A Study of Ligand Substitution and its Importance in the C–H Activation of Methane and Methanol

Thesis by
Jonathan S. Owen

In Partial Fulfillment of the
Requirements for the Degree of
Doctor of Philosophy

Division of Chemistry
and Chemical Engineering

California Institute of Technology
Pasadena, CA

2005
(Defended May 27th, 2005)

For my parents

Acknowledgments

My time at Caltech has been great, and like most of my experiences in life, I'm lucky to have spent that time with excellent people. This good fortune is mostly due to my parent's hard work and guiding hand. Their watchful eye and open-minded support is always welcome and never fails to make me feel comfortable. Thanks Mom and Dad, much of my success is your own, as I'm sure you are aware. Thanks also to my brothers. I've learned a lot from watching you make choices and find the things you love. Can't wait to see you next Christmas!

Thanks to John and Jay! Being a graduate student with you two has been perfect. Although it took me a while to fully appreciate it, I really enjoyed the freedom you gave me. Your help and opinions usually came at just the right time and fit my style of learning well. I can't imagine a better set of thesis advisors. It's been fun at bp meetings, on the group hike and numerous parties. You've both helped make my time here enjoyable!

My thesis committee has been good to me, accepting my tardiness and forgetfulness with good-natured smiles. Bob, we should go "climbing on Table Mountain" someday! Your lighthearted and creative approach to chemistry has helped me to take a step back and look at the big picture. Thanks for the advice and laughter and I look forward to joining you in Yosemite this summer. Nate, your commitment to teaching, and your interest in renewable energy has been especially motivating. Learning from you and your group has been the primary motivator for my interest

in semiconductors and Nanoscience. I'll no doubt be asking for your help someday soon. Brian, it's been fun watching you get your start here at Caltech. Your organic chemistry class is one of the best classes I've ever taken, and a testament to your enthusiasm for chemistry! Best of luck with the tenure decision, Caltech would be lucky to have you.

The Bercaw group - woohoo, its been fun! Though things seem to have changed a lot from the beginning to the end of my time here, people in the Bercaw group have always been hard working and willing to drink more than is healthy. People in this group have always been supportive and willing to share time to help new people get started.

In my first year Joseph Sadighi, Seva Rostovtsev, Chris Brandow Anita Zhong, and Antek Wong-foy really helped me get rolling. Joseph, you are one of the few people that exceeds my expectations of greatness. If it weren't for your kindness and relentless good manners I'd find your facility with language and perfect memory intimidating. I learned more about *chemistry* from you than anyone other student or post doc I interacted with at Caltech. Theory, I've really enjoyed our time together! You and Maggie are lucky to have eachother and such healthy kids. From talks about DFT and kinetics to the NMR facility, it's always a hoot! Few people are so lucky to be blessed with a good-natured humor and persistent kindness like yours. Seva, thanks for your help during my first year and for hosting my visit to Dupont. I really enjoyed having you Olga and Daniel as friends. Annita and Antek, thanks for helping me get started and for your encouragement early on.

Our group was lucky to have two friendly visiting professors while I was at Caltech. Both Gerry Niccolai and John Moss were good friends of mine while they visited, and my time here will always remind me of them. Gerry, I sincerely appreciate the encouraging words and advice you and Veronique offered me. Thanks again to you Laura and Luca for showing me and Susan a good time in Lyon last summer. I'd love to return the favor someday. John Moss, what can I say, you've got to be everyone's favorite person! I really admire your good nature and kind heart. I hope I can come and visit you Lynn, Miranda and Tara one day. I will never forget the trips we took together to Yosemite and Joshua Tree.

More recent members of the Bercaw group might as well have been family for the last few years. Lily Ackerman, thanks for helping with kinetics and for arguments at the chalk board. You're incredibly effective and are likely to be successful anywhere you apply yourself. It will be fun watching you climb the ladder at Symyx. Sara Klamo and Endy Min, thanks for the good times we've had together. Mans-pants, I'll never forget our group Christmas parties and group hikes. From welding glasses, to voyeuristic spanking, olive oil facials and piles of purple puke, it's been memorable. Good luck to you and Ramez in Michigan. To the members of the Bercaw Bulls, sorry I suck so bad. Jeff Byers, thanks for sticking by as coach even though I never listened. Keep up the hard work Jeff, it will take you a long way. Steve Baldwin, you are the man! You've improved on the basketball court and infront of the vac-line. Best of luck getting out of here. Paul Elowe, thanks for sharing a piece (or several) of Switzerland with the group. Don't let your ambition get the better of you

and continue to pound out the stellar results. Dave Weinberg, I was happy to know you were joining the group the day I met you. Thanks for the many trips to Lucky Baldwins, Joshua Tree, Tahquitz, and Yosemite. Thanks also for keeping the green box alive, it helped me get out of here on time. Theo Agapie, you win the award for hardest working (with several close runner-ups). I'm glad we became good friends, and I can't wait to see where we end up. I'll never forget our first climb at Tahquitz or the group ski trip to Mammoth. You and Dave are like pack mules on the hiking trail. I just hope that doesn't prevent your brain from working there as well as it does in the lab. Bolin Lin, its been fun watching you get started in the lab. It's really impressive that you can make the transition from a computational group to an experimental one without such ease. Good luck finishing up. George Chen joined the group in my last year, and is one hell of a character. You're off to a great start George - don't blow yourself up.

Several excellent post-docs have come and gone while I was in the group. Joseph Sadighi, John Scollard, Christoph Balzarek, Cliff Baar, Alan Heyduk, Parisa Mehrkhodavandi, Tom Driver and Reto Dorta have all been helpful around the lab, and for advice on manuscripts etc. Alan Heyduk broke trail for the anhydrous trifluoroethanol chemistry, and I couldn't have made my science work without his innovation. Thanks to John Scollard and Christoph Balzarek who infected me with Macaholism and got me started as computer czar. Cliff Baar was an all around fun person to have in the group, with a particularily memorable Christmas party. Parisa Mehrkhodavandi, Pat Andersen, Mark Thompson and Ged

Parkin were a great team for John's 60th birthday party. Parisa, I think you're a good scientist and I'm sure you'll have success at UBC. Tom Driver was a great collaborator and critic in my last year at Caltech. Tom I really enjoyed being able to talk about kinetics and mechanism with you. No doubt you'll find a good academic job, even if that means Adrian has to work in wastewater treatment. Reto Dorta was a good friend during his brief visit, I can't wait to visit you in Lausanne! Looking forward to seeing all of you at the next Bercawfest.

Raissa Trend and Andrew Waltman, I really enjoyed our time together. You two have been great friends. Raissa, I've always appreciated your sincere interest in scientific analysis. It was nice to have a friend who is so frequently willing to go to the bar and then still interested in talking chemistry. Drew, most people at Caltech won't forget your good humor. From birthday cake war paint to drunken beat-boxing, life was a whole lot more fun with you around. And lets not forget the "cotton gin." It was a shame that you and Victor didn't meet sooner.

Victor Rucker, Susan and I agree that you are the funniest person on earth. Victor, thank you for your honest opinion and numerous insightful conversations. You heard a side of me that few are patient enough to listen to. Thank you to both you and Lily for your friendship. It will be fun to live close to one another next year!

Susan Schofer deserves many thanks for reading my props, my papers, my candidacy, for her enthusiasm for chemistry, for unending encouragement, for a willingness to drop everything and have a good time, for being forgiving and patient and still analytical and critical.

Susan, we had a great time at in Southern California and I wouldn't trade our time together for anything. I think we learned a lot from one another and I'm infinitely grateful for that.

There are many people at Caltech that helped me with some aspects of my experiments and who contributed greatly to my success. Larry Henling and Mike Day taught me everything I know about crystallography. Larry, thanks for teaching how to use the diffractometer, and how to analyze data. It was really fun working together to extract crystal structures. Mike, thanks for all your help with data analysis and for helping me get a feel for the refinement process and what it means. Dan Neiman, built most of the high-pressure manifold in 201 and taught me how to build it right the first time. Dan, I really enjoyed working together, you work harder than most graduate students, you certainly talk more and somehow you've maintained more enthusiasm for what you do. I think you are one of the most fortunate people I know. Thanks to Mike Roy and Steve Olson for help with machining. Also a big thanks to Dean Roddick for help with the high pressure NMR tube design. A special thanks to Scott Ross and Tom Dunn for help with NMR spectroscopy. The NMR facility has come a long way since I first came to Caltech, and both Tom and Scott are the people who helped make that possible. Tom, I don't see how this place could run without you. Thanks for helping to keep the spectrometers alive before Scott started. Scott, thanks for many hours sitting in front of the spectrometer. I learned a lot from you and am thankful for your patient help.

I also want to say thanks to Jonas Peters, Ted Betley, Steve Brown, Seth Harkins, Bruce MacKay, Cora MacBeth for their friendship and scientific perspective. It's been fun watching you from downstairs, and it will be fun to have you as colleagues. Thanks also to many friends in the Stoltz and Grubbs groups!

Bp deserves a big thanks for a well run MC^2 program. We are lucky to have your support! I really benefited from learning to interface academic ideals with a long-term practical thinking. Thanks for accommodating our intellectual interests.

Abstract

Pyridinium and indolium-derived aminocarbene complexes of platinum and palladium were prepared by oxidative addition of pyridinium and 2-chloro-indolium carbene precursors. These complexes were synthesized in order to study the degree to which aminocarbene ligands π-bond with the transition-metals to which they are bound. X-Ray crystal structures show minimal multiple bonding in the indole examples and a measurable shortening of the pyridine-2-ylidene Pt–C distance (1.959(3) Å) compared with typical Pt–C bonds (2.01(1) Å). The kinetics of associative DMSO substitution *trans* to the pyridine-2-ylidene ligand indicate a stabilization of the trigonal bipyramidal transition structure that is due to π-acidity of the carbene carbon. This π-acidity is responsible for 4-orders of magnitude acceleration in the associative substitution rate compared with a structurally similar phenyl donor.

The relative rates of methane, methanol and dimethylether C–H activation by $[(N\text{-}N)PtMe(TFE\text{-}d_3)]^+$ ((N-N) = ArN=C(Me)-C(Me)=NAr Ar = 3,5-di-*tert*-butylphenyl, TFE-d_3 = CF_3CD_2OD) were studied by ^1H and ^{13}C NMR spectroscopy. Methane activation kinetics were conducted at 300-1000 psi of methane pressure in single crystal sapphire NMR tubes ($k = 1.6 \pm 0.4 \times 10^{-3}$ $M^{-1}s^{-1}$, 330 K; $k = 2.7 \pm 0.2 \times 10^{-4}$ $M^{-1}s^{-1}$, 313 K). Deuterium scrambling studies indicate that displacement of TFE-d_3 from the platinum center by methane's C–H bond is slower than the subsequent C–H oxidative cleavage and hence the rate-determining step in methane C–H activation. The kinetics of methanol and dimethylether C–H activation

were studied with ^{1}H NMR spectroscopy and shown to be inhibited by a preequilibrium binding of the substrates oxygen lone-pair to the metal center. A small kinetic isotope effect ($k_H/k_D = 1.4 \pm 0.1$) and the observed concentration dependence suggest that the reaction proceeds by rate determining displacement of the coordinated trifluoroethanol by the C-H bonds of methanol ($k = 2.0 \pm 0.2 \times 10^{-3}$ $M^{-1}s^{-1}$, $K_{eq} = 0.0042 \pm 0.0006$, 330 K). A similar concentration dependence is observed in the activation of dimethylether ($k = 5.5 \pm 0.5 \times 10^{-4}$ $M^{-1}s^{-1}$, $K_{eq} = 0.020 \pm 0.002$, 313 K). Comparison of these second order rate constants ($k_{(Methane)}/k_{(Methanol)} = 1/1.3$, 330 K; $k_{(Methane)}/k_{(Dimethylether)} = 1/2$, 313 K) shows that the selectivity of this ligand substitution step matches the selectivity previously reported by our group for oxidizing methyl and hydroxymethyl groups with aqueous tetrachloroplatinate (1.5/1). These data strongly suggest a similar rate-determining step under the Shilov conditions.

Table of Contents

List of Figures

Chapter 1

Chapter 2

Appendix A

List of Tables

Chapter 1

Chapter 2

Chapter 3

Chapter 1

Pyridinium-Derived *N*-Heterocyclic Carbene Complexes of Platinum: Synthesis, Structure and Ligand Substitution Kinetics

This chapter was taken in part from:

Owen, J. S.; Labinger, J. A.; Bercaw, J. E. *J. Am. Chem. Soc.* **2004,** *126*(26), 8247-8255.

Abstract

A series of [(R-*iso*-BIPY)Pt(CH_3)L]$^+$X$^-$ complexes [R-*iso*-BIPY = N-(2-pyridyl)-R-pyridine-2-ylidene; (R = 4-H, **1**; 4-*tert*-butyl, **2**; 4-dimethylamino, **3**; 5-dimethylamino, **4**); L = SMe_2, **b**; dimethylsulfoxide (DMSO), **c**; carbon monoxide (CO), **d**; X = OTf^- = trifluoromethanesulfonate and/or $[BPh_4]^-$] were synthesized by cyclometalation of the [R-*iso*-BIPY-H]$^+$[OTF]$^-$ salts **1a - 4a** ([R-*iso*-BIPY-H]$^+$ = N-(2-pyridyl)-R-pyridinium) with dimethylplatinum-μ-dimethylsulfide dimer. X-ray crystal structures for **1b**, **2c - 4c** as well as complexes having bipyridyl and cyclometalated phenylpyridine ligands, [(bipy)Pt(CH_3)(DMSO)]$^+$ (**5c**) and ($C_{11}H_8N$)Pt(CH_3)(DMSO) (**6c**), have been determined. The pyridinium-derived N-heterocyclic carbene complexes display localized C-C and C-N bonds within the pyridinium ligand that are indicative of carbene π-acidity. The significantly shortened platinum-carbon distance, for "parent" complex **1b**, together with NMR parameters and the ν(CO) values for carbonyl cations **1d – 4d** support a degree of Pt-C10 multiple bonding, increasing in the order **3** < **4** < **2** < **1.** Degenerate DMSO exchange kinetics have been determined to establish the nature and magnitude of the *trans*-labilizing ability of these new N-heterocyclic carbene ligands. Exceptionally large second order rate constants (k_2 = 6.5 ± 0.4 $\underline{M}^{-1}\cdot s^{-1}$ (**3c**) to 2300 ± 500 $\underline{M}^{-1}\cdot s^{-1}$ (**1c**)) were measured at 25 °C using ^{1}H-NMR magnetization transfer kinetics and variable temperature line shape analysis. These rate constants are as much as four orders of magnitude greater than those of a series of structurally similar cationic *bis*(nitrogen)-donor complexes [(N-N)Pt(CH_3)(DMSO)]$^+$ reported earlier, and a factor of 32 to 1800 faster than an analogous charge neutral complex derived from cyclometalated 2-

phenylpyridine, $(C_{11}H_8N)Pt(CH_3)(DMSO)$ (k_2 = 0.21 ± 0.02 $\underline{M}^{-1}\cdot s^{-1}$ (**6c**)). The differences in rate constant are discussed in terms of ground state *versus* transition state energies. Comparison of the platinum-sulfur distances with second-order rate constants suggests that differences in the transition-state energy are largely responsible for the range of rate constants measured. The π-accepting ability and *trans*-influence of the carbene donor are proposed as the origin of the large acceleration in associative ligand substitution rate.

Introduction:

The development of imidazolium-derived N-heterocyclic carbene ligands has had a major impact on catalysis,[1] including more active ruthenium olefin metathesis catalysts[2] and improved palladium and nickel catalysts for aryl halide cross-couplings.[1,3] Enhanced activity for catalysts bearing N-heterocyclic carbene ligands may be attributable to the strong σ-donating[4] and weak π-accepting properties of imidazole-2-ylidenes.[5] Carbene ligands derived from deprotonation of pyridinium rather than imidazolium cations would be stabilized by only one mesomeric nitrogen and thus should be even better σ-donors and π-acceptors (Scheme 1).[6] These differences should magnify their *trans*-influence and *trans*-effect, making metal complexes based on this class of N-heterocyclic carbene ligand more substitutionally labile.

Scheme 1

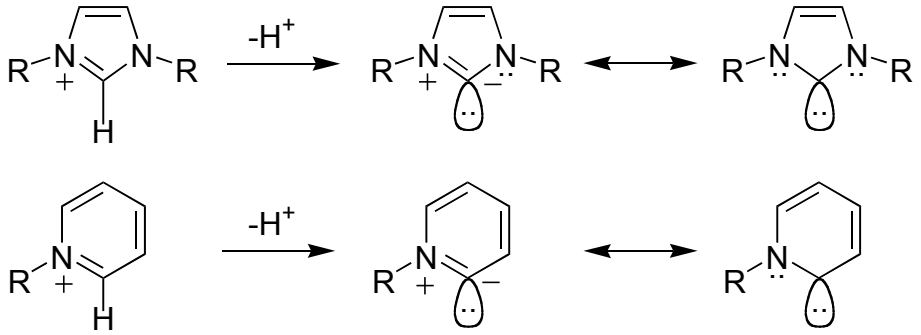

In recent model studies of the "Shilov cycle", the rate of benzene C–H bond activation by $[(N\text{-}N)M(CH_3)L]^+$ ((N-N) = α-diimine; M = Pt, Pd; L = H_2O, 2,2,2-trifluoroethanol = TFE) complexes in TFE solution was found to be strongly dependent on the position of the pre-equilibrium substitution of TFE for water.[7] Regardless of whether the rate-determining step is associative benzene displacement of TFE or oxidative addition of a benzene C-H bond,

more electron-rich α-diimine ligands were found to decrease the thermodynamic preference for water binding and increase the overall rate of C–H activation. Based on these findings, we reasoned that electron-rich ligands capable of favoring the binding of TFE *versus* water and facilitating ligand substitution should enhance the propensity for a platinum(II) or palladium(II) complex to activate C–H bonds. We envisioned that the enhanced σ-donor and π-acceptor capabilities of pyridinium-derived N-heterocyclic carbenes might be ideal for facilitating substitution of a trans ligand.

We describe herein the synthesis of a series of square planar platinum(II) complexes having a new class of chelating pyridine/N-heterocyclic carbene donors, N-(2-pyridyl)-R-pyridine-2-ylidene (R = H, 4-*tert*-butyl, 4-dimethylamino, 5-dimethylamino).[8] (Since these ligands are isomers of 2,2′-bipyridyl, we abbreviate them as R-*iso*-BIPY.) To establish the σ- and π-bonding properties of this new ligand type, we determined the X-ray crystal structures for $[(R\text{-}iso\text{-}BIPY)Pt(CH_3)(DMS)]^+$ and $[(R\text{-}iso\text{-}BIPY)Pt(CH_3)(DMSO)]^+$ cations (DMS = dimethylsulfide; DMSO = dimethylsulfoxide), examined their NMR parameters and the carbonyl stretching frequencies for the corresponding methyl-carbonyl cations, and undertook studies of the kinetics of DMSO substitution trans to the carbene donor.

Results

Synthesis and Isolation of $[(R\text{-}iso\text{-}BIPY)Pt(CH_3)L]^+$ Salts and Related Complexes. To avoid the need for preparation of a free, likely very reactive

carbene, we designed pyridinium salts that would provide the desired carbene complexes upon cyclometalation.[9] Pyridinum salts **1a - 4a** (Scheme 2) were prepared by heating the appropriately substituted pyridine with 2-pyridyl triflate at 150 ˚C under argon. These salts react with $[(\mu\text{-}SMe_2)Pt(CH_3)_2]_2$ in acetone or dichloromethane solution at room temperature, with liberation of one equivalent of methane, to give ~50-90% isolated yields of the cyclometalated products **1b - 4b**. Pyridinium salt **1a** reacts most rapidly giving an immediate color change and vigorous evolution of methane gas upon mixing.

Scheme 2

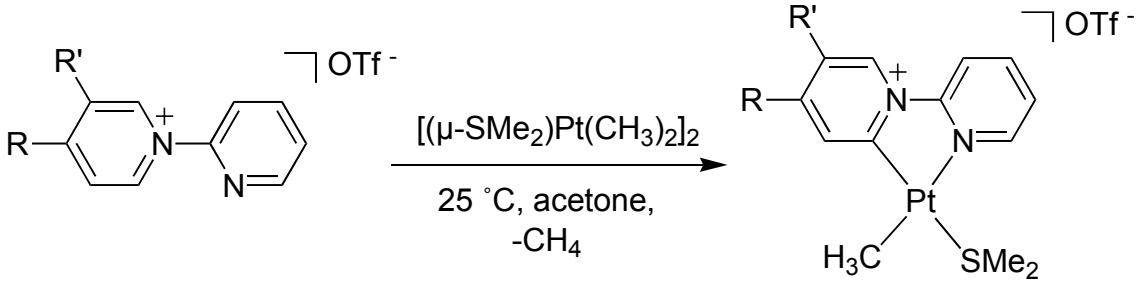

1a R = R' = H
2a R = CMe_3, R' = H
3a R = NMe_2, R' = H
4a R = H, R' = NMe_2

1b R = R' = H
2b R = CMe_3, R' = H
3b R = NMe_2, R' = H
4b R = H, R' = NMe_2

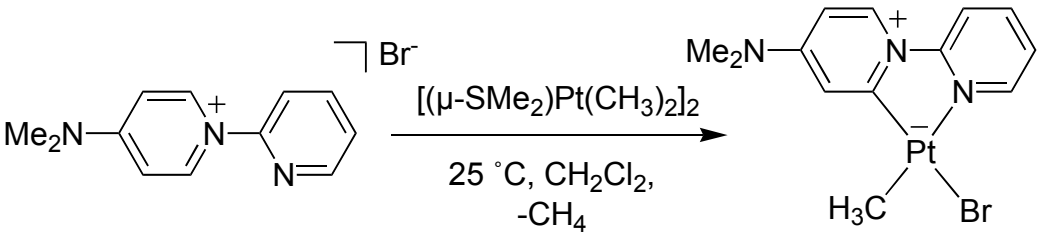

3e **3f**

The dimethylsulfide complexes **1b - 4b** are useful synthons, providing access to the corresponding DMSO (**1c, 2c, 4c**) and carbonyl (**1d - 4d**) complexes (Scheme 3).[10] The triflate salts were crystallized directly or were converted to

tetraphenylborate salts (the bromide complex in the case of **3f**) by precipitation from methanol to generate more crystalline complexes suitable for X-ray structural analysis. All complexes can be handled and stored in air as solids at room temperature; however, solutions oxidize slowly in air.

Scheme 3

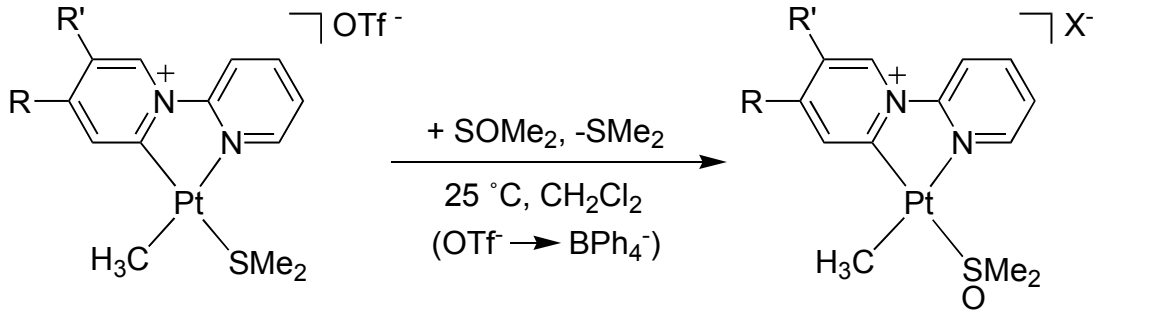

1b R = R' = H
2b R = CMe_3, R' = H
3b R = NMe_2, R' = H
4b R = H, R' = NMe_2

1c R = R' = H; X^- = $SO_3CF_3^-$
2c R = CMe_3, R' = H; X^- = $SO_3CF_3^-$

4c R = H, R' = NMe_2; X^- = BPh_4^-

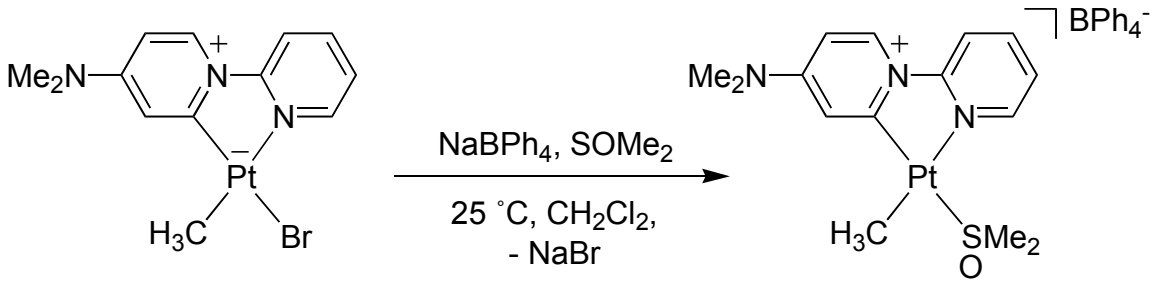

3f **3c**

In order to compare the carbene complexes with closely related ones, $[(bipy)Pt(CH_3)(DMSO)]^+[BPh_4]^-$ (**5c**) and the cyclometalated 2-phenylpyridine adduct, $(C_{11}H_8N)Pt(CH_3)(DMSO)$ (**6c**), were synthesized (Figure 1). Protonolysis of $(bipy)Pt(CH_3)_2$ in the presence of DMSO and precipitation from methanol using $NaBPh_4$ provided **5c.** Complex **6c** was prepared analogously to **1c-4c**, using 2-phenylpyridine as the ligand precursor. The unstable dimethylsulfide

product was immediately trapped with DMSO and isolated. Attempts to prepare the platinum-carbonyl complex $(C_{11}H_8N)Pt(CH_3)(CO)$ unfortunately proved unsuccessful.

Figure 1

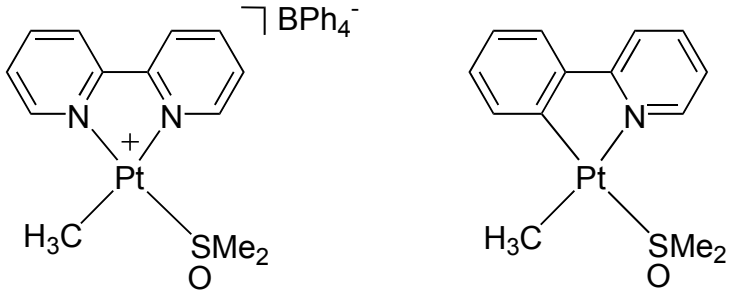

5c **6c**

X-ray Crystal Structures, NMR and Infrared Spectral Parameters. X-ray quality crystals of **1b** and **2c-6c** were grown by diffusion of petroleum ether or diethyl ether into their acetone or dichloromethane solutions. Their structures are shown in Figure 2. In all cases the platinum methyl group is located trans to the pyridine nitrogen, and the dimethylsulfide or dimethylsulfoxide ligands trans to the carbene or phenyl donor. Table 1 gives ligand to platinum bond lengths for all complexes.

Bonding of the sulfur and carbene donors with platinum is of particular interest. The Pt-S distances for complexes **2c**-**4c** and **6c** are indistinguishable (within 3σ (σ_{AVG}= 0.0012Å)), while in complex **5c** it is shorter by 0.08 Å (Table 1). The Pt-C10 distances fall in the order **1b** < **2c** < **4c** < **3c** = **6c** < **5c** (**5c**, the bipy adduct, has no C10**;** the differences for **2c** and **4c** are comparable to the uncertainties). The Pt-C10 bond length of 1.959(3) Å for **1b** is significantly shorter than that of the typical sp^2-carbon-platinum single bond (2.01(1) Å) [11]

while the values for **3c** and **6c** (2.011(2) and 2.011(3) Å respectively) are closer. (It should be noted however that the ligand trans to C10 is DMS for **1b** but DMSO for **3c** and **6c**.)

Figure 2

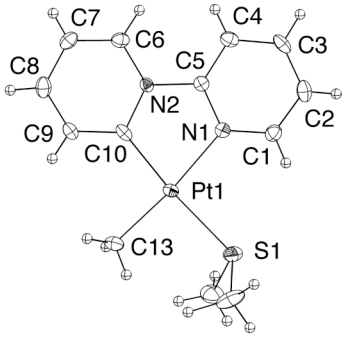

1b

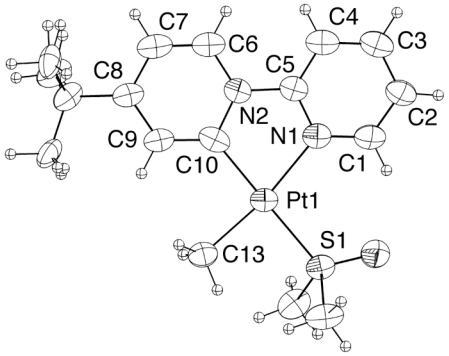

2c

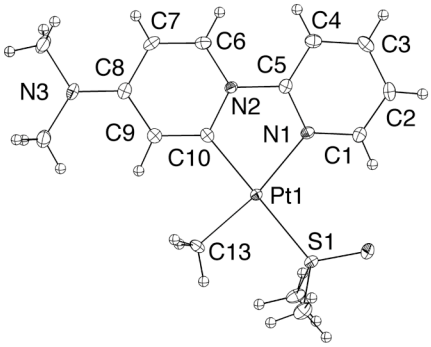

3c

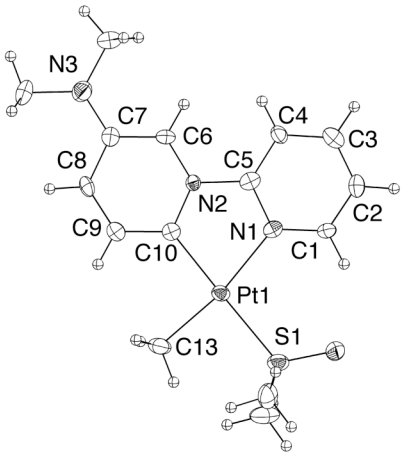

4c

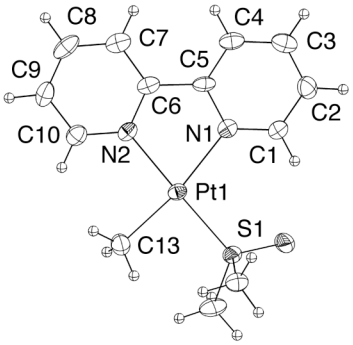

5

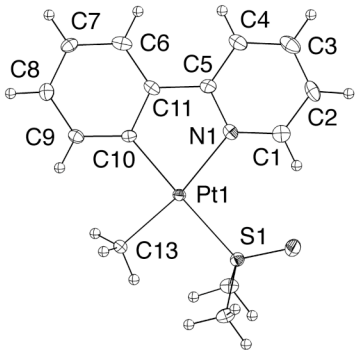

6c

The quality of the X-ray structure determinations for **1b, 3c,** and **6c** also allows discrimination of C–C and C–N bond lengths within the ligand. Ring C-C and C-N distances for complexes **3c, 4c, 6c** and **1b** are given in Table 2. Figure 3 shows the bond length patterns in **1b**, **3c** and **6c**.

Table 1. Selected Pt-X bond lengths [Å] for complexes **1b**, **2c**, **3c**, **4c**, **5c**, and **6c**.

	Pt-S(1)	Pt-C(13)	Pt-N(1)	Pt-C(10)
1b	2.3447(8)	2.037(3)	2.092(2)	1.959(3)
2c	2.2758(19)	2.077(7)	2.101(6)	1.996(7)
3c	2.2693(5)	2.046(2)	2.100(2)	2.011(2)
4c	2.2841(17)	2.050(6)	2.095(5)	2.004(6)
5c	2.1961(11)	2.053(4)	2.130(3)	2.066(3)[a]
6c	2.2759(9)	2.047(3)	2.114(3)	2.011(3)

[a]Pt-N(2).

Table 2. Selected ring bond lengths [Å] for complexes **1b**, **3c**, **4c**, and **6c**.

	N(2)-C(10)	C(10)-C(9)	C(9)-C(8)	C(8)-C(7)	C(7)-C(6)	C(6)-N(2)	Me_2N-C_{Ar}
1b	1.389(3)	1.410(4)	1.356(4)	1.393(4)	1.359(4)	1.369(2)	
3c	1.395(3)	1.376(3)	1.408(3)	1.423(3)	1.347(3)	1.370(3)	1.351(3)
4c	1.359(8)	1.405(9)	1.356(9)	1.394(9)	1.400(9)	1.355(8)	1.359(8)
6c	1.407(5)[a]	1.390(5)	1.386(5)	1.395(5)	1.376(5)	1.397(5)[b]	

[a]C(11)-C(10). [b]C(6)-C(11).

Downfield ^{13}C-NMR chemical shifts are characteristic features of carbene donors. Lappert and coworkers reported a range of δ = 175-218 ppm for a series of imidazolium-derived platinum-carbene complexes.[12] In complexes **2c-4c** and **6c** the signal for the carbon bound directly to platinum can be unequivocally identified by the satellites due to the large ^{195}Pt-^{13}C coupling constants. ^{13}C{^{1}H} NMR spectra of complexes **2c-4c** have peaks in the range of δ = 160-175 ppm

($^1J_{Pt\text{-}C}$ ~ 1200-1300 Hz), while **6c** shows a chemical shift of δ = 152 ppm with a significantly smaller $^1J_{Pt\text{-}C}$ of 1071 Hz.[13] $^{13}C\{^1H\}$

Figure 3

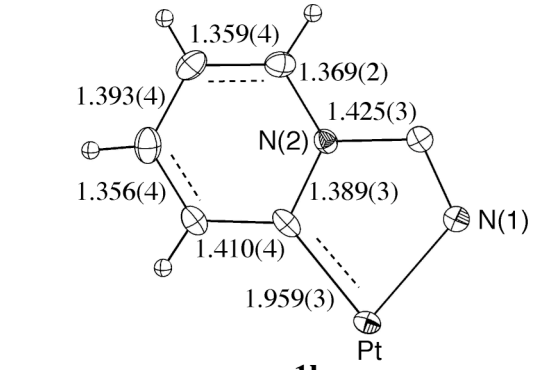

1b

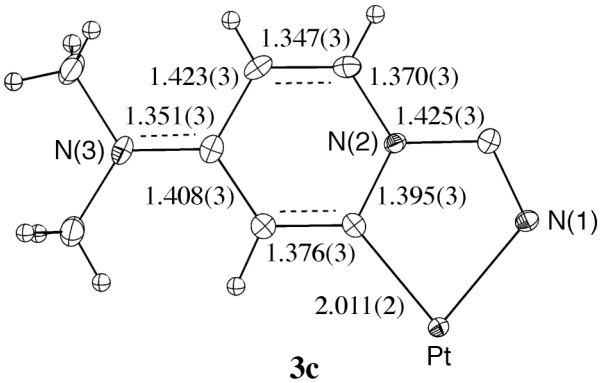

3c

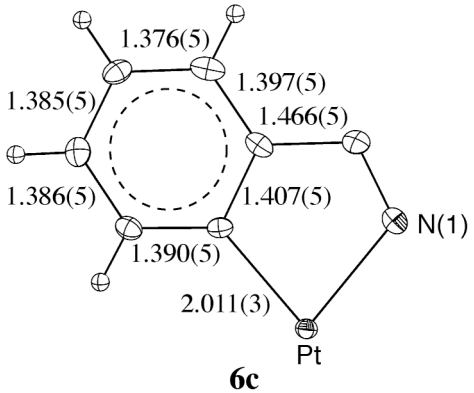

6c

Table 3. Selected spectroscopic, crystallographic, and kinetics parameters.

	δ [ppm]	$^{1}J^{195}$Pt-^{13}C [Hz]	r(Pt-C) [Å]	ν(CO) [cm^{-1}][a]	k_2^{298} [M^{-1}s^{-1}][b]
1c	174.0	nd	nd	2099.4	382(50)
2c	172.2	1231.2	1.996(7)	2097.9	175(25)
3c	164.3	1203.8	2.011(2)	2088.9	6.51(36)
4c	160.9	1323.8	2.004(6)	2090.2	28.8(1.5)
6c	152.1	1070.9	2.011(3)	nd	0.21(2)

[a] For [OTf$^-$] salts of carbonyl adducts, **1d-4d**, in acetone-d_6. [b] In $C_2D_2Cl_4$.

NMR data for complexes **2c-4c** and **6c** are included in Table 3, along with relevant crystallographic, infrared and kinetics data (see above).

At room temperature, complexes **1c-4c** show ^{1}H NMR spectra consistent with their solid state structures. The $^{2}J_{\text{Pt-H}}$ satellites observed for the methyl signals (~ 81 Hz) are consistent with methyl *trans* to the pyridine nitrogen (as observed in the spectrum of **5c**). Notably, the 300 MHz ^{1}H NMR spectrum of **3c** shows inequivalent [N(CH_3)$_2$] resonances at room temperature, that coalesce at 70 ˚C.[14] In contrast complex **4c** shows one sharp [N(CH_3)$_2$] resonance at room temperature.

Ligand Substitution Kinetics. In order to investigate the *trans*-labilizing ability of these pyridine-2-ylidene ligands, DMSO exchange rates for complexes **1c-4c** and **6c** were measured in $C_2D_2Cl_4$ and acetone-d_6 solution, using magnetization transfer and variable temperature line shape simulation. Kinetic data are shown in Tables 4 and 5. Complexes **1c** and **2c** substitute most quickly, giving broad ^{1}H NMR spectra in the presence of free DMSO at room temperature. Simulation of their temperature-dependent spectra provided first-order rate constants (k_{obs}) and activation parameters. Plots of

k_{obs} *versus* [DMSO] indicate an associative substitution mechanism with a first-order DMSO dependence[15] and a contribution from a DMSO-independent substitution pathway (k_i). Complexes **3c**, **4c** and **6c** undergo slower associative DMSO exchange and were studied using magnetization transfer techniques at 298 K.[16] At the concentrations studied, the substitution rates display a linear dependence on DMSO concentration with no evidence for a DMSO-independent substitution path. The second-order rate constant for the parent pyridine-2-ylidene complex **1c** is four orders of magnitude greater than that measured for its structural isomer, bipy complex **5c**, and three orders of magnitude greater than its neutral 2-phenyl pyridine analog **6c**.

Table 4. Second-order rate constants and activation parameters for complexes **1c** and **2c** from variable temperature line shape simulation.

	[Pt][b]	[DMSO][b]	T range	k_{obs}^{298c}	k_2^{298d}	k_i^{298e}	$\Delta H^{\ddagger f}$	$\Delta S^{\ddagger g}$
1c[a]	0.0308	0.0308	255 - 313	109			11.3	-11.3
	0.0416	0.0416	245 - 312	130			11.2	-11.3
	0.0525	0.0525	254 - 303	159	2300 ± 500	37	10.8	-12.3
1c[h]	0.0197	0.0197	314 - 347	20.5			10.7	-16.7
	0.0504	0.0504	304 - 338	36.3			10.2	-17.1
	0.0738	0.0738	304 - 336	40.8	382 ± 50	14	11.2	-13.6
2c[h]	0.0527	0.0264	314 - 348	8.4[i]			11.8	-14.6
	0.0527	0.0527	314 - 348	17.3			10.3	-18.2
	0.0527	0.0791	304 - 348	22.5			10.4	-17.3
	0.0527	0.1054	304 - 348	26.6	175 ± 25	8.3	10.3	-17.4

[a] In acetone-d_6. [b] M. [c] s^{-1}, calculated. [d] $M^{-1} s^{-1}$ slope from plot of k_{obs} vs. DMSO. [e] s^{-1}, intercept from plot of k_{obs} vs. DMSO. [f] kcal/mol. [g] e. u.. [h] In $C_2D_2Cl_4$.
[i] excluded from determination of k_2.

Table 5. Second order rate constants for complexes **3c, 4c, 5,** and **6** from magnetization transfer kinetics in $C_2D_2Cl_4$.

	[Pt][a]	[DMSO][a]	k_{obs}^{298} [b]	k_2^{298} [c]	$[k_2^{298}]_{ave}$ [c]
3c	0.0240	0.0530	0.34	6.42	
	0.0570	0.1610	1.00	6.21	
	0.0760	0.1365	0.94	6.89	
	0.0760	0.2795	1.87	6.69	6.51 ± 0.36
4c	0.0387	0.1550	4.35	28.1	
	0.0388	0.0775	2.16	27.9	
	0.0389	0.3114	9.54	30.6	28.8 ± 1.5
5c[d]					0.16 ± 0.01
6c	0.0414	1.240	0.236	0.190	
	0.0413	2.063	0.419	0.203	
	0.0309	3.094	0.692	0.224	0.21 ± 0.02

[a] M. [b] s^{-1}. [c] M^{-1} s^{-1}. [d] In acetone-d_6. See reference 14a.

Discussion

Previous theoretical studies of complexes bearing imidazolium-derived N-heterocyclic carbenes suggest that they are primarily strong carbon σ-donor ligands.[5] Still unresolved, however, is whether π-bonding becomes important in the transition states and intermediates of catalytic reaction cycles, and has any consequence for catalytic activity. The major resonance contributors describing the interactions of a transition metal with N-heterocyclic carbenes derived from imidazolium (**A**) and pyridinium (**B**) cations are shown in Scheme 4. Analogy to the imidazolium-derived carbenes suggests that the σ-only form **B1** would be the most important contributor for pyridinium-derived carbenes, but as discussed below, our structural data and fast associative substitution kinetics suggest a significant role for π-acidity as well.

Scheme 4

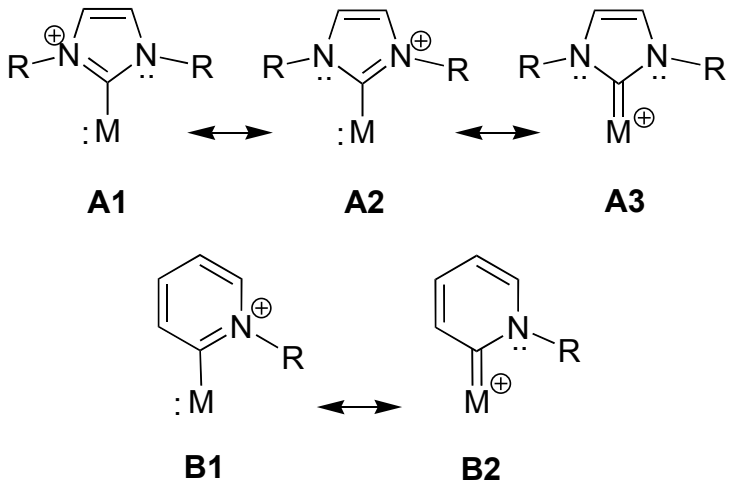

Scheme 5

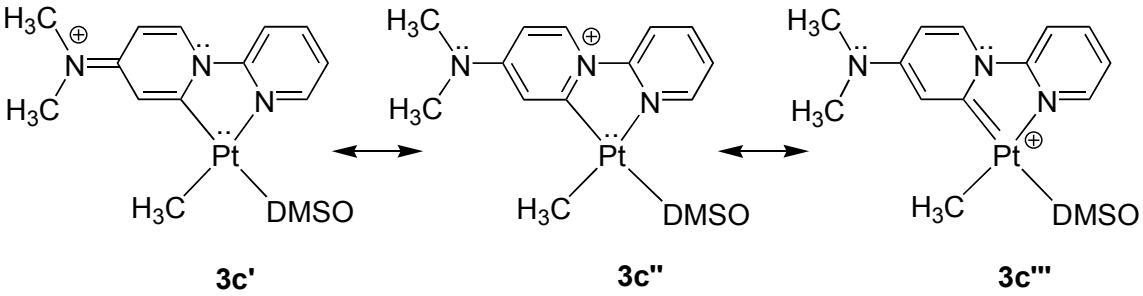

Structural and Spectroscopic Evidence. Bond length patterns in the X-ray structures of **3c** and **1b** demonstrate the importance of π–acidity of the carbene ligand. Resonance structures for complex **3c** (Scheme 5) reflect competition between the N pπ electrons of the dimethylamino substituent, the pyridinium N pπ electrons, and the dπ electrons of the platinum for the empty carbon pπ orbital. The X-ray structure of **3c** agrees best with the resonance depiction **3c′**, showing a platinum-carbon single bond with appropriate short/long alternations for double and single C-C bonds within the ring. The Pt-C10 distance (2.011(2) Å) indicates a relatively minor contribution from **3c′′′**. In contrast, the absence of a dimethylamino substituent in **1b** leaves the

empty carbene orbital to be stabilized only by interaction with the filled platinum dπ orbital and the pyridinium N pπ electrons. The former interaction results in the shortest Pt-C10 bond in the series (1.959(3) Å) and ligand C–C and C–N distances (Figure 3) consistent with significant contributions for both resonance structures **B1** and **B2** (Scheme 4). Both structures differ from that of metalated 2-phenylpyridine analog **6c,** which shows delocalized bonding in the phenyl ring (Table 2, Figure 3), and a platinum–carbon distance (2.011(3) Å) not significantly different from that for **3c** (2.011(2) Å). The Pt-C10 distance of 1.959(3) Å for the "parent" example, **1b**, is significantly shorter than that expected for a single bond. We conclude, therefore, that the X-ray structural data support a degree of Pt-C10 π-bonding as depicted in resonance structure **B2** (Scheme 4).

Scheme 6

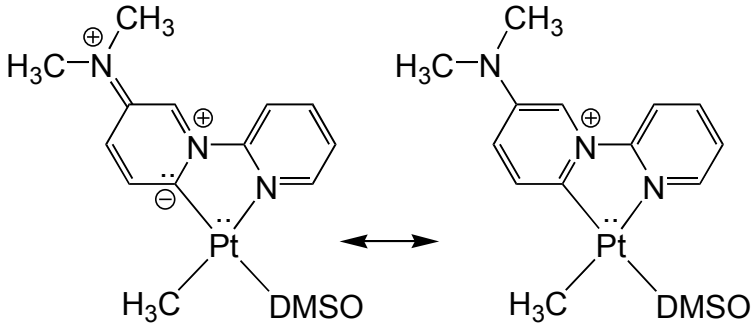

4c' **4c"**

The NMR and infrared parameters for these complexes also suggest some modest Pt-C10 π-bonding. While the ^{13}C NMR chemical shifts for the Pt-bonded carbon for **1c** - **4c** (δ 160.9 – 174.0) are significantly downfield of that for the metalated 2-phenylpyridine complex **6c** (δ 152.1), they are not so far downfield as those for the imidazolium-derived carbenes (δ = 175 – 218) or

alkylidenes ($\delta \geq 200$).[17] Moreover, the $^{1}J_{Pt\text{-}C}$ values for **2c** - **4c** are larger (1203.8 – 1323.8 Hz) than that for **6c** (1070.9 Hz), suggesting a higher Pt-C10 bond order for the (2-pyridyl)-R-pyridine-2-ylidene complexes. The carbonyl stretching frequencies for **1d** - **4d** lie in the order of increasing ν(CO): **3c** (2088.9 cm^{-1}) < **4c** (2090.2 cm^{-1}) < **2c** (2097.9 cm^{-1}) < **1c** (2099.4 cm^{-1}), approximately the order expected, as the "parent" ligand of **1c** should be most π acidic; **2c** and **4c** less so, because of the electron-releasing substituents; and **3c** least, because of the 4-amino nitrogen πp donation (form **3c'**, Scheme 5).

An additional manifestation of the importance of resonance structure **3c'** (Scheme 5) is the measurable barrier to rotation about the $[(CH_3)_2N]\text{–}C_{Ar}$ bond in **3c** ($\Delta G^{\ddagger}_{343K}$ = 16.8 kcal/mol). The much smaller barrier for **4c** is expected, because the analogous double bonded resonance structure (**4c'**) is disfavored by charge separation; the higher CO stretching frequency for **4d** *vs.* **3d** is also consistent with this argument (Scheme 6).

Structural and Kinetics Evidence. Studies of degenerate DMSO exchange reveal effects of ligand bonding properties both on the ground state (*trans*-influence) and transition state (*trans*-effect). Romeo and coworkers have extensively studied associative, degenerate DMSO exchange at cationic alkyl platinum centers. For $[(N\text{-}N)Pt(CH_3)(DMSO)]^{+}$ complexes (N-N = a *bis*(nitrogen donor)) in acetone-d_6 solution second order rate constants range from [(9.49 ± 0.05) x 10^{-6} $\underline{M}^{-1}s^{-1}$] for (N-N) = tetramethylethylenediamine to [0.920 $\underline{M}^{-1}$ s^{-1}] for (N-N) = 1,4-dicyclohexyl-1,4-diazabutadiene.[18,19] Romeo's findings can serve as a basis for comparison, in attempting to quantify the

extent to which these new pyridinium-derived N-heterocyclic carbene ligands accelerate ligand substitution.

Langford and Gray[20] and others[21] have suggested that strong s-bonding between a ligand and the platinum 6s and 5p orbitals limits the availability of those metal-based orbitals for interacting with the *trans*-ligand, thus weakening its bonding interaction, a phenomenon termed "*trans*-influence." Experimentally, stronger s-donation results in greater *trans*-influence, with carbon and hydride donors being among the strongest.[21]

π-Bonding, on the other hand, generally exerts its greatest influence in the transition state structure, with ligands of greater π-acid character accelerating associative ligand substitution.[21] The importance of this π-bonding to the relative energies of similar trigonal bipyramidal structures can be understood by examining the equatorial orbital interactions. A qualitative diagram of the frontier orbitals of the square planar ground state and trigonal bipyramidal transition state on an associative substitution pathway is shown in Figure 4. In this representation π-acceptors lower the transition state energy, while strong σ-donors raise it.

Figure 4

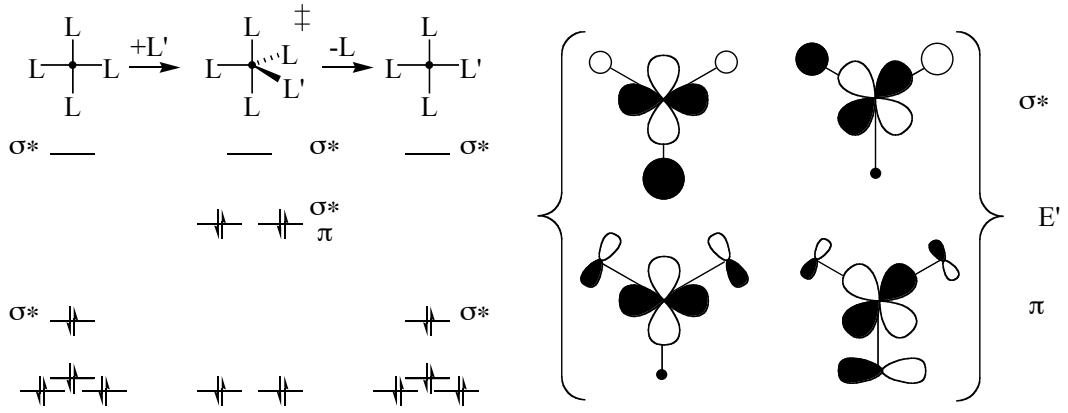

Relative ligand *trans*-influence can be measured by examining the bond lengths of the ligand trans to the N-heterocyclic carbene ligand.[21] Thus, any differences in the platinum–sulfur bond lengths among the series **2c** – **6c** should allow an assessment of relative ground-state energies on the associative substitution reaction profile. X-ray crystal structures of the DMSO cations **2c** - **4c, 6c** show very similar platinum–sulfur distances (Table 1), whose average of 2.274 Å is significantly longer (by about 0.08 Å) than the Pt-S distance (2.1961(11) Å) for the bipy complex **5c**. This indicates, as expected, a substantially greater *trans*-influence for ligands having a Pt-C bond (**2c** - **4c, 6c**) as compared with a Pt-N bond. The similarity between the platinum-sulfur distances in **2c** - **4c** and **6c** is important and suggests that formally neutral N-heterocyclic carbene and anionic sp^2-hybridized phenyl carbon donors have a similar *trans*-influence.[22] This property is maintained despite the lower basicity of a carbene carbon, and is likely the result of the π-acceptor character and greater bond order documented above. However, this is not reflected in the substitution rates: that for **6c** is 1-3 orders of magnitude lower than those for the carbene complexes.[23]

We conclude, therefore, that the large acceleration of ligand substitution for **1c** - **4c** compared to **6c**, is primarily due to stabilization of the transition state energies. This result can be rationalized using the orbital diagram shown above in Figure 4, where both π-acceptors and weaker σ-donors stabilize the transition structure. The trend in the associative DMSO substitution rates (**1c** > **2c** > **4c** > **3c**) parallels the relative ground state π-acidities for the N-heterocyclic carbene ligands.

The distinctive σ-donating/π-accepting characteristics of carbene-donor ligands are undoubtedly quite relevant to their increasing role in homogeneous catalysis. Structural, spectroscopic and kinetics evidence cited here indicates that it is an augmentation of π-accepting capability that distinguishes the pyridine-2-ylidene donors from their formally anionic phenyl analogs, and make them particularly well suited for accelerating associative ligand substitution. We are currently working on exploiting this property for enhancing C-H activation and related chemistry.

Experimental

General Methods. All air and/or moisture sensitive compounds were manipulated using standard Schlenk techniques or in a glove box under a nitrogen atmosphere, as described previously.[24] 4-*tert*-butylpyridine, 4-dimethylaminopyridine, and pyridine were purchased from Aldrich, distilled from CaH_2 and stored under argon. 2-phenylpyridine, 2,2′-bipyridyl, and sodium tetraphenylborate were purchased from Aldrich and used as received. 3-dimethylaminopyridine[25], 2-pyridyl triflate[26], and $[(\mu\text{-}SMe_2)Pt(CH_3)_2]_2$[27] were prepared as described previously. $C_2D_2Cl_4$ and acetone-d_6 were purchased from Cambridge Isotope Laboratories, distilled from CaH_2 and $CaSO_4$, respectively, and stored under argon. Dimethylsulfoxide used in kinetic experiments was passed through an activated alumina column and stored under argon. NMR spectra were recorded on a Varian ^{UNITY}INOVA 500 (499.853 MHz for ^{1}H) spectrometer.

Table 6. Crystal[a] and refinement data for complexes **1b, 2c-4c, 5, 6**.

	1b $[BPh_4]^-$	**2c $[OTf]^-$**	**3c $[BPh_4]^-$**
Empirical formula	$[C_{13}H_{17}N_2SPt]^+$ $[B(C_6H_5)_4]^- \cdot (C_3H_6O)$	$[C_{17}H_{22}N_2OSPt]^+$ $[SO_3CF_3]^- \cdot (C_6H_6)$	$[C_{15}H_{22}BN_3OSPt]^+$ $[B(C_6H_5)_4]^-$
a, Å	11.0611(6)	21.8153(11)	11.0499(4)
b, Å	13.0966(7)	10.4419(5)	11.3835(4)
c, Å	14.2868(7)	22.0778(11)	14.9527(6)
α, deg	114.0150(10)		67.7790(10)
b, deg	91.9270(10)		74.5460(10)
γ, deg	111.0610(10)		88.1200(10)
Volume, Å^3	1724.46(16)	5029.2(4)	1673.33(11)
Z	2	8	2
Crystal system	Triclinic	Orthorhombic	Triclinic
Space group	P-1	Pbcn	P-1
d_{calc}, g/cm^3	1.552	1.811	1.601
θ range, deg	1.60 to 28.30	1.84 to 28.42	1.53 to 28.35
μ, mm^{-1}	4.163	4.291	4.291
Abs. Correction	None	None	None
GOF	1.215	1.86	1.365
R_1,[b] wR_2[c] [I>2σ(I)]	0.0244, 0.0509	0.0496, 0.0806	0.0203, 0.0470
	4c $[BPh_4]^-$	**5c $[BPh_4]^-$**	**6c**
Empirical formula	$[C_{15}H_{22}N_3OSPt]^+$ $[B(C_6H_5)_4]^- \cdot (C_3H_6O)$	$[C_{13}H_{17}N_2OPtS]^+$ $[B(C_6H_5)_4]^- \cdot (C_3H_6O)$	$C_{14}H_{17}NOSPt$
a, Å	11.1872(6)	23.0688(8)	10.3677(9)
b, Å	15.3712(8)	13.1532(5)	14.9165(13)
c, Å	20.8806(10)	23.9873(9)	17.3745(15)
α, deg			
β, deg	90.4650(10)	115.5560(10)	
γ, deg			
Volume, Å^3	3590.5(3)	6566.3(4)	2687.0(4)
Z	4	8	8
Crystal system	Monoclinic	Monoclinic	Orthorhombic
Space group	$P2_1$	$P2_1/c$	Pbca
d_{calc}, g/cm^3	1.546	1.604	2.187
θ range, deg	1.65 to 28.39	1.71 to 28.60	2.34 to 28.49
μ, mm^{-1}	4.004	4.373	10.586
Abs. Correction	None	Face-indexed Gaussian	Face-indexed Gaussian
GOF	1.074	1.29	1.272
R_1,[b] wR_2[c] [I>2σ(I)]	0.0343, 0.0601	0.0359, 0.0538	0.0235, 0.0364

[a] 98(2) K. [b] $R_1 = \sum||F_o| - |F_c||/\sum|F_o|$. [c] $wR_2 = [\sum[w(F_o^2-F_c^2)^2]/\sum[w(F_o^2)^2]]^{1/2}$.

Magnetization Transfer Experiments and Line Shape Analysis Experiments.

Both types of experiments were carried out in J. Young nmr tubes under 1 atmosphere of argon. Solutions were prepared in 1.0 mL volumetric flasks. Reaction temperatures were determined by measuring the peak separation of an ethylene glycol or methanol standard before and after the experiment at each temperature.

Magnetization transfer experiments were conducted at 25 ˚C by inversion of the signal for free DMSO using a selective DANTE inversion sequence.[28] Relaxation times (T_1) for the resonances of interest were measured before the magnetization transfer experiment using the inversion recovery method. Signals for free and bound DMSO were integrated at delay times t and fit to a two-site exchange model using the program CIFIT. (Figure 5). Pseudo-first-order rate constants obtained from these fits were plotted versus DMSO concentration. All plots showed a linear dependence on DMSO concentration and a zero intercept within experimental error (Figure 6).

Variable temperature line shape data for complexes **1c** and **2c** were recorded in 10-degree increments from the static spectrum (-40 ˚C) until the boiling point of the solvent or temperature limitation of the NMR probe (<100 ˚C). In all cases a coalescence point was reached. Line broadening of the platinum bound DMSO was used to calculate first order rate constants in the slow exchange region according to equation (1).[29] The temperature dependence of the ^{195}Pt satellites of the platinum- bound DMSO signal introduces error in the

$$k_{obs}{}^{t} = 1/\tau_t = \pi(w_t{}^{1/2} - w_o{}^{1/2}) \qquad (1)$$

measured line widths at half height ($w_t^{1/2}$). Spectra with significant contributions to the width at half height from the platinum satellites were discarded in the Eyring analysis. Eyring plots of these pseudo-first order rate constants (Figure 7) provided a method of determining pseudo-first order rate constants at 298K (k_{obs}^{298}). These rate constants were plotted *versus* DMSO to determine rate constants for the DMSO dependent (k_2) and independent (k_i) substitution paths.

Figure 5. Magnetization transfer data for **(4c)** at 298K in CD_2Cl_4[a].

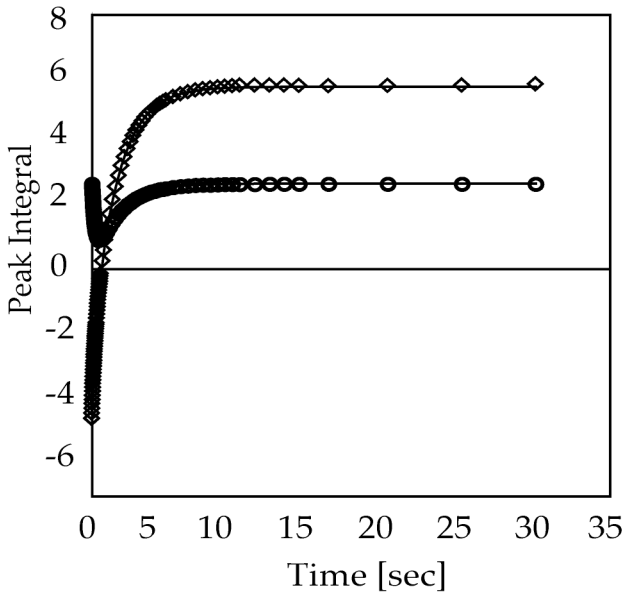

[a] (o) Bound DMSO. (◊) Free DMSO. (–) The best fit line from a two-site exchange model. $k_{obs} = 2.16\ s^{-1}$; $k_2 = 27.9\ \underline{M}^{-1}s^{-1}$

Figure 6. k_{obs} versus [DMSO] for (**4c**) at 298 K in $C_2D_2Cl_4$[a].

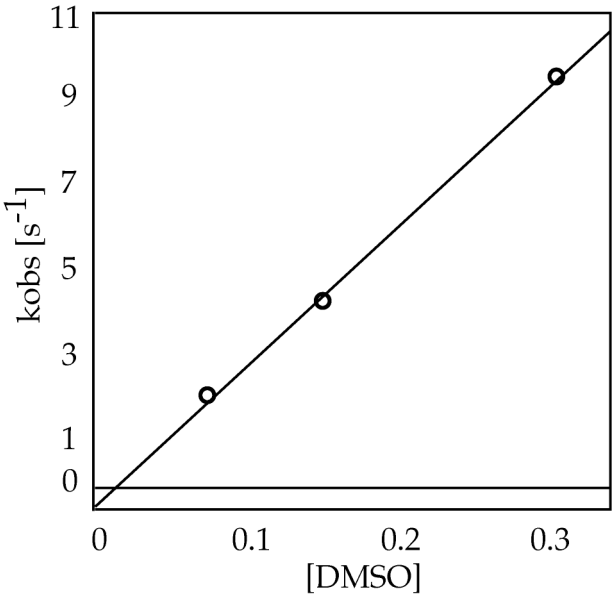

[a] $k_2 = 27.9\ \underline{M}^{-1}s^{-1}$

Figure 7. Eyring plot for (**1c**) in Acetone-*d6* from 255 - 313 K.[a,b]

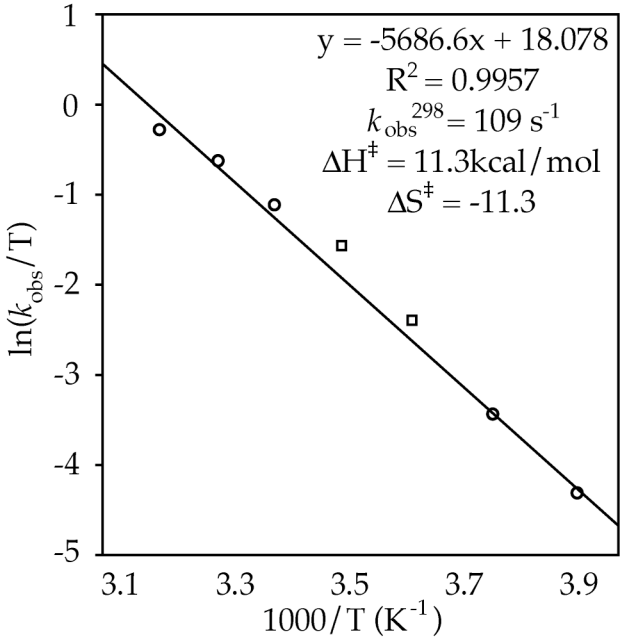

[a] The value for k_2 was calculated from the linear best-fit at 298 K. [b] (o) k_{obs}^{T}, (□) Data points excluded due error from ^{195}Pt satellites.

Pyridinium Salts. All pyridinium triflate salts were prepared by a procedure analogous to the one detailed for **2a** below, with exceptions noted.

N-(2-pyridyl)-4-*tert*-butylpyridinium triflate. (**2a**) 2-Pyridyl triflate (7.33 g, 32.3 mmol) and 4-*tert*-butylpyridine (8.73 g, 64.5 mmol) were combined under argon in a Teflon-stoppered Schlenk tube equipped with a stir bar. The solution was degassed, sealed under vacuum and heated to 140 ˚C. After stirring overnight (~12 hr) the colorless solution turned black and upon cooling partially solidified. Dissolving the mixture in CH_2Cl_2 and addition of diethyl ether precipitated a dark purple solid that was isolated on a glass frit. Several recrystallizations from hot ethyl acetate provided 6.88 g (59%) of **2a** as purple crystals. ^{1}H NMR (300 MHz, $CDCl_3$): δ = 1.47 (s, 9H, $C(CH_3)_3$), 7.64 (dd, 1H, ^3J = 7.7 Hz, ^3J = 4.9 Hz), 8.15 (ddd, 1H, ^3J = 8.1 Hz, ^3J = 8.1 Hz, ^4J = 1.6 Hz), 8.24 (d, 2H, ^3J = 7.1 Hz), 8.20 (d, 1H, ^3J = 8.2 Hz), 8.65 (dd, 1H, ^3J = 2.8 Hz, ^4J = 1.6 Hz), 9.58 (d, 2H, ^3J = 7.1 Hz); ^{13}C{^{1}H] NMR (75 MHz, $CDCl_3$): δ = 24.3, 32.4, 122.1, 131.5, 132.7, 148.78, 148.79, 148.9, 158.2, 185.8; Anal. Calcd for $C_{15}H_{17}F_3N_2O_3S$: C, 49.72; H, 4.73; N, 7.73. Found: C, 49.65; H, 4.66; N, 7.66.

N-(2-pyridyl)-pyridinium triflate (**1a**). 2-Pyridyl triflate (7.33 g, 32.3 mmol) and pyridine (10.21g, 129.1 mmol) were stirred for 18 hr at 140 ˚C. The crude material was recrystallized from $CHCl_3$ and diethyl ether. 1.942 g (20%) of **1a** as pink plates were obtained. ^{1}H NMR (300 MHz, CD_2Cl_2): δ = 7.71 Hz (dd, 1H, ^3J = 7.7 Hz, ^3J = 4.9 Hz), 8.23 (ddd, 1H, ^3J = 8.2 Hz, ^3J = 8.2 Hz, ^4J = 1.6 Hz), 8.35 (t, 2H, ^3J = 7.7 Hz), 8.51 (d, 1H, ^3J = 8.2 Hz), 8.68-8.75 (m, 2H), 9.74 (d, 2H, ^3J = 6.0

Hz); $^{13}C\{^{1}H]$ NMR (75 MHz, CD_2Cl_2): δ = 118.0, 127.7, 129.2, 141.8, 142.5 (br, 2C), 148.4, 150.3; Anal. Calcd for $C_{11}H_9F_3N_2O_3S$: C, 43.14; H, 2.96; N, 9.15. Found: C, 43.35; H, 2.99; N, 9.02.

N-(2-pyridyl)-4-dimethylamino-pyridinium triflate (**3a**). 2-Pyridyl triflate (2.932 g, 12.9 mmol) and 4-dimethylaminopyridine (3.154 g, 25.8 mmol) were stirred 5 hr at 150 ˚C. The crude material was recrystallized from ethanol and diethyl ether giving **3a** as a high yield of pink plates. ^{1}H NMR (300 MHz, $CDCl_3$): δ = 3.36, 8.23 (ddd, 1H, ^{3}J = 8.2 Hz, ^{3}J = 8.2 Hz, ^{4}J = 1.6 Hz), 7.14 (d, 2H, ^{3}J = 8.2), 7.45 (ddd, 1H, ^{3}J = 7.1 Hz, ^{3}J = 4.9 Hz, ^{4}J = 1.1 Hz), 7.92 (d, 1H, ^{3}J = 8.2 Hz), 8.02 (ddd, 1H, ^{3}J = 6.9 Hz, ^{3}J = 6.9 Hz, ^{4}J = 1.9 Hz), 8.53 (d, 2H, ^{3}J = 4.8 Hz), 8.91 (d, 2H, ^{3}J = 7.7 Hz); $^{13}C\{^{1}H]$ NMR (125 MHz, $CDCl_3$): δ = 40.7, 108.4, 114.6, 124.7, 138.3, 140.6, 149.2, 150.5, 157.3; Anal. Calcd for $C_{13}H_{14}F_3N_3O_3S$: C, 44.70; H, 4.04; N, 12.03. Found: C, 44.63; H, 4.01; N, 11.97.

N-(2-pyridyl)-5-dimethylamino-pyridinium triflate (**4a**). 2-Pyridyl triflate (4.279, 18.8 mmol) and 3-dimethylaminopyridine (2.303 g, 18.8 mmol) were heated to 140 ˚C overnight. Addition of diethyl ether to a CH_2Cl_2 solution of the crude product caused a black oil to separate. Decanting the solvent and removing the volatiles *in vacuo* provided a dark brown solid that was recrystallized from CH_2Cl_2 and diethyl ether to give 3.444 g (52%) of **4a** as very dark yellow crystals. ^{1}H NMR (300 MHz, $CDCl_3$): δ = 3.23 (s, 6H, $N(CH_3)_2$), 7.64 (dd, 1H, ^{3}J = 7.7 Hz, ^{3}J = 4.7 Hz), 7.79 (dd, 1H, ^{3}J = 9.1 Hz, ^{3}J = 3.0 Hz), 7.95 (dd, 1H, ^{3}J = 8.8 Hz, ^{3}J = 6.0 Hz,), 8.17 (ddd, 1H, ^{3}J = 6.3 Hz, ^{3}J = 6.3 Hz, ^{4}J = 1.7 Hz),

8.31 (d, 1H, ^3J = 8.2 Hz), 8.57 (m, 1H), 8.63 (dd, 1H, ^3J = 2.8 Hz, ^4J = 1.7 Hz), 8.69 (d, 1H, ^3J = 6.0 Hz); $^{13}C\{^1H]$ NMR (75 MHz, $CDCl_3$): δ = 40.5, 100.1, 118.3, 123.9, 127.0, 127.5, 128.1, 128.4, 141.5, 148.7, 149.5; Anal. Calcd for $C_{13}H_{14}F_3N_3O_3S$: C, 44.70; H, 4.04; N, 12.03. Found: C, 44.57; H, 4.02; N, 11.93.

Cylclometalation of the pyridinum salts 1a-4a. All of the carbene complexes were prepared and purified according to the procedure described for **1b** below. Complex **3b** was only prepared *in situ* and was immediately converted to **3d**, and isolated as a carbonyl cation.

[(*iso*-BIPY)Pt(CH$_3$)(DMS)]$^+$ [OTF]$^-$ (1b). [(μ-SMe_2)Pt(CH_3)$_2$]$_2$ (0.984 g, 1.71 mmol) was added, in one portion, to a solution of N-(2-pyridyl)-pyridinium triflate (**1a**) (1.049g 3.43 mmol) in 50 mL of methylene chloride under argon purge. Evolution of methane was immediately observed upon mixing, and the solution quickly became a yellow orange color. After stirring for 1 hour a small amount of diethyl ether was slowly added to precipitate a dark solid. After stirring for 30 minutes the solution was cannula-filtered to remove the dark solids and the filtrate concentrated. Addition of diethyl ether precipitated a mustard colored powder which was isolated on a glass frit and dried under vacuum. Yield 1.887 g (95%). ^1H NMR (500 MHz, acetone-d_6) δ = 1.17 (s, 3H, $^2J_{Pt-H}$ = 82.04 Hz, Pt-CH_3), 2.60 (br s, 6H, $^3J_{Pt-H}$ = ~28 Hz S(CH_3)$_2$), 7.88 (ddd, 1H, ^3J = 6.9 Hz, ^3J = 6.9 Hz, ^4J = 1.4 Hz), 8.03 (ddd, 1H, ^3J = 5.5 Hz, ^3J = 5.5 Hz, ^4J = 0.9 Hz), 8.22-8.42 (m, 2H), 8.63 (ddd, 1H, ^3J = 7.3 Hz, ^3J = 7.3 Hz, ^4J = 1.4 Hz), 8.7 (d, 1H, ^3J = 8.4 Hz), 9.22 (br d, 1H ^3J = 5.06 Hz), 9.6 (br d, 1H ^3J = 6.14 Hz); $^{13}C\{^1H]$ NMR

(125 MHz, acetone-d_6): δ = -9.40 (^1JPt-C = 792.2, Pt-CH_3), 20.39, 116.8, 122.5, 128.8, 133.9 (JPt-C = 113.8 Hz), 140.5 (JPt-C = 34.7 Hz), 143.2, 144.42 (JPt-C = 53.7 Hz), 147.8, 157.0, 176.1 (^1JPt-C = 1317.1 Hz, Pt-C_{car}); Anal. Calcd for $C_{14}H_{17}F_3N_2O_3PtS_2$: C,29.12; H, 2.97; N, 4.85. Found: C, 29.05; H, 2.88; N, 4.77.

[(4-*tert*-butyl-*iso*-BIPY)Pt(CH_3)(DMS)]$^+$ [OTF]$^-$ (2b). [(μ-SMe_2)Pt(CH_3)$_2$]$_2$ (0.954 g, 1.66 mmol) and N-(2-pyridyl)-4-*tert*-butyl-pyridinium triflate (**2a**) (1.203 g, 3.32 mmol) were allowed to react to yield 1.904 g (94%) of **2b** as a yellow powder. ^{1}H NMR (300 MHz, CD_2Cl_2) δ = 1.22 (s, 3H, ^{2}JPt-H = 81.3 Hz Pt-CH_3), 1.44 (s, 9H), 2.52 (br s, 6H, ^{3}JPt-H = ~32 Hz, S(CH_3)$_2$), 7.75-7.81 (m, 2H), 8.28 (d, 1H, ^4J = 2.2 Hz, ^{3}JPt-H = 54.9 Hz), 8.46 (ddd, 1H, ^3J = 7.1 Hz, ^3J = 7.1 Hz, ^4J = 1.7 Hz), 8.63 (d, 1H, ^3J = 8.2 Hz), 9.09 (dd, 1H, ^3J = 5.5 Hz, ^3J = 1.1 Hz, ^{3}JPt-H = 7.1 Hz), 9.43 (d, 1H, ^3J = 7.7 Hz); ^{13}C{^{1}H} NMR (125 MHz, CD_2Cl_2): δ = -9.31 (^1JPt-C = 791.8 Hz, Pt-CH_3), 20.77, 30.14, 37.08, 116.2, 120.5, 127.6, 129.9 (JPt-C = 120.8 Hz), 138.7 (JPt-C = 39.5 Hz), 142.8, 146.7, 156.3 (JPt-C = 49.6 Hz), 169.0 (JPt-C = 49.6 Hz), 179.2 (^1JPt-C = 1321.6 Hz, Pt-C_{car}); Anal. Calcd for $C_{18}H_{25}F_3N_2O_3PtS_2$: C, 33.28; H, 3.88; N, 4.31. Found: C, 34.03; H, 4.08; N, 4.16.

[(5-dimethylamino-*iso*-BIPY)Pt(CH_3)(DMS)]$^+$ [OTF]$^-$ (4b). (μ-SMe_2)Pt(CH_3)$_2$]$_2$ (0.758 g, 1.318 mmol) and N-(2-pyridyl)-3-dimethylamino-pyridinium triflate (**4a**) (0.921 g 2.64 mmol) were allowed to react to yield 1.176 g (72%) of **4b** as a yellow powder. ^{1}H NMR (300 MHz, CD_2Cl_2) δ = 1.15 (s, 3H, ^{2}JPt-H = 80.85 Hz, Pt-CH_3), 2.51 (s, 6H, ^{3}JPt-H = 31.5 Hz, S(CH_3)$_2$), 3.14 (s, 6H, NMe_2), 7.53 (dd, 1H, ^3J = 9.3 Hz, ^4J = 2.8Hz, JPt-C = 6.0 Hz), 7.76 (ddd, 1H, ^3J = 5.5 Hz, ^3J =

5.5 Hz, ^4J = 1.1 Hz), 8.06 (d, 1H, ^3J = 9.3 Hz, J_{Pt-H} = 23.6 Hz), 8.40 (d, 1H, ^3J = 2.75 Hz, J_{Pt-H} = 4.2 Hz), 8.51 (ddd, 1H, ^3J = 7.7 Hz, ^3J = 7.7 Hz, ^4J = 1.6 Hz), 8.67 (d, 1H ^3J = 8.24 Hz), 9.07 (dd, 1H ^3J = 6.04 Hz, ^4J = 1.1 Hz); $^{13}C\{^1H\}$ NMR (125 MHz, CD_2Cl_2): δ = -10.31 ($^1J_{Pt-C}$ = 789.2 Hz, Pt-CH_3), 20.77, 40.5, 116.8 (J_{Pt-C} = 13.6 Hz), 120.3 (J_{Pt-C} = 40.1 Hz), 127.7, 128.8 (J_{Pt-C} = 117.5 Hz), 132.5 (J_{Pt-C} = 117.5 Hz), 142.4, 145.5, 146.2, 156.7 (J_{Pt-C} = 51.2 Hz), 176.1 ($^1J_{Pt-C}$ = 1323.3 Hz, Pt-C_{car}); Anal. Calcd for $C_{16}H_{22}F_3N_3O_3PtS_2$: C,30.97; H, 3.57; N, 6.77. Found: C, 30.92; H, 3.54; N, 6.58.

Substitution of dimethylsulfide by dimethylsulfoxide. The dimethylsulfide complex is mixed with sufficient DMSO (~20 eq) to fully dissolve the sample, and is left stirring under vacuum for 1 hr. The residue is then dissolved in a small amount of dichloromethane under argon, and the product precipitated with diethyl ether, filtered and dried under vacuum.

[(*iso*-BIPY)Pt(CH_3)(DMSO)]$^+$ [OTf]$^-$ (**1c**). The reaction was carried out according to the above procedure. [(*iso*-BIPY)Pt(CH_3)(DMS)]$^+$[OTf]$^-$ (**1b**) (0.257 g, 0.445 mmol), DMSO (0.63 mL , 8.9 mmol, 20 eq); yield 93%. ^{1}H NMR (300 MHz, $CDCl_3$) δ = 0.89 (s, 3H, $^2J_{Pt-H}$ = 80.2 Hz, Pt-CH_3), 3.34 (br s, 6H, $^3J_{Pt-H}$ = 21.1 Hz, S(CH_3)$_2$), 7.74 (at, 1H, ^3J = 6.2 Hz), 7.98 (at, 1H, ^3J = 6.2 Hz), 8.10 (at, 1H, ^3J = 7.51 Hz), 8.25 (d, 1H, ^3J = 8.0 Hz, J_{Pt-H} = 23.9 Hz), 8.48 (at, 1H, ^3J = 7.73 Hz), 9.01 (d, 1H, ^3J = 8.7 Hz), 9.85 (d, 1H ^3J = 5.55 Hz), 10.03 (d, 1H ^3J = 5.55 Hz); $^{13}C\{^1H]$ NMR (125 MHz, acetone-d_6): δ = -11.20 ($^1J_{Pt-C}$ = 757.8 Hz, Pt-CH_3), -43.15 (Pt-OS(CH_3)$_2$),

116.1, 123.3, 127.6, 133.4, 140.2 , 143.0, 144.1, 150.8, 156.4, 174.0; Anal. Calcd for $C_{14}H_{17}F_3N_2O_4PtS_2$: C,28.33; H, 2.89; N, 4.72. Found: C, 28.07; H, 2.81; N, 4.58.

[(4-*tert*-butyl-*iso*-BIPY)Pt(CH_3)(DMSO)]$^+$ [OTf]$^-$ (**2c**). The reaction was carried out according to a procedure similar to the above. [(*tert*-butyl-*iso*-BIPY)Pt(CH_3)(DMS)]$^+$[OTf]$^-$ (**2b**) (0.122 g, 0.199 mmol), DMSO (0.30 mL , 3.98 mmol, 20 eq); yield 107 mg (86%). ^{1}H NMR (300 MHz, CD_2Cl_2) δ = 0.90 (s, 3H, $^2J_{Pt\text{-}H}$ = 80.4 Hz, Pt-CH_3), 1.44 (s, 3H, *tert*-Bu), 3.30 (s, 6H, $^3J_{Pt\text{-}H}$ = 21.2 Hz, OS$(CH_3)_2$), 7.74 (at, 1H, ^3J = 6.8 Hz), 7.87 (dd, 1H, ^3J = 7.1 Hz, ^4J = 2.2 Hz), 8.25 (d, 1H, ^3J = 2.3 Hz, $J_{Pt\text{-}H}$ = 26.1 Hz), 8.43 (ddd, 1H, ^3J = 7.7 Hz, ^3J = 7.7 Hz, ^2J = 1.8 Hz), 8.68 (d, 1H, ^3J = 8.6 Hz), 9.87 (d, 1H, ^3J = 7.0 Hz), 9.88 (dd, 1H, ^3J = 5.8 Hz, ^4J = 1.4 Hz); ^{13}C{^{1}H] NMR (125 MHz, CD_2Cl_2): δ = -10.2 ($^1J_{Pt\text{-}C}$ = 757.4 Hz, Pt-CH_3), 30.2, 37.2, 44.3 (-43.15, $^1J_{Pt\text{-}C}$ = 44.5 Hz, (Pt-OS$(CH_3)_2$), 116.1, 121.5 ($^1J_{F\text{-}C}$ = 321.9 Hz, $F_3CSO_3^-$) 121.9, 127.4, 130.1 ($J_{Pt\text{-}C}$ = 112.4 Hz), 139.2 ($J_{Pt\text{-}C}$ = 35.4 Hz) , 143.3, 151.2, 156.1 ($J_{Pt\text{-}C}$ = 47.7 Hz), 169.6($J_{Pt\text{-}C}$ = 47.7 Hz), 172.2 ($^1J_{Pt\text{-}C}$ = 1231.2 Hz, Pt-C); Anal. Calcd for $C_{18}H_{25}F_3N_2O_4PtS_2$: C, 33.28; H, 3.88; N, 4.31. Found: C, 34.03; H, 4.08; N, 4.16.

[(5-dimethylamino-*iso*-BIPY)Pt(CH_3)(DMSO)]$^+$ [OTF]$^-$ (**4c**). The reaction was carried out according to the above procedure to yield 1.176 g (72%) of **4c** as an orange powder. ^{1}H NMR (300 MHz, CD_2Cl_2) δ = 1.15 (s, 3H, $^2J_{Pt\text{-}H}$ = 81.0 Hz, Pt-CH_3), 2.51 (s, 6H, $^3J_{Pt\text{-}H}$ = 31.7 Hz, OS$(CH_3)_2$), 3.14 (s, 6H, N$(CH_3)_2$), 7.53 (dd, 1H, ^3J = 9.3 Hz, ^4J = 2.8 Hz, $J_{Pt\text{-}C}$ = 6.4 Hz), 7.76 (ddd, 1H, ^3J = 5.5 Hz, ^3J = 5.5 Hz, ^4J = 1.1 Hz), 8.06 (d, 1H, ^3J = 9.3 Hz, $J_{Pt\text{-}C}$ = 24.0 Hz), 8.40 (d, 1H, ^3J = 2.8 Hz, $J_{Pt\text{-}C}$ =

4.3 Hz), 8.51 (ddd, 1H, ^3J = 7.7 Hz, ^3J = 7.7 Hz, ^4J = 1.6 Hz), 8.67 (d, 1H ^3J = 8.7 Hz), 9.07 (dd, 1H ^3J = 5.5 Hz, ^4J = 1.1 Hz, JPt-C = 7.3 Hz); $^{13}C\{^1H\}$ NMR (125 MHz, CD_2Cl_2): δ = -10.31 (^1JPt-C = 789.2, Pt-CH_3), 20.77, 40.5, 116.8 (JPt-C = 13.9 Hz), 120.3 (JPt-C = 39.8 Hz), 127.7 (JPt-C = 9.0 Hz), 128.8 (JPt-C = 117.5 Hz), 132.8 (JPt-C = 117.5 Hz), 142.7, 145.9, 146.6, 157.0 (JPt-C = 51.2 Hz), 160.94 (^1JPt-C = 1323.3 Hz, Pt-C_{car}); Anal. Calcd for $C_{16}H_{22}F_3N_3O_4PtS_2$: C, 30.19; H, 3.48; N, 6.60. Found: C, 30.35; H, 3.47; N, 6.62.

Substitution of tetraphenylborate for triflate. The triflate salts were dissolved in a small amount of methanol, and a concentrated solution of sodium tetraphenylborate (1 eq) was added dropwise, immediately precipitating the product. Cooling to –40 ˚C in the freezer and isolation on a glass frit gave >90% yield of the tetraphenylborate salts. A representative preparation is shown below.

[(5-dimethylamino-*iso*-BIPY)Pt(CH_3)(DMSO)]$^+$ [BPh_4]$^-$ (4c). A few drops of DMSO were added to complex (**4b)** (0.400g, 0.644mmol) to dissolve it. After stirring the dark liquid under vacuum for 30 min. methanol (15 ml) was added. A solution of sodium tetraphenylborate (0.221g, 0.644mmol) in methanol (20, ml) was added dropwise with stirring to the orange solution. An orange precipitate formed upon addition. The mixture was filtered and the orange powder washed with diethylether and dried under vacuum. 0.467g (yield = 90%). ^{1}H NMR (500 MHz, CD_2Cl_2) δ = 0.878 (s, 3H, ^{2}JPt-H = 80.32 Hz, Pt-CH_3), 3.03 (s, 6H, NMe_2), 3.26 (s, 6H, ^{3}JPt-H = 20.9 Hz, S(CH_3)$_2$), 6.86 (at, 4H, ^3J = 7.33 Hz), 7.02 (at, 8H, ^3J = 7.33 Hz), 7.35 (bs, 8H), 7.45 (d, 1H, ^3J = 8.64 Hz), 7.49 (dd, 1H, ^3J = 9.25 Hz, ^4J = 2.75

Hz), 7.63 (at, 1H, ^3J = 6.2 Hz), 7.73 (d, 1H, ^3J = 2.57 Hz), 7.99 (at, 1H, ^3J = 8.44 Hz), 8.03 (d, 1H, ^3J = 9.18 Hz), 9.90 (dd, 1H ^3J = 5.60 Hz, ^4J = 1.65 Hz); $^{13}C\{^1H\}$ NMR (125 MHz, CD_2Cl_2) δ = -11.12 ($^1J_{Pt\text{-}C}$ = 788.8 Hz, Pt-CH_3), 39.96, 43.92, 114.6, 118.76 ($J_{Pt\text{-}C}$ = 40.92 Hz), 122.0, 125.9, 127.2, 128.1 ($J_{Pt\text{-}C}$ = 51.1 Hz), 133.3 ($J_{Pt\text{-}C}$ = 110.0 Hz), 136.1, 142.5, 146.0, 146.2, 151.0, 156.0, 159.0, 164.2 ($^1J_{B\text{-}C}$ = 49.2 Hz); Anal. Calcd for $C_{39}H_{42}BN_3OPtS$: C, 58.06; H, 5.25; N, 5.21. Found: C, 57.79; H, 5.40; N, 5.11.

(4-dimethylamino-*iso*-BIPY)Pt(CH_3)Br (**3f**). [(μ-SMe_2)Pt(CH_3)$_2$]$_2$ (0.6920 g, 1.20 mmol) was dissolved in 225 mL of methylene chloride to which was added N-(2-pyridyl)-4-dimethylamino-pyridinium bromide (**3e**) (0.6749 g, 2.41 mmol). Upon stirring the solution became yellow, and methane evolved. The reagents were left stirring for 8 hr, and a crystalline yellow powder slowly precipitated from the solution. The volume was concentrated to 5 mL , and the solids isolated on a glass frit to give 0.660 g (56%) of **3f** as a bright yellow powder. Further concentration of the filtrate provided additional material. ^1H NMR (300 MHz, CD_3NO_2) δ = 0.91 (s, 3H, $^3J_{Pt\text{-}H}$ = 83.79 Hz, Pt-CH_3), 3.16 (s, 6H, N(CH_3)$_2$), 6.72 (dd, 1H, ^3J = 8.19 Hz, ^3J = 3.11 Hz), 7.04 (d, 1H, $^3J_{Pt\text{-}H}$ = 70.18 Hz ^3J = 3.27 Hz), 7.39 (m, 1H), 7.67 (d, 1H, ^3J = 8.96 Hz), 8.12 (m, 1H), 8.33 (d, 1H, ^3J = 8.04 Hz, $^3J_{Pt\text{-}H}$ = 6.42 Hz), 9.61 (dd, 1H ^3J = 5.51 Hz, ^4J = 1.60 Hz, $^3J_{Pt\text{-}H}$ = 6.63 Hz); Anal. Calcd for $C_{13}H_{16}BrN_3Pt$: C, 31.91; H, 3.30; N, 8.59. Found: C, 38.43; H, 4.49; N, 10.11.

[(4-dimethylamino-*iso*-BIPY)Pt(CH_3)(DMSO)]$^+$ [BPh_4]$^-$ (**3c**). N-(2-pyridyl)-4-dimethylamino-pyridine-2-ylidene platinum methyl bromide (**3f**) (0.2400 g, 0.491 mmol), sodium tetraphenylborate (0.1679 g, 0.491 mmol) and

dimethylsulfoxide (105 μl, 1.484 mmol) were mixed with 250 mL of methylene chloride and left stirring overnight. In the morning the bright yellow solution had turned nearly colorless, and a white precipitate had formed. The mixture was filtered through Celite, and the volume concentrated to a total of 10 mL. Diethylether was slowly added to give a white precipitate. The suspension was placed in a –20˚C freezer, and the white solids were isolated on a glass frit, washed with diethyl ether, and dried under high vacuum to give 0.365 g (92%) of **3c** as an off-white powder. ^{1}H NMR (300 MHz, CD_2Cl_2) δ = 0.70 (s, 3H, $^{2}J_{Pt\text{-}H}$ = 80.79 Hz Pt-CH_3), 3.09 (s, 3H, NCH_3), 3.21 (s, 3H, NCH_3), 3.21 (s, 6H, $^{2}J_{Pt\text{-}H}$ = 20.20 Hz Pt-S(CH_3)$_2$), 6.18 (dd, 1H, ^{3}J = 8.16 Hz, ^{3}J = 3.22 Hz), 6.83 (m, 5H), 6.94-7.04 (m, 9H), 7.33-7.47 (m, 10H), 7.90 (m, 1H), 9.61 (dd, 1H ^{3}J = 5.72 Hz, ^{4}J = 1.29 Hz, $^{3}J_{Pt\text{-}H}$ = 6.15 Hz); ^{13}C{^{1}H] NMR (125 MHz, CD_2Cl_2) δ = -10.40 ($^{1}J_{Pt\text{-}C}$ = 761.3 Hz, Pt-CH_3), 105.8, 110.4 ($J_{Pt\text{-}C}$ = 118.79 Hz), 113.1, 123.7, 136.7, 141.7, 148.9, 153.8 ($J_{Pt\text{-}C}$ = 60.5 Hz), 155.1, 163.6 ($^{1}J_{Pt\text{-}C}$ = 1202.89 Hz, Pt-C_{car}). Anal. Calcd for $C_{39}H_{42}BN_3OPtS$: C, 58.06; H, 5.25; N, 5.21. Found: C, 57.79; H, 5.40; N, 5.11.

Synthesis of carbonyl cations 1d-4d. The dimethylsulfide complexes **1b-4b** were dissolved in acetone (**1,2,4**) or prepared *in situ* (**3**) and degassed. Carbon monoxide (1 atmosphere) was added and the solutions allowed to stir for one hour. The carbonyl cations were precipitated by addition of diethyl ether and isolated on a glass frit. IR spectra were acquired in acetone. Anal. **2d** Calcd for $C_{17}H_{19}F_3N_2O_4PtS$: C, 34.06; H, 3.19; N, 4.67. Found: C, 33.73; H, 3.12; N, 4.40. **4d** Calcd for $C_{15}H_{16}F_3N_3O_4PtS$: C, 30.72; H, 2.75; N, 7.17. Found: C, 31.02; H, 2.73; N, 6.90.

($C_{11}H_8N$)Pt(CH_3)(DMSO) (**6c**). 2-Phenylpyridine (481 μL, 3.37 mmol) was added dropwise via syringe to a solution of [(μ-SMe_2)Pt(CH_3)$_2$]$_2$ (0.967 g, 1.68 mmol) in 50 mL of acetone at room temperature in air. The solution quickly became yellow, and small bubbles formed. After stirring for 1.5 hr DMSO (477 μL, 6.73 mmol) was added, and the solution stirred for another 30 min. The yellow solution was concentrated, and pentane was added, precipitating the bright yellow product. The suspension was filtered and dried under vacuum giving 0.864 g (58%) of **6c** as a bright yellow solid. ^{1}H NMR (300 MHz, acetone-d_6) δ = 0.66 (s, 3H, $^2J_{Pt-H}$ = 83.52 Hz, Pt-CH_3), 3.21 (s, 6H, $^2J_{Pt-H}$ = 17.6 Hz, S(CH_3)), 7.11 (dt, 1H, ^3J = 7.69 Hz, ^3J = 1.65 Hz), 7.21 (dt, 1H, ^3J = 7.74 Hz, ^3J = 1.65 Hz), 7.31-7.36 (m, 1H), 7.50 (d, 1H, ^3J = 1.1 Hz, $^2J_{Pt-H}$ = 28.6 Hz), 7.34-7.79 (m, 1H), 8.03 (dd, 2H ^3J = 3.85 Hz, ^4J = 1.10 Hz) 9.80 (d, 1H ^3J = 5.60 Hz, $^2J_{Pt-H}$ = 7.1 Hz); ^{13}C{^{1}H] NMR (125 MHz, CD_2Cl_2) δ = -12.4 ($^1J_{Pt-C}$ = 776.1, Pt-CH_3), 43.3 (J_{Pt-C} = 34.6), 118.4, 122.5, 123.3 (J_{Pt-C} = 39.3), 124.8, 129.0 (J_{Pt-C} = 66.7 Hz), 132.5 (J_{Pt-C} = 88.9 Hz), 137.9, 146.6, 150.3, 150.4 (J_{Pt-C} = 1062.8 Hz, Pt-C_{ph}), 164.0 ($^1J_{Pt-C}$ = 74.9 Hz). Anal. Calcd for $C_{14}H_{17}NOPtS$: C, 38.01; H, 3.87; N, 3.17. Found: C, 38.12; H, 3.84; N, 3.15.

References and Notes.

---

1) Herrmann, W. A. *Angew. Chem., Int. Ed. Engl.* **2002**, *41*, 1290-1309.

2) a) Bielawski C. W.; Grubbs, R. H. *Angew.Chem.Int.Ed.*, **2000**, *39*, 2903-2906. b) Scholl, M.; Ding, S.; Lee, C. W.; Grubbs, R. H. *Org. Lett.*, **1999**, *1*, 953-956. c) Chaterjee, A. K.; Morgan, J. P.; Scholl, M.; Grubbs, R. H. *J.Am.Chem.Soc.*, **2000,** *122*, 3783-3784. d) Sanford, M.S.; Ulman, M.; Grubbs, R.H. *J. Am. Chem. Soc.* **2001**, *123*, 749-750. e) Sanford, M.S.; Ulman, M.; Grubbs, R.H. *J. Am. Chem. Soc.* **2001**, *123*, 6543-6554.

3) a) Littke, A.F.; Fu, G.C. *Angew. Chem., Int. Ed. Engl.* **2002**, *41*, 4176-4211. b)

4) Kocher, C.; Herrmann, W. A. *J. Organomet. Chem.* **1997**, *532* 261.

5) a) Green, J.C.; Scurr, R.G.; Arnold, P.L.; Cloke, F.G.N. *J. Chem. Soc, Chem. Comm.* **1997**, 1963. b) Boehme, C.; Frenking, G. *Organometallics* **1998**, *17*, 5801-5809.

6) Gleiter, R.; Hoffmann, R. *J. Am. Chem. Soc.* **1968**, *90*, 5457-5460.

7) a) Zhong, H. A.; Labinger, J. A.; Bercaw, J. E. *J. Am. Chem. Soc.* **2002**, *124*, 1378-1399. b) Ackerman, L. J.; Sadighi, J. P.; Kurtz, D. M.; Labinger, J. A.; Bercaw, J. E. *Organometallics* **2003,** *22*, 3884-3890.

8) A few examples of monodentate pyridin-2-ylidene complexes of platinum and palladium have been prepared by protonation or methylation of the nitrogen of 2-pyridyl complexes. a) Crociani, B.; Di Bianca, F.; Giovenco, A.;

Scrivanti, A. *J. Organomet. Chem.* **1983**, *251*, 393-411. b) Crociani, B.; Di Bianca, F.; Giovenco, A.; Scrivanti, A. *J. Organomet. Chem.* **1984**, *269*, 295-304.

9) This strategy has been documented before: a) McGuinnes, D. S.; Cavell, K. J.; Yates, B. F. *Chem, Commun.* **2001**, 355. b) Herrmann, W. A.; Köcher, C.; Gooßen, L. J.; Artus, G. R. J. *Chem. Eur. J.* **1996**, *2*, 162. c) Herrmann, W. A.; Kohl, F. J.; Scwarz, J. *Synthetic Methods of Organometallic and Inorganic Chemistry*, *Vol. 9*, Stuttgart ; New York : Georg Thieme Verlag ; New York : Thieme Medical Publishers, **2000**, p.84.

10) Isolation of the dimethylsulfide complex **3b** proved troublesome, so this complex was made *in situ* as a precursor to **3d**.

11) Several Pt-C (sp2) bond lengths *trans* to dimethylsulfide or DMSO donors have been reported, with an average of 2.019 Å and maximum uncertainty of ± 0.007Å. a) 2.036(7) and 2.010(7): Alibrandi, G.; Bruno, G.; Lanza, S.; Minniti, D.; Romeo, R.; Tobe, M. L. *Inorg. Chem.* **1987**, *26*, 185-190. b) 2.018(5): Zucca, A.; Doppiu, A.; Cinellu, M. A.; Stoccoro, S.; Minghetti, G.; Manassero, M. *Organometallics* **2002**, *21*, 783-785. c) 2.011(5) and 2.022(6): Unpublished results for (7,8-Benzoquinoline)Pt(CH_3)(SMe_2), CCDC# 170367.

12) Cardin, D.J.; Cetinkay, B.; Lappert, M. F.; Randall, E. W. ; Rosenberg, E. *J. Chem. Soc., Dalton Trans.* **1973**, *19*, 1982-1973.

13) The lower solubility of **1c** prevented the determination of its ^{1}JPt-C coupling constant.

14) The $\Delta G^{\ddagger}$ at 70 ˚C was estimated at 16.8 kcal/mol, and was found to be invariant to added DMSO.

15) k_2 was determined from the slope of the k_{obs} versus [DMSO].

16) Complex **6c** has a substitution rate nearly too slow to study by magnetization transfer at room temperature. Concentrated samples with several equivalents of DMSO were used to achieve reliably measurable rates of magnetization transfer.

17) Crabtree, R.H. *The Organometallic Chemistry of the Transition Metals*, John Wiley & Sons, Inc., 2001, pp. 265,298.

18) a) Romeo, R.; Scolaro, L. M.; Nastasi, N.; Arena, G. *Inorg. Chem.* **1996**, *35*, 5087-5096. b) Romeo, R.; Nastasi, N.; Scolaro, L. M.; Plutino, M. R.; Albinati, A.; Macchioni, A. *Inorg. Chem.* **1998**, *37*, 5460-5466. c) Romeo, R.; Fenech, L.; Scolaro, L. M.; Albinati, A.; Macchioni, A.; Zuccaccia, C. *Inorg. Chem.* **2001**, *40*, 3293. d) Romeo R.; Fenech L.; Carnabuci, S.; Plutino, M. R.; Romeo, A. *Inorg. Chem.* **2002**, *41*, 2839-2847.

19) [(2,9-dimethylphenanthroline)platinum(methyl)(DMSO)]$^+$ had a substitution rate much faster than the all other complexes in Romeo's study, but it was determined to substitute by a different mechanism.

20) Langford, C. H.; Gray, H. B. *Ligand Substitution Processes*, W. A. Benjamin, Inc., New York, NY, **1966**.

21) a) Spessard, G. O.; Miessler, G. L. *Organometallic Chemistry*, Prentice Hall, Upper Saddle River, New Jersey, 1997. b) Basolo, F.; Pearson, R. G. *Prog. Inorg. Chem.* **1962**, *4*, 381. c) Wendt, O. F. *Platinum(II) and Palladium(II) Complexes with Group 14 and 15 Donor Ligands*, Ph.D. Thesis, **1997,** Lund

University, Lund, Sweden. d) Crabtree, R.H. *The Organometallic Chemistry of the Transition Metals*, John Wiley & Sons, Inc., **2001**.

22) Crociani *et al.* inferred from ν(Pt-Cl) stretching frequencies that the *trans*-influence of 2-pyridyl decreased compared to its ylidene analogue. Ref. 8b.

23) Romeo[18a] has observed that stronger σ-donation need not result in a greater *trans*-effect. In the context of the bonding model described in Figure 3, this would depend upon the relative importance of σ-antibonding interactions in the ground and transition states for substitution.

24) Burger, B. J.; Bercaw, J. E. *New Developments in the Synthesis, Manipulation, and Characterization of Organometallic Compounds*; Wayda, A.; Darensbourg, M. Y., Eds.; American Chemical Society: Washington, DC, **1987**; Vol. 357.

25) Giam, C. S.; Hauck, Albert E. *Organic Preparations and Procedures International*; **1977**, 9(1), 9-11.

26) Keumi, T.; Yoshimura, K.; Shimada, M.; Kitajima, H. *Bull. Chem. Soc. Jap.* **1988**, *61*(2), 455-9.

27) Hill, G. S.; Irwin, M. J.; Levy, C. J.; Rendina, L. M.; Puddephatt, R. J. *Inorg. Synth.* **1998**, *32*, 149-153.

28) Morris, G. A.; Freeman, R. *J. Magn. Reson.* **1978**, *29*, 433-462.

29) Günther, H. *NMR Spectroscopy, Second Edition*, John Wiley & Sons Limited: West Sussex, England, 1995, pp. 335 – 346.

Chapter 2

Selectivity in the C–H Activation of Methane and its Oxidation Products: Kinetics and Mechanism

Abstract

The relative rates of methane and methanol C–H activation by [(N-N)PtMe(TFE-d_3)]$^+$ ((N-N) = ArN=C(Me)-C(Me)=NAr Ar = 3,5-di-*tert*-butylphenyl, TFE-d_3 = CF_3CD_2OD) (**2**) were studied by ^{1}H and ^{13}C NMR spectroscopy. Methane activation kinetics were conducted at 300-1000 psi of methane pressure in single crystal sapphire NMR tubes ($k = 1.6 \pm 0.4 \times 10^{-3}$ $M^{-1}s^{-1}$, 330 K; $k = 2.7 \pm 0.2 \times 10^{-4}$ $M^{-1}s^{-1}$, 313 K). Protonolysis of the dimethyl complex (N-N)$PtMe_2$ (**1**) with D^+ gives statistical scrambling of the label in all the available sites of the methane and [(N-N)Pt($CH_{3-n}D_n$)(CF_3CD_2OD)]$^+$ products. These results indicate that the C–H bond making and breaking steps happen more readily than loss of the bound methane, and hence that displacement of TFE-d_3 by methane's C–H bond is slower than its subsequent C–H oxidative cleavage. Addition of anhydrous methanol to solutions of **2** rapidly establishes equilibrium between methanol **2(MeOH)** and trifluoroethanol **2(TFE)** adducts ($K_{eq} = 0.0042 \pm 0.0006$). Increasing the methanol concentration inhibits the rate of C–H activation from 0.12 - 4.4 M. A small kinetic isotope effect ($k_H/k_D = 1.4 \pm 0.1$) and the observed concentration dependence suggest that the reaction proceeds by rate determining displacement of the coordinated trifluoroethanol by the C-H bonds of methanol ($k = 2.0 \pm 0.2 \times 10^{-3}$ $M^{-1}s^{-1}$, 330 K). A similar mechanism is observed in the activation of dimethylether ($k = 5.5 \pm 0.5 \times 10^{-4}$ $M^{-1}s^{-1}$, $K_{eq} = 0.020 \pm 0.002$, 313 K). Comparison of these second order rate constants ($k_{(Methane)}/k_{(Methanol)} = 1/1.3$, 330 K; $k_{(Methane)}/k_{(Dimethylether)} = 1/2$, 313 K) shows that this step is unselective with respect to coordinating the C–H bonds of methane, methanol, or dimethylether. This selectivity matches the one previously reported by our group for oxidizing methyl and hydroxymethyl groups with aqueous

tetrachloroplatinate estimated from the catalytic oxidation of ethanol and toluene sulfonic acid (1.5/1). These data strongly suggest a similar rate-determining step under the Shilov conditions.

Introduction:

The rising cost of oil and the fear of high carbon dioxide levels in the atmosphere are leading scientists to search for cheap alternatives to coal and oil. The most immediately practical solution to this problem is the efficient use of abundant natural gas. Unfortunately, because many of the known natural gas reserves are far removed from where they are needed most, the gas must be transported long distances. The high cost of building pipelines, ~1 million dollars per kilometer[1], and the need to refrigerate the gas, so that it can be shipped as a liquid, limit the efficiency of this resource and raise the cost of its production. A much more environmentally and economically friendly alternative would be to convert the natural gas directly to useful and more easily transported products at the well-head.[2]

The direct aerobic oxidation of methane to useful chemicals is the most clear and simple solution to this problem. Unfortunately, this process is complicated by the increasing reactivity of its oxidation products. For instance, most oxidants capable of reacting with methane (BDE(C–H) = 104 kcal/mol) react more readily with the weaker C–H bonds of methanol (BDE(C–H) = 93 kcal/mol), placing an inherent limit on the yield.[3] Nonetheless, a few examples of catalysts based on platinum(II), palladium(II), and mercury(II) salts have been shown to produce high yields of partially oxidized products.[4] Based on the yields obtained with these catalysts, it was estimated that methane can be as much as 100 times more reactive than its oxidation product.[3c] Direct studies on the aqueous tetrachloroplatinate system pioneered by Shilov suggest that the reactivity of methyl groups (or methane) and hydroxymethyl groups (or

methanol) is similar (1.5/1) under those conditions.[5] Though these estimates were the first demonstrations of such an unusual selectivity, the origin of this relative reactivity is not clear.

We have previously exploited diimine-ligated platinum(II) alkyl complexes as model systems for extensive mechanistic studies of C–H activation.[6] Using this system we were able to determine the relative rates of methane, methanol and dimethylether C–H activation, and the steps responsible for their rates of reaction.

Results

Methane Activation with $[(N\text{-}N)Pt(^{13}CH_{3-n}D_n)(DOCD_2CF_3)]^+$ $[CF_3CD_2OB(C_6F_5)_3]^-$ (2-^{13}C(TFE)). In order to study the kinetics of methane activation, **1-^{13}C** was prepared from the diimine ligand (ArN=C(Me)-C(Me)=NAr Ar = 3,5-di-*tert*-butylphenyl) and ^{13}C-labeled (μ-dimethylsulfide) platinumdimethyl dimer. Protonolysis of (diimine)platinumdimethyl (**1-^{13}C**) with 2 equivalents of tris(pentafluorophenyl)borane ($B(C_6F_5)_3$) in anhydrous CF_3CD_2OD (TFE-d_3) produces **2(TFE)** and methane as a statistical mixture of

Scheme 1

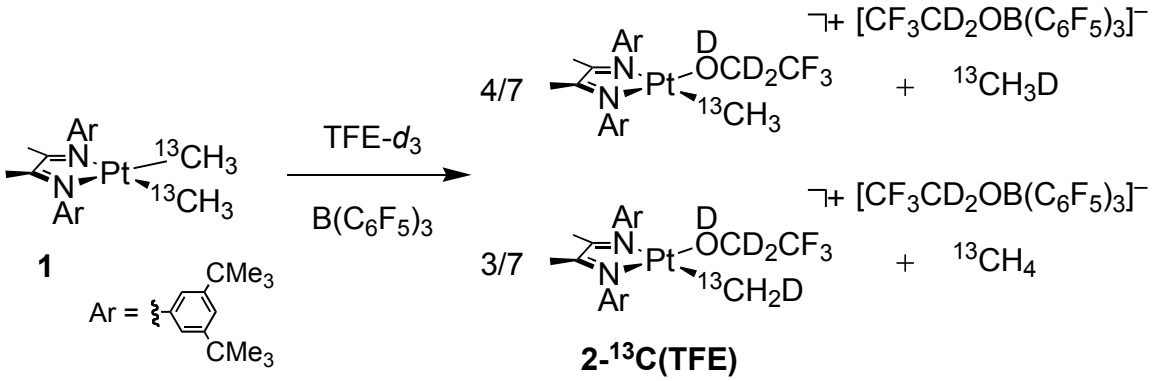

$^{13}CH_4$ and $^{13}CH_3D$ ~(3:4) (Scheme 1).[6c] Isotopically shifted upfield from the all protio platinum methyl group (δ = 0.74 ppm, $J_{C\text{-}H}$ = 128.3 Hz, fwhm = 1.8 Hz @ 500 MHz) the H,D coupling of the Pt-CH_2D fragment (δ = 0.73 ppm, fwhm = 4.2 Hz @ 500 MHz) is not resolved in the ^1H NMR spectrum, however ^{13}C-D coupling is observed in its ^{13}C NMR spectrum (δ = -8.6 ppm, $J_{C\text{-}D}$ = 19.5 Hz @ 125.7 MHz).

Upon addition of dry methane-^{12}C to solutions of **2-^{13}C(TFE)** in single-crystal sapphire NMR tubes the appearance of **2-^{12}C(TFE)** is observed in the ^1H NMR spectrum (Scheme 2). The disappearance of the platinum methyl group of **2-^{13}C(TFE)** and the appearance of the platinum methyl group of **2-^{12}C(TFE)** show a similar rate. The disappearance of **2-^{13}C(TFE)** was monitored by ^{13}C NMR at 330 K and 313 K in the presence of 300-1000 psi of added methane. First-order decay of the ^{13}C label has a rough linear concentration dependence at 330 K (k = 1.6 ± 0.4 × 10^{-3} $M^{-1}s^{-1}$) and a more precisely linear dependence at 313 K (k = 2.7 ± 0.2 × 10^{-4} $M^{-1}s^{-1}$) (Tables 1,2 and Figure 1).

Methane activation happens in parallel with a much slower decomposition to a pentafluorophenyl platinum complex **3** as well as CH_3D and CH_2D_2 evident by the nonzero intercept in Figure 1 (k_{decomp} = 1.8 × 10^{-5} s^{-1}, 330K; k_{decomp} = 6.8 × 10^{-6} s^{-1}, 313K) (Scheme 3). Electrospray mass spectra of these

Scheme 2

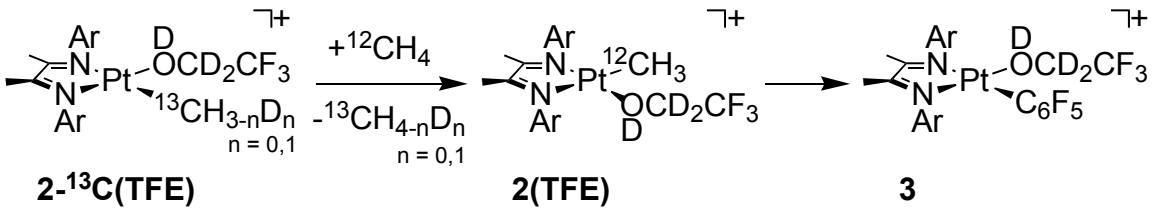

2-^{13}C(TFE) **2(TFE)** **3**

Table 1. Methane activation kinetics at 313 K with **2**.

[Pt] (M)	Methane (psi)	$[CH_4]$ (M)	k_{obs} (s^{-1})	k_2[a] ($M^{-1}s^{-1}$)
0.0145	570	0.393	0.000059	0.000266
0.0145	835	0.690	0.000101	0.000275
0.0145	1020	0.855	0.000121	0.000266

[a] Calculated from $\{k_2 = (k_{obs}-k_i) / [CH_4] \times 2\}$ where $k_i = 6.77 \times 10^{-6}$ is taken from intercept of k_{obs} versus [methane] and factor of two included for the equal rates of the forward and back reaction.

Table 2. Methane activation kinetics at 330 K with **2**.

[Pt] (M)	Methane (psi)	$[CH_4]$ (M)	k_{obs} (s^{-1})	k_2[a] (s^{-1})
0.00944	300	0.298	0.000288	0.00181
0.00944	400	0.370	0.000283	0.00143
0.01454	500	0.423	0.000350	0.00157
0.02181	503	0.510	0.000376	0.00140
0.01454	550	0.488	0.000385	0.00150
0.01454	700	0.617	0.000540	0.00169

[a] Calculated from $\{k_2 = (k_{obs}-k_i) / [CH_4] \times 2\}$ where $k_i = 1.85 \times 10^{-5}$ is taken from intercept of k_{obs} versus [methane] and factor of two included for the equal rates of the forward and back reaction.

Figure 1. k_{obs} versus [methane] at 330 K (left) and 313 K (right).

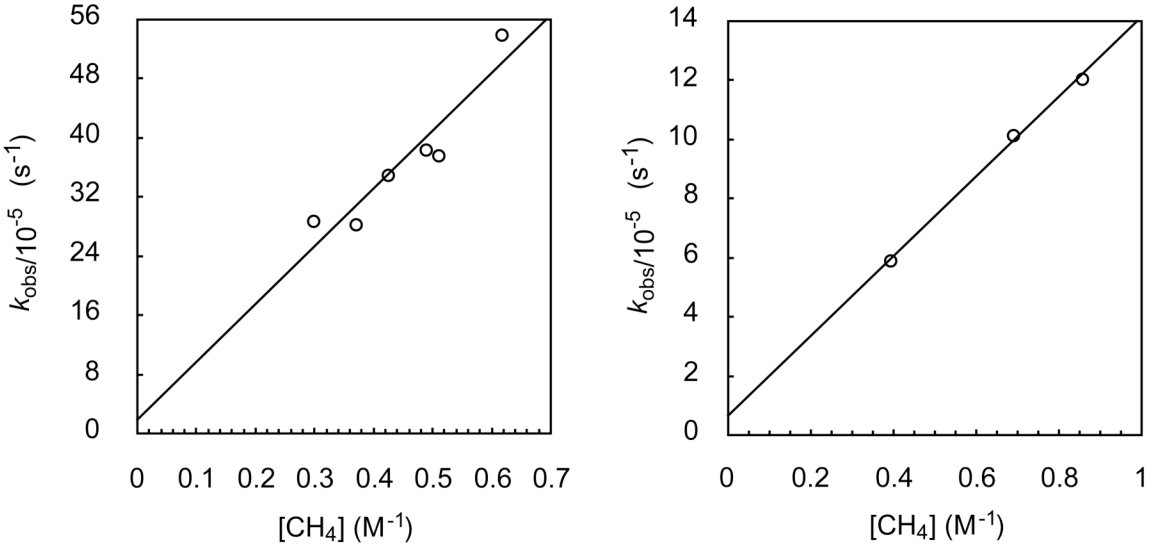

samples diluted with methanol-d_0 show a large peak at M/Z = 854.3 amu consistent with a methanol bound pentafluorophenyl platinum cation (**3**). Monitoring the decomposition of **2** in the absence of added substrate ([**2**] = 15.2

mM, $[B(C_6F_5)_3]$ = 30.3 mM, k_{obs} = 4 × 10^{-5}, 330K) shows an initial first-order rate similar to the y-intercept in Figure 1 on the left. Additional evidence for **3** comes from several NMR samples of **2** left exposed to air that produce crystals of the pentafluorophenyl complex shown below in Figure 2.[7]

Scheme 3

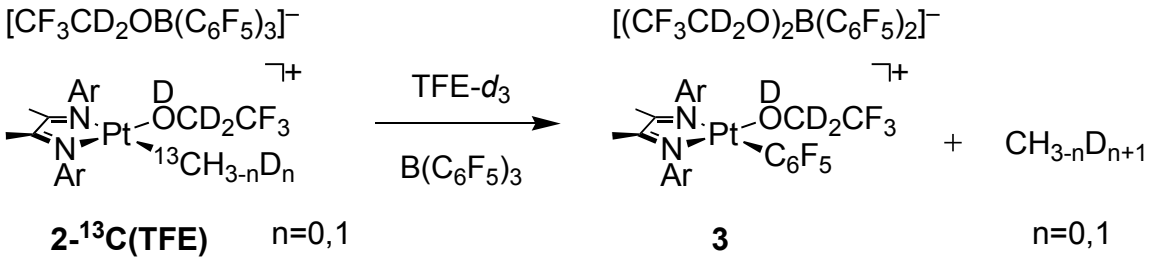

Figure 2

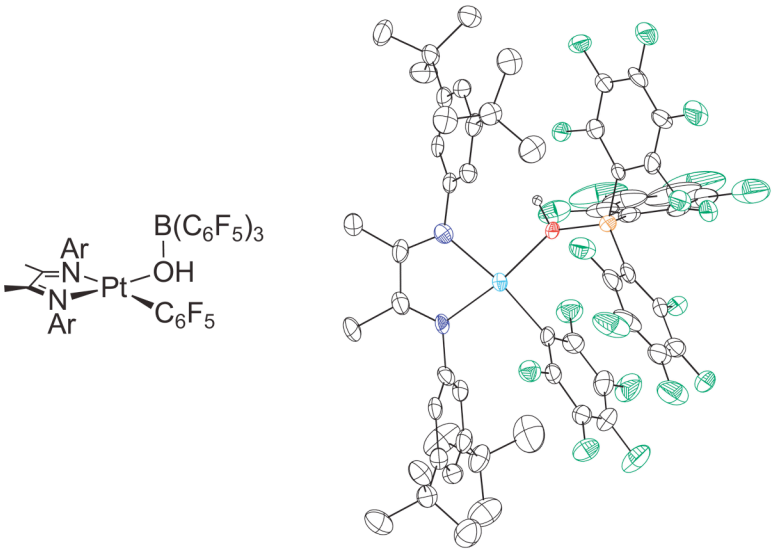

Methanol Activation with 2. Addition of anhydrous methanol-d_1 to solutions of **2** rapidly establishes equilibrium between methanol-d_1 bound (**2(MeOH)**) and trifluoroethanol bound (**2(TFE)**) (K_{eq} = 0.0042 ± 0.0006, 330K) platinum cations. Additional broad signals for methanol bound to borane are visible in the ^{1}H and ^{13}C NMR spectra, the shape and frequency of which, depend

on the temperature and concentration of added methanol. Over several hours, the appearance of methane (CH_4/CH_3D), as well as 1-2 platinum complexes that convert to a methanol bound pentafluorophenyl platinum cation (**3**), is observed in the ^{1}H NMR spectrum (Scheme 4). The methane liberated in activations of CD_3OD *versus* CH_3OD carries *one* additional deuterium from the substrate.

An intermediate hydroxymethyl complex could be observed at lower concentrations of added methanol. Reaction of **2** with three equivalents of $^{13}CH_3OH$ produces a new ^{13}C NMR signal at δ = -4 ppm with broad ^{195}Pt satellites (J = 732 Hz). In the ^{1}H-coupled ^{13}C NMR spectrum this resonance appears as a 1:2:1 triplet (J = 134 Hz), which is consistent with a platinum-bound sp^3-hybridized CH_2 fragment. HMQC spectra show a correlation between this ^{13}C resonance and a ^{1}H resonance (δ = 2.72 ppm) within the region of other O-bound methanol signals for the starting material (**2**) and pentafluorophenyl product (**3**) (δ = 2.5 - 3.0 ppm) (Figures 3, 4). On the basis of these data, we formulate this intermediate as $[(NN)Pt(CH_2OD)(DOCH_3)]^+$ (**4**).[8]

Scheme 4

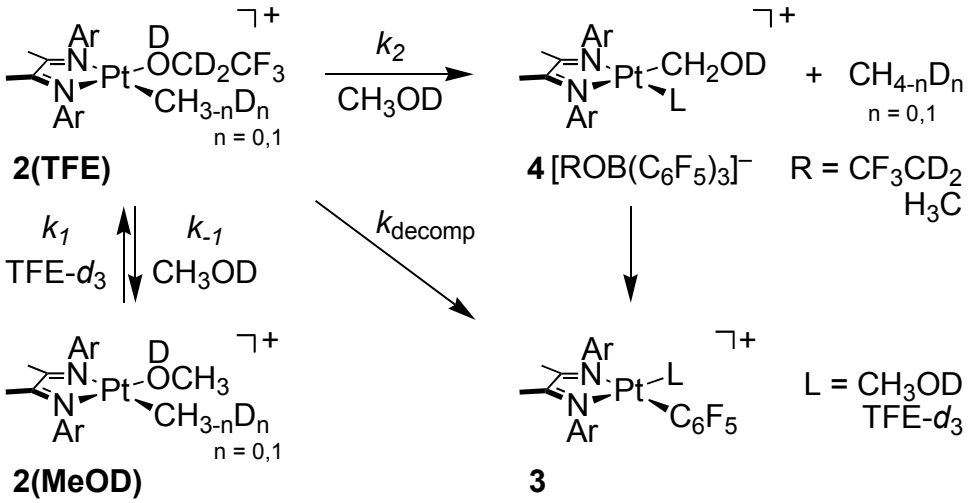

Figure 3. 1D-HMQC from $^{13}CH_3OH$ activation.[a]

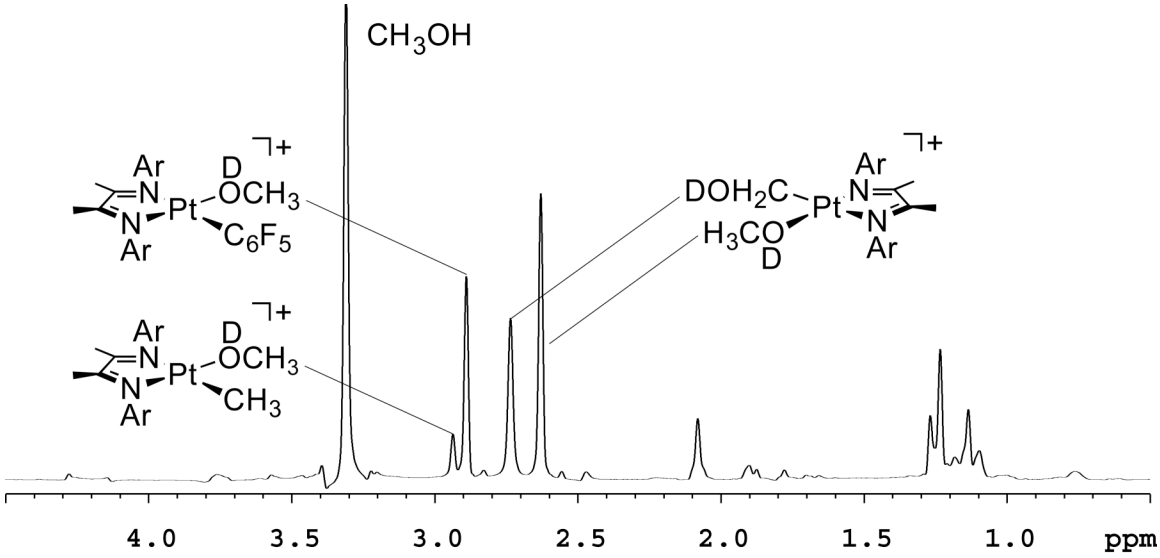

[a] Peaks appear without ^{13}C–^{1}H couplings. Solvent presaturation was used to minimize the intensity of free methanol signal.

Figure 4. 2D-HMQC of **3** derived from $^{13}CH_3OH$ activation.[a]

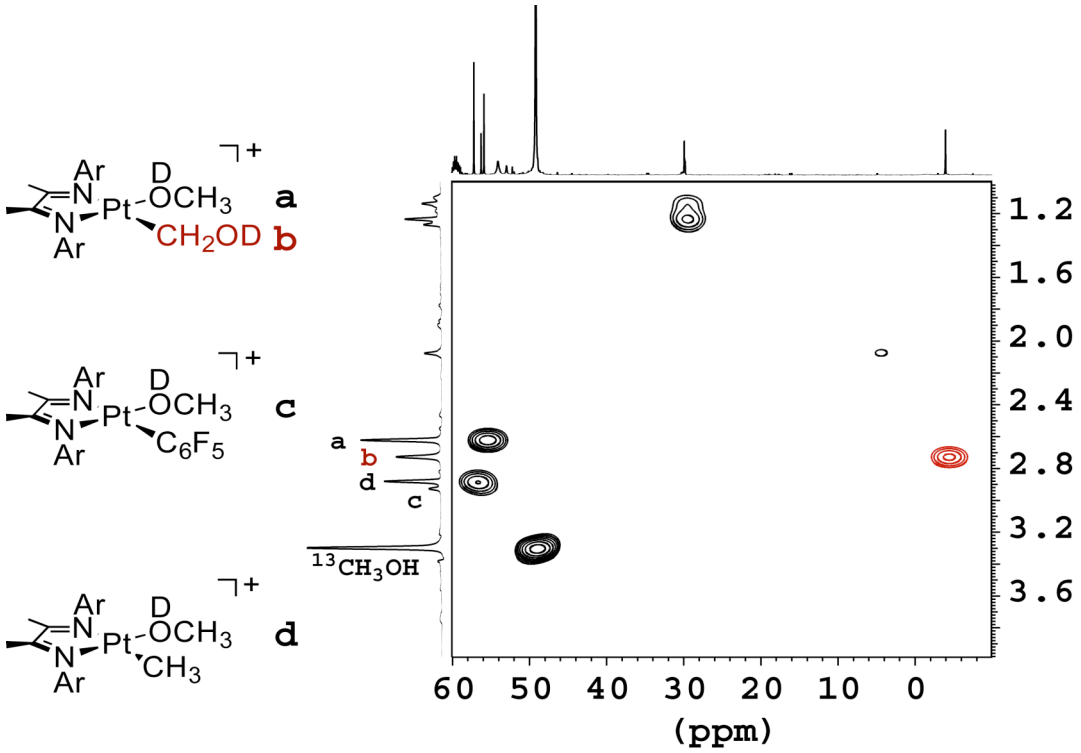

[a] A 1D HMQC spectrum as well as a higher resolution ^{13}C NMR spectrum (both acquired separately) are superimposed on the axes of the 2D plot.

Kinetics of Methanol Activation with 2. The kinetics of methanol activation were studied by following the disappearance of **2(MeOD)** at 330 K by ^{1}H NMR. The reaction exhibits well-behaved pseudo first-order kinetics, with the observed rate constant *decreasing* with *increasing* methanol concentration. Assuming that productive methanol C–H activation proceeds via a bimolecular reaction between **2(TFE)** and methanol, the observed rate constants can be expressed as a function of the calculated concentration of **2(TFE)** where [**2(TFE)**] = $[Pt_{Tot}](\alpha_{TFE})$ (Equations 1-3). When the observed rate constants are corrected

Equations 1 - 3

$$\frac{d[Pt_{Prod}]}{dt} = (k_2[MeOD] + k_{decomp})[\mathbf{2(TFE)}] = (k_2[MeOD] + k_{decomp})[Pt_{Tot}](\alpha_{TFE})$$

$$(\alpha_{TFE}) = \frac{1}{1 + \frac{[MeOD]}{K_{eq}[TFE]}} \qquad k_{obs} = (k_2[MeOD] + k_{decomp})(\alpha_{TFE})$$

by the calculated mole percent of **2(TFE)** ($k_{obs}/(\alpha_{TFE})$) they show a linear dependence on the methanol concentration over a wide concentration range (Figure 6, right) ($k_2 = 2.0 \pm 0.2 \times 10^{-3}$ $M^{-1}s^{-1}$, $k_H/k_D = 1.4 \pm 0.1$, $k_{decomp} = 2 \pm 1 \times 10^{-4}$ s^{-1}). Tables 4 and 5 list important kinetics data (below).

Table 3. Methanol-d_1 activation kinetics at 330 K with **2**.

[Pt] (M)	[CH_3OD] (M)	[TFE][a] (M)	k_{obs}(H) (s^{-1})	k_{obs}(H)/α(TFE) (s^{-1})
0.00933	0.1233	13.46	0.000136	0.000435
0.00933	0.2466	13.39	0.000135	0.000731
0.00949	0.5073	13.25	0.000135	0.00137
0.00949	0.7380	13.11	0.000132	0.00191
0.00949	1.2254	12.84	0.000119	0.00284
0.00949	2.4508	12.15	0.000105	0.00518

[a] The concentration of TFE was calculated assuming volume additivity.

Table 4. Methanol-d_4 activation kinetics at 330K with **2**.

[Pt] (M)	[CD_3OD] (M)	[TFE] [a] (M)	k_{obs}(D) (s^{-1})	k_{obs}(D)/α(TFE) (s^{-1})
0.00947	0.6155	13.18	0.000100	0.00152
0.00933	1.2309	12.84	0.0000839	0.00253
0.00890	2.4619	12.15	0.0000622	0.00389
0.00949	4.4314	11.05	0.0000585	0.00719

[a] The concentration of TFE was calculated assuming volume additivity.

Figure 5. Plot of k_{obs} (s^{-1}) versus [methanol] (M) (left) and of k_{obs}/α_{TFE} (s^{-1}) versus [methanol] (M) (right).[a]

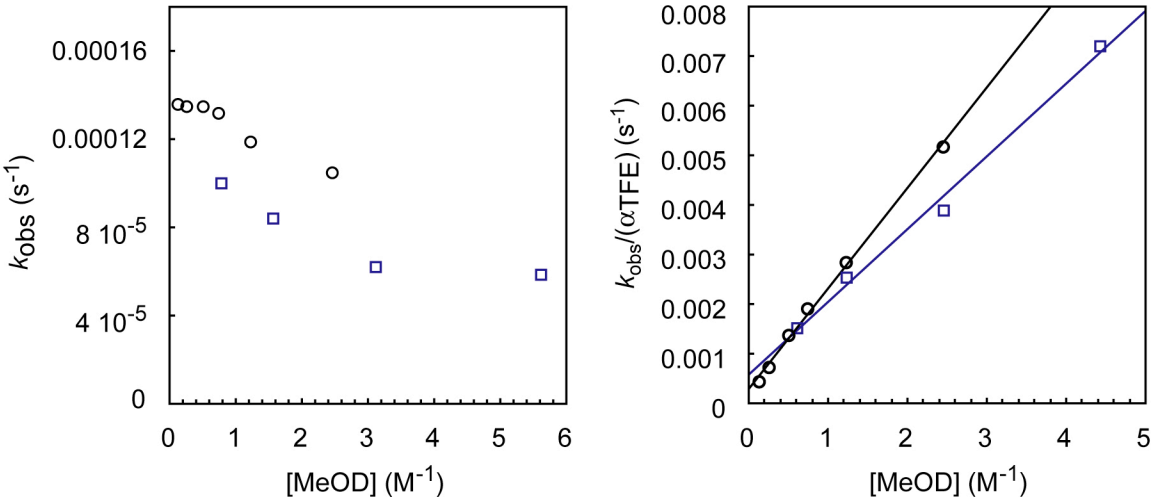

[a] CH_3OD (○) and CD_3OD (□)

Activation of Dimethylether with 2. Addition of anhydrous dimethylether to solutions of **2** establishes equilibrium between a dimethylether bound platinum cation (**2(DME)**) and **2(TFE)** (K_{eq} = 0.020 ± 0.002, 313 K)**.** Decomposition of these starting complexes (313 K) proceeds with the formation of methane, an unusual new species with eight aromatic ligand resonances, and **3**. An additional resonance for this complex downfield of the ligand peaks shows weak platinum coupling (Acetone-d_6: d, δ = 10.4 ppm, $J_{Pt\text{-}H}$ = 24.4 Hz, $J_{H\text{-}H}$ = 1.7 Hz 1H). Continued monitoring shows these resonances decrease at the same time that crystals appear in the NMR tube. An X-ray crystal structure of this

material reveals an unusual example of a Pt-Pt dimer (**5**) with μ-CH_2 and μ-$CH(OCH_3)$ bridges ($d_{average}$(Pt-C) = 2.005 (3)), as well as two counter-anions from the protonolysis ($[CF_3CH_2OB(C_6F_5)_3]^-$) (FAB-HRMS: M+ = 1368.73) (Figure 5).[9] A short Pt-Pt distance d(Pt-Pt) = 2.6053(2) is indicative of a metal–metal bond. Reaction of **2** with DME-$^{13}C_2$ produces a similar dimer with fully ^{13}C-labeled bridging ligands, allowing analysis of its ^{1}H and ^{13}C NMR parameters (Table 3).

Figure 6

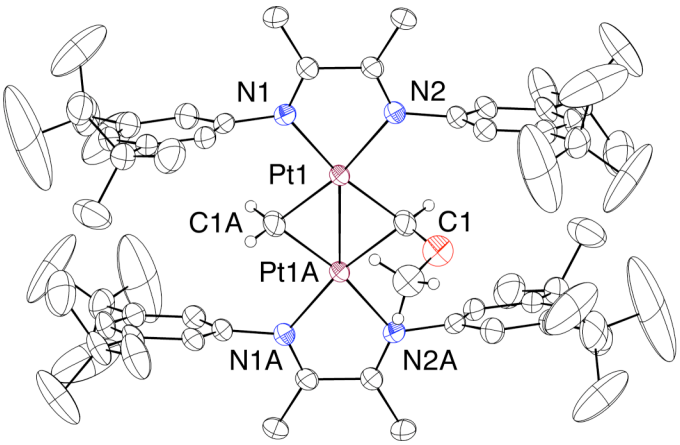

Bond Lengths [Å] and Angles [°]	
Pt1 - Pt1A	2.6053 (2)
Pt1 - C1	2.0055 (34)
C1 - O1	1.5157 (74)
Pt1 - C1 - Pt1A	81.02 (0.13)
C1 - Pt1 - C1A	98.98 (0.13)

Table 5. ^{1}H and ^{13}C NMR parameters for **5**.[a]

	δ (^{1}H) (ppm)	J_{CH2-H}[b] (Hz)	$J_{CH(OMe)-H}$ (Hz)	J_{C-H}[c] (Hz)	δ (^{13}C) (ppm)	J_{Pt-C} (Hz)
CH_{2A}	8.15	5.25	1.74	154.3	133.2	560.2
CH_{2B}	8.01	5.25	-	153.4	133.2	560.2
CH(OMe)	10.35	1.74	-	177.7	190.0	637.2
OCH_3	3.79	-	-	146.5	67.1	NA

[a] Acetone-d_6. [b] Indicates geminal coupling. [c] Average coupling.

Kinetics of Dimethylether Activation with 2. The disappearance of **2** was monitored by ^{1}H NMR at 313 K over more than five half-lives. A plot of first-order rate constants extracted from the data *versus* [dimethylether] is shown in Figure 7 on the left. A best fit line is drawn through the data according to equations 1-3 with the appropriate substitution of dimethylether for methanol.

In analogy to the methanol kinetics discussed above, correcting the first-order rate constants for [**2(TFE)**] and plotting *versus* [dimethylether] shows the rate depends linearly on [dimethylether] ($k = 5.4 \pm 0.5 \times 10^{-4}$ $M^{-1}s^{-1}$) with a negligible intercept (Figure 7).

Table 6. Dimethylether activation kinetics at 313 K with **2**.

[Pt] (M)	$[CH_3OCH_3]$ (M)	[TFE] [a] (M)	k_{obs}(D) (s^{-1})	k_{obs}(D) / α(TFE) (s^{-1})
0.0105	0.1628	13.637	0.0000563	0.0000899
0.0105	0.1909	13.609	0.0000564	0.0000959
0.0100	0.5735	13.227	0.0000987	0.000313
0.00983	0.9212	12.879	0.000110	0.000503

[a] The concentration of TFE was calculated assuming volume additivity.

Figure 7. Plot of k_{obs} (s^{-1}) versus [methanol] (M) (left) and of k_{obs}/α_{TFE} (s^{-1}) versus [methanol] (M) (right).

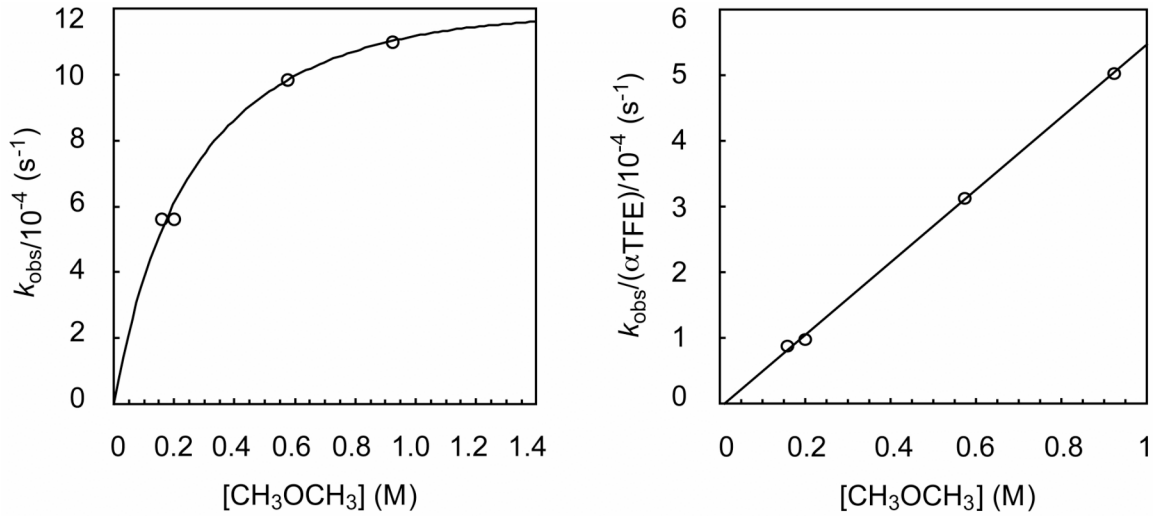

Discussion

The important microscopic steps in a C–H activation reaction with **2** are shown below (Scheme 4). First, association of the substrate (***i***) and loss of the coordinated solvent lead to an alkane σ-complex (**A**). Subsequent oxidative

cleavage (***ii***) of the coordinated C–H bond generates a platinum(IV)hydride (**B**), which goes on to reductively eliminate methane (not shown). Although it is not clear whether discreet platinum(IV)hydrides are intermediates in the Shilov cycle, steps (***i***) and (***ii***) characterize the mechanisms of many carefully studied C–H activation reactions.[10] Previous studies in our group have outlined examples where either (***i***) or (***ii***) is the rate-determining step.[6] The observations described above support a common mechanism where formation of an alkane σ-complex (***i***) is the rate-determining step. Hence the kinetic selectivity measured above for methane, methanol, and dimethylether C–H activation is due to their respective rate of forming **A**.

Scheme 5

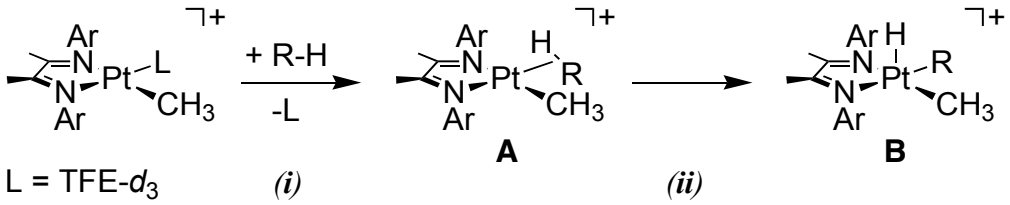

Scrambling in the Protonolysis of 1 and the Reversibility of Methane Activation with 2. The statistical scrambling of a single deuterium into the available sites of the methane and platinummethyl products (Scheme 1) suggests that step ***ii*** is rapid and reversible prior to the loss of methane (-***i***) (Scheme 5). This rapid C–H bond making and breaking requires that in the activation of methane the coordination of the substrate is the slowest step and hence the rate determining step. Furthermore, the measured rate of disappearance of the ^{13}C label in the starting material is only half of the actual rate of methane activation. This factor of two arises because decomposition of the symmetric platinum(IV)

intermediate (**B**) produces the ^{12}C product at the same rate as the reverse reaction.

Scheme 6

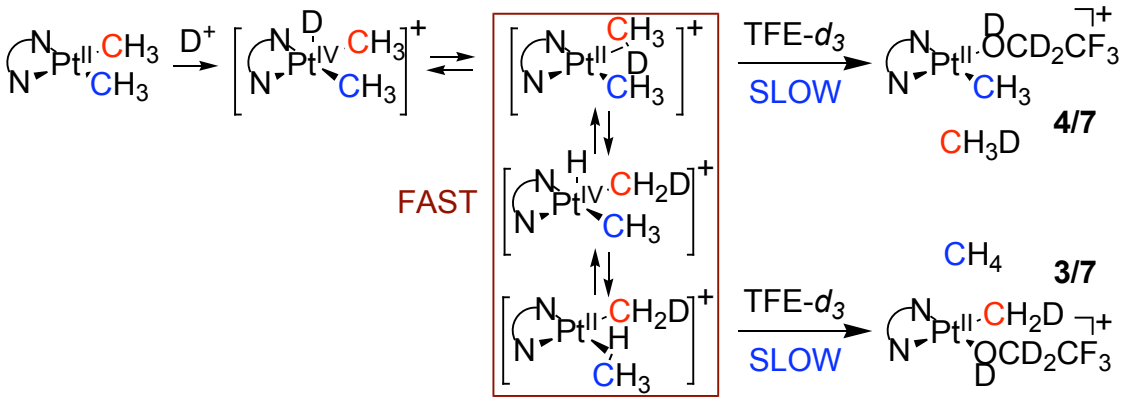

Pentafluorophenyl Transfer and the Production of 3. The appearance of **3** accompanied all of the reactions presented above. Higher concentrations of the starting materials gives rise to a faster decomposition rate that may arise from a first order dependance on both the concentration of platinum and added borane. These observations are tentatively explained by a bimolecular transmetallation of a pentafluorophenyl group from the borane to the platinum center and of a methylgroup to the borane. Subsequent alcoholysis of the boron-carbon bond produces methane with incorporation of only one additional deuterium from the solvent. The appearance of **3** is accelerated in samples contaminated by air and water, though it was also observed in rigorously dry samples. The initial first order decomposition rate, in the absence of added substrate, is similar to the intercepts of the k_{obs} *versus* [methane] plots, though these intercepts are nearly an order of magnitude slower than those observed in reactions with methanol. The increased rate of pentafluorophenylation in methanol activation reactions is due to the methanol-borane complex being a more potent transmetallating agent.

Contamination by adventitious water may also lead to a faster rate of decomposition, which may explain the different intercepts in the activation of methanol-d_4 and methanol-d_1.

Substrate Inhibition in the Activation of Methanol and Dimethylether. Methanol and dimethylether coordinate to the platinum center more tightly than the trifluoroethanol solvent by a factor of 240 and 50, respectively. When bound by the substrates oxygen lone-pair the rate of C–H activation is inhibited leading to a reaction rate that depends on [**2(TFE)**]. Assuming that C–H activation as well as decomposition to **3** proceed *exclusively* from **2(TFE)**, the observed rates can be corrected by its concentration under the reaction conditions (k_{obs}/(α-TFE)) according to Equations 1-3 above (Figures 5 and 7). Plots of these corrected rates show a very good linear correlation on the concentration of the substrate confirming this assumption and allowing a determination of the second order rate constant for the bimolecular reaction of **2(TFE)** with the substrate C–H bond and the first order decomposition rate.

Calculated first-order C–H activation rate constants at each methanol concentration ($k_{obs\text{-}C\text{–}H} = k_2 \times$ [MeOD] × (α-TFE)) are plotted below with the measured first-order rate constants for the disappearance of the starting material (Figure 8). As is expected from pre-equilibrium behavior, the calculated C–H activation rate saturates as the [methanol] increases from zero. As [methanol] approaches 100%, [TFE] decreases to zero and the rate also decreases to zero. The observed first-order rates do not show this saturation behavior because the parallel decomposition reaction dominates at low concentrations of methanol. This side reaction results in a set of observed rate constants that decrease from

nearly 100% decomposition and approach 100% methanol C–H activation. This change in reaction pathway is supported by the observation that methane liberated from reactions at low [methanol-d_1] carry more deuterium than under high [methanol]. This background pentafluorophenylation incorporates an additional deuterium from solvent into the methane that is liberated (Scheme 3).

Figure 8. Observed and calculated first-order rate constants for methanol activation.

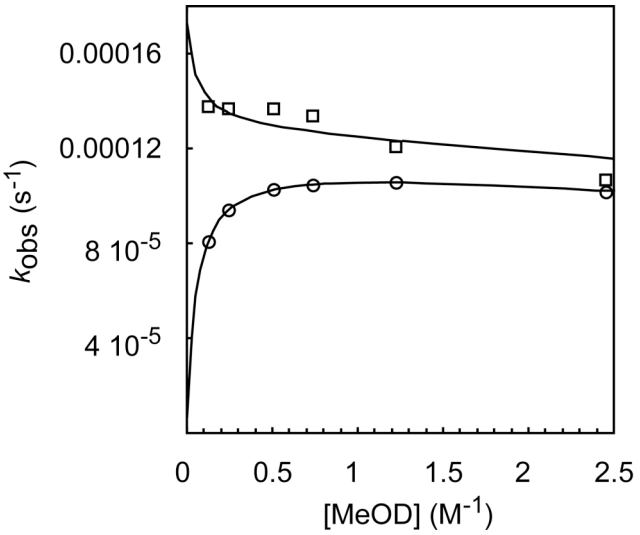

Calculated first-order rate constants (○) and observed rate constants (□) for methanol C–H activation with best fit lines drawn based on Equations 1-3.

The kinetics of dimethylether activation were pursued with the hope that the parallel decomposition reaction could be suppressed with this more easily dried, aprotic substrate. Activations of dimethylether proceed with the appearance of **3** but without any contamination of the first-order rate constants from this side reaction. This is clear from the intercept in Figure 7 which indicates a negligible contribution to the observed rate constant. The lack of a significant side-reaction allows observation of the saturation-like behavior of the k_{obs} versus [dimethylether] plots.

Isotope Effects and the Irreversibility of Methanol-d_4 C–H Activation. The small but measurable isotope effect on the rate of methanol-d_4 activation suggests that, much like in the methane reaction, the C–H bond coordination, rather than the bond breaking, is the slow step in the reaction. The incorporation of only one additional deuterium into the methane produced in the activation of methanol-d_4 suggests that some of the steps in the production of **4** are irreversible. This result contrasts the methane activation where all of the hydrogens of the methane and methyl group exchange during the course of the activation. The irreversibility of this reaction and the slow coordination step requires that the measured second order rate constant is the actual rate of methanol C–H bond coordination rather than a fraction of the rate as in the case of methane.

Hydroxyalkyl and Alkoxyalkyl Platinum Intermediates from Methanol and Dimethylether Activation. The products observed in the activation of methanol and dimethylether are important to the study of methane oxidation as well as the hydrogenation of carbon monoxide. Though not common, many examples of transition-metal α-oxygen substituted alkyl complexes exist. Few of these examples are hydroxymethyl complexes, and the few characterized examples are octahedral, making **4** unique.[11] Alkoxyalkyl complexes, on the other hand, are more common.[12] In two cases these complexes are proposed intermediates in the C–H activation of tetrahydrofuran (THF) or diethylether, ultimately leading to Fischer carbene hydride complexes by α-elimination.[13] An example of this reaction published by our group is shown below, where the C–H activation of diethylether eventually leads to an α-ethoxyethylidene complex

(Scheme 7).[13a] In light of these observations the stability of **4** and the lack of a stable methoxyalkylplatinum complex in the reactions dimethylether with **2** are interesting. This difference in reactivity may be due to a more favorable α-

Scheme 7

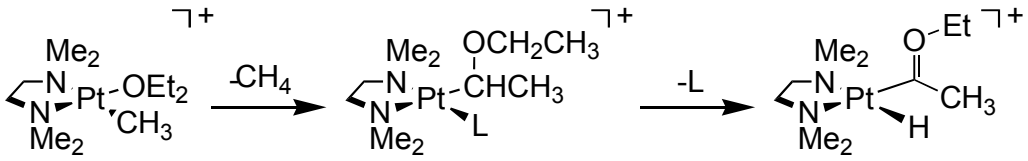

elimination from the methoxymethyl intermediate. In the case of dimethylether activation, α-elimination produces an electron rich methoxymethylidene complex versus an electron-poor hydroxymethylidene that would result from **4.** A higher concentration of this methoxymethylidene hydride complex might then encourage dimerization to produce **5** and an equivalent of methanol. Alkylgroups with α-oxygen ligands have also been shown to undergo C–O bond cleavage in the presence of strong acids.[14] This mechanism is enticing both for the observation of the *μ*-methylidene ligand in **5** and the presence of excess *tris*(pentafluorphenyl)borane. In the absence of the appropriate crossover experiment, it is not possible to rule out either mechanism.

The bonding in **5** is interesting because of the unusual connectivity of this dimer. The short Pt-Pt distance as well as the charge and diamagnetism of this complex point to a metal-metal bonded Pt(III)/Pt(III) description analogous to the only other examples of alkyl bridged platinum-platinum dimers published by Cotton.[15] The ^{1}H and ^{13}C spectroscopic parameters of **5** also provide some insight into the bonding within this dimer. In particular the downfield chemical shifts of the bridging groups in both the ^{1}H and ^{13}C spectra are most likely due to a large paramagnetic contribution to the chemical shift characteristic of terminal

alkylidene ligands. The especially large C–H coupling constants of both methylidene bridges and especially in the methoxymethylidene suggest a high *2s*-character in this C–H bond that may arise from the acute Pt-C-Pt bond angles and the electron deficient nature of the platinum center. Consistent with a high partitioning of *2s*-character in the C–H bonds the small platinum-carbon coupling constants suggest a bond with a large contribution from the carbon *3p*-orbital.

Conclusions

The relative rates of methane, methanol, and dimethylether C–H activation show that the platinum center is relatively unselective with respect to which C–H bond it prefers to coordinate: $k_{methane}/k_{methanol}$ = 1/1.3, 330K and $k_{methane}/k_{dimethylether}$ = 1/2, 313K. For both methane and methanol, this selectivity was shown to derive from the rate of associative displacement of TFE by the substrate C–H bond to form a σ-complex. A lack of selectivity was also observed in the reactivity ratios estimated from studies of toluenesulfonate, ethanol and other alcohol oxidations with aqueous tetrachloroplatinate (see above),[3] strongly implying that formation of an alkane σ-complex is the rate- and selectivity-determining step in these conditions.

Experimental

General Methods. All air and/or moisture sensitive compounds were manipulated using standard Schlenk techniques or in a glovebox under a nitrogen atmosphere, as described previously.[16] **1** was prepared as described previously,[6a] and purified by filtering a saturated methylene chloride solution

followed by precipitation of the platinum complex at -78 ˚C. The dark purple solid was then stored under high vacuum for three days to remove co-crystallized solvent molecules and stored in a P_2O_5 dessicator in the glovebox. $B(C_6F_5)_3$ was sublimed at 90 ˚C at full vacuum and stored in a P_2O_5 dessicator in the glove box. All deuterated solvents and ^{13}C labeled compounds were purchased from Cambridge Isotope Laboratories, with the exception of dimethylether-$^{13}C_2$ which was purchased from Isotec. Methanol-d_1 and methanol-d_4 were stored over 3 Å molecular sieves and then distilled from sodium. Trifluoroethanol-d_3 was dried over 3Å molecular sieves for at least 5 days and then was vacuum distilled onto $B(C_6F_5)_3$ and shortly thereafter distilled into a Strauss flask and stored in the glove box. Ultra high purity methane (99.95%) was purchased from Matheson and stored over activated alumina prior to use. Dimethylether was purchased from Matheson and stored as a solution in tetraglyme over sodium and benzophenone at <1 atmosphere of vapor pressure for at least one week. NMR spectra were recorded on a Varian Mercury 300, Varian INOVA 500 or Varian Innova 600 spectrometer.

Kinetics of Methane Activation. Stock solutions of **2** were prepared by weighing **1** and *tris*(pentafluorophenyl)borane (2 equivalents) into 5.0 mL volumetric flasks and adding TFE-d_3 (approximately 3 mL). The suspension was mixed by shaking until the solids had dissolved. Additional TFE-d_3 was added to dilute the sample to 5.0 mL, the solution mixed and then transferred to a vial and stored at -30 ˚C in the glove box freezer. Solutions prepared from anhydrous reagents in this way are stable for days with minimal decomposition (~5-10%) after 1 week. 400 μL was measured into a sapphire NMR tube using a

volumetric syringe, the cap tightly closed and the sample taken to the high-pressure manifold. After evacuating the manifold, the tube was charged with the desired pressure of dry methane gas and the tube taken to the NMR spectrometer that had been preheated to 330 ± 0.1 K or 300 ± 0.1 K as determined by an ethylene glycol temperature calibration standard. After allowing the sample to reach the probe temperature (5 minutes) the tube was removed and mixed by rocking the sample ~10 revolutions and then reinserted into the probe. A ^{1}H NMR spectrum was taken to measure the methane concentration *versus* the known concentration of platinum in the solution. Kinetics were monitored by following the disappearance of the ^{13}C-labeled platinum methyl signal in the ^{13}C NMR. After the run, the sample height was measured to ± 0.5 mm and compared with the starting height to correct the concentration for the change in volume due to the dissolved gas.

CAUTION: Handling high-pressures of gas in sapphire NMR tubes is extremely dangerous and should be approached with caution. Many steps were taken to minimize exposure to the tubes while under pressure. The tubes and high-pressure manifold used in this work were tested regularly at pressures well above those employed under working conditions.

Kinetics of Methanol Activation. Stock solutions were made by weighing **1** and tris-pentafluorophenylborane (2 equiv.) into 1.0 mL volumetrtic flasks and adding TFE-d_3 (approximately 0.5 mL). The suspension was shaken until the all solids had dissolved. After the solids had dissolved, the desired amount of methanol was added with a μL syringe followed by enough TFE-d_3 to dilute to 1.0 mL total volume. 700 μL was measured into a J. Young NMR tube

using a volumetric syringe, the cap tightly closed and the sample taken to the NMR spectrometer that had been preheated to 330 ± 0.1 K as determined by an ethylene glycol temperature calibration standard. Kinetics were monitored by following the disappearance of the starting material in the ^{1}H NMR spectrum.

Kinetics of Dimethylether Activation. 5.0 mL stock solutions were prepared as described above and 700μL measured into J. Young NMR tubes. The samples were degassed on a high vaccum line and dimethylether added to the NMR tube. After mixing, the sample height was measured to determine the change in volume due to the added gas and the sample taken to the NMR spectrometer that had been preheated to 300 ± 0.1 K with the help of an ethylene glycol temperature calibration standard. Kinetics were monitored by following the disappearance of the starting material in the ^{1}H NMR spectrum.

$^{13}CH_3Li \bullet LiI$. $^{13}CH_3I$ (8.13 g, 56.88 mmole) that had been distilled from copper pellets and calcium hydride was dissolved in petroleum ether (10 mL) and cooled to -78 ˚C under argon. 2.06 equivalents of *t*-BuLi in pentane (1.7 M, 69.0 mL, 117 mmole) were added dropwise to this solution with vigorous stirring, causing the formation of a white precipitate. After stirring for 15 minutes at -78 ˚C the white suspension was warmed to 0 ˚C in an ice bath and then stirred for 4 hours at this temperature. The stirring was then stopped and the suspension left standing until the solids had settled to the bottom of the flask. The liquids were removed via cannula filtration and the solids pumped to dryness. The white precipitate was then taken into the glove box where it was washed three times with petroleum ether and then dried under high vacuum

overnight. Roughly half of the material was spilled in the glove box. The unspilled portion weighed 4.13g (46% yield).

[(μ-SMe_2)Pt($^{13}CH_3$)$_2$]. [(μ-SMe_2)Pt($^{13}CH_3$)$_2$] was prepared similarly to the unlabeled version[17] using $^{13}CH_3Li$•LiI (2.484 g, 15.84 mmole) dissolved in 25 mL of diethylether. A slightly darker color of the reaction mixture and the product resulted from the use of this reagent. The product was dissolved in THF and additional carbon was added. The suspension was filtered, and the product reprecipitated with petroleum ether at -78 ˚C. This procedure was repeated a second time yielding 1.09g (49% based on platinum) of white powder. ^{1}H NMR (300 MHz, C_6D_6) δ = 1.00 (m, $J_{C\text{-}H}$ = 128.1 Hz, $J_{Pt\text{-}H}$ = 87.53 Hz, 12H), 2.05 (s, $J_{Pt\text{-}H}$ = 20.32 Hz, 12H); ^{13}C NMR (75.4 MHz, C_6D_6) δ = -6.41 ($J_{Pt\text{-}C}$ = 791.7 Hz);

[(diimine)Pt($CH_{3-n}D_n$)($DOCH_3$)]$^+$[$CF_3CD_2OB(C_6F_5)_3$]$^-$ (2(MeOD)). ^{1}H NMR (600 MHz, TFE-d_6) δ = 0.75 (s, 3H), 1.35 (s, 9H), 1.37 (s, 9H), 1.81 (s, 3H), 2.02 (s, 3H), 3.04 (s, 3H), 6.84 (s, 2H), 7.06 (s, 2H), 7.52 (s, 1H), 7.60 (s, 1H);

[(diimine)Pt($CH_{3-n}D_n$)(CH_3OCH_3)]$^+$[$CF_3CD_2OB(C_6F_5)_3$]$^-$ (2(DME)). ^{1}H NMR (600 MHz, TFE-d_6) δ = 0.85 (s, 3H), 1.37 (s, 9H), 1.38 (s, 9H), 1.89 (s, 3H), 1.99 (s, 3H), 6.84 (s, 2H), 7.04 (s, 2H), 7.54 (s, 1H), 7.54 (s, 1H);

[(diimine)Pt(μ-CH_2)(μ-($CH(OCH_3)$)Pt(diimine)]$^+$[$CF_3CD_2OB(C_6F_5)_3$]$^-_2$ (5). Crystals that precipitated at the end of dimethylether activations were isolated by filtration and dried under vacuum. These crystals were very soluble in organic solvents including diethylether. Removing the solvent from these solutions gave oily residues rather than solids. Redissolving the crystals in Acetone-d_6 gave a sample that is 90% **5**. ^{1}H NMR (500 MHz, Acetone-d_6) δ = 1.278 (s, 9H), 1.283 (s, 9H), 1.29 (s, 9H), 1.30 (s, 9H), 2.25 (s, 3H), 2.26 (s, 3H), 3.79 (s,

3H), 6.78 (at, $J_{H\text{-}H}$ = 1.8 Hz, 1H), 6.83 (at, $J_{H\text{-}H}$ = 1.8 Hz, 1H), 6.91 (at, $J_{H\text{-}H}$ = 1.8 Hz, 1H), 6.93 (at, $J_{H\text{-}H}$ = 1.8 Hz, 1H), 7.46 (m, 2H), 8.01 (d, $J_{H\text{-}H}$ = 5.25 Hz, 1H), 8.15 (dd, $J_{H\text{-}H}$ = 5.25 Hz, $J_{H\text{-}H}$ = 1.74 Hz, 1H), 10.35 (d, $J_{H\text{-}H}$ = 1.74 Hz, 1H); HRMS (FAB) *m*/*z* calcd for $[C_{67}H_{102}N_4OPt_2]^+$ 1368.735, found 1368.733.

X-ray Structure Details for 5. The Pt dimer sits on a center of symmetry in the *P*-1 solution with the methoxy group of the μ-CH(OCH_3) fragment disorder over this center of symmetry. Refinement of its population showed that the ligand occupies each site with equal probability. Attempts to solve the structure in *P*1 gave less reliable results.

Table 7. Crystal and Refinement Data for **5** (CCDC 267189).[a]

Empirical formula	$[C_{67}H_{102}N_4OPt_2]^{+2}$ $2(C_{20}H_2BF_{18}O)^-$
Formula weight, g/mole	2591.76
Crystal size, mm^3	0.29 x 0.25 x 0.18
θ range, deg	2.42 to 34.86
a, Å	12.3114(3)
b, Å	15.4916(4)
c, Å	16.6024(4)
A, deg	63.6320(10)
β, deg	73.3540(10)
γ, deg	88.6650(10)
Volume, $Å^3$	2698.14(12)
Z	1
Crystal system	Triclinic
Space group	P-1
d_{calc}, g/cm^3	1.595
θ range, deg	1.74 to 40.43
Completeness to θ = 40.43°	87.30%
Reflections collected	74339
Independent reflections	29995 [R_{int}= 0.0603]
Absorption correction	SADABS (μ = 2.703 mm^{-1})
Max. and min. transmission	1.000000 and 0.831789
Goodness-of-fit on F^2	1.748
R indices (all data)	R_1 = 0.1021, wR_2 = 0.1148

[a] 100(2) K, [b] $R_1 = \Sigma||F_o|| - |F_o||/ \Sigma|F_o|$. [c] $wR_2 = [\Sigma[w(F_o^2 - F_c^2)^2]/ \Sigma[w(F_o^2)^2]]^{1/2}$.

References

1) Theo Fleish, bp Gast to Products Executive: personal communication.

2) Marks, T. J. *et al. Chem. Rev.* **2001**, *101*, 953–996.

3) (a) Labinger, J. A. *Catal. Let.* **1988**, *1*, 371–375. (b) Crabtree, R. H. *Chem. Rev.* **1995**, *95,* 987-1007. (c) Labinger, J. A.; Bercaw, J. E.; Luinstra, G. A.; Lyon, D. K.; Herring, A. M. *International Gas Conversion Symposium, Sydney, Australia, July 4-9, 1993* (R. F. Howe and E. Curry-Hyde, Eds.), Elsevier, Amsterdam, **1994**, 515-520.

4) (a) Stahl, S. S.; Labinger, J. A.; Bercaw, J. E.; *Angew. Chem. Int. Ed.* **1998**, *37*, 2180-2192, and references cited therein. (b) Periana, R. A.; Taube, D. J.; Evitt, E. R.; Loffler, D. G.; Wentrcek, P. R.; Voss, G.; Masuda, T. *Science* **1993**, *259*, 340–343. (c) Periana, R. A.; Taube, D. J.; Gamble, S.; Taube, H.; Satoh, T.; Fujii, H. *Science* **1998**, *280*, 560–564.

5) (a) Labinger, J. A.; Herring, A. M.; Bercaw, J. E. *J. Am. Chem. Soc.* **1990**, *112*, 5628-5629. (b) Labinger, J. A.; Herring, A. M.; Lyon, D. K.; Luinstra, G. A.; Bercaw, J. E.; Horvath, I. T.; Eller, K. *Oganometallics* **1993**, *12* 895-905. (c) Sen, A.; Benvenuto, M. A.; Lin, M. R.; Hutson, A. C.; Basickes, N. *J. Am. Chem. Soc.* **1994**, *116*, 998-1003. These results are uncertain due to the ubiquitous formation of metallic Pt, which is a good alcohol oxidation catalyst.

6) (a) Zhong, A. H.; Labinger, J. A.; Bercaw, J. E. *J. Am. Chem. Soc.* **2002**, *124*, 1378-1399. (b) Johansson, L.; Tilset, M.; Labinger, J. A.; Bercaw, J. E. *J. Am.*

Chem. Soc. **2002**, *122,* 10846-10855. (c) Heyduk, A. F.; Driver, T, G.; Labinger, J. A.; Bercaw, J. E *J. Am. Chem. Soc.* **2004**, *126,* 15034–15035.

7) CCDC#: 213879.

8) Alcoholysis of the C–O bond to produce a trifluoroethoxymethyl platinum complex has not been ruled out.

9) CCDC#: 213879.

10) (a) Jones, W. D. *Acc. Chem. Res.* **2003**, *36*, 140-146. (b) Crabtree, R. H. *Chem. Rev.* **1995**, *95*, 987-1007. (c) Shilov, A. E.; Shul'pin, G. B. *Chem. Rev.* **1997**, *97*, 2879–2932. (d) Hall, C.; Perutz, R. N. *Chem. Rev.* 1996, 96, 3125-3146.

11) (a) Thorn, D. L.; Tulip, T. H. *Organometallics* **1982**, *1*, 1580-1586. (b) Blackmore, T.; Bruce, M. I.; Davidson, P. J.; Iqbal, M. Z.; Stone, F. G. A. *J. Chem. Soc. A* **1970**, 3153. (c) Casey, C. P.; Andrews, M. A,; McAlister, D. R.; Rinz, J. E. *J. Am. Chem. Soc.* **1980**, *102*, 1927. (d) Sweet, J. R.; Graham, W. A. G. *J. Organomet. Chem.* **1979**, *173*, C9. (e) Headford, C. E. L.; Roper, W. R. *J. Organomet. Chem.* **1980**, *198*, C7. (f) Espenson, J. H.; Bakac, A. *J. Am. Chem. Soc*. **1981**, *103*, 2721 and references therein.

12) Thorn, D. L. *Organometallics*, **1986**, *5*, 1897–1903 and references therein.

13) (a) Holtcamp, M. W.; Labinger, J. A.; Bercaw, J. E. *J. Am. Chem. Soc.* 1997, 119, 848–849. (b) Luecke, H. F.; Arndtsen, B. A.; Burger, P.; Bergman, R. G. *J. Am. Chem. Soc*. **1996**, *118*, 2517–2518.

14) And references cited therein: Thorn, D. L. *Organometallics* **1986,** *5*, 1897.

15) (a) Uson, R.; Fornies, J.; Tomas, M.; Casas, J. M.; Cotton, F. A.; Falvello, L. R. *J. Am. Chem. Soc.* **1985**, *107*, 2556. (b) Uson, R.; Fornies, J.; Tomas, M.; Casas, J. M.; Cotton, F. A.; Falvello, L. R.; Llusar, R. *Organometallics* **1988**, *7*, 2279. (c) Uson, R.; Fornies, J.; Tomas, M.; Casas, J. M.; Cotton, F. A.; Falvello, L. R.; Feng, X. *J. Am. Chem. Soc.* **1993**, *115*, 4145.

16) Burger, B. J.; Bercaw, J. E. *New Developments in the Synthesis, Manipulation, and Characterization of Organometallic Compounds*; Wayda, A.; Darensbourg, M. Y., Eds.; American Chemical Society: Washington, DC, **1987**; Vol. 357.

17) Hill, G.S.; Irwin, M.J.; Levy, C.J.; Rendina, L.M.; Puddephatt, R. J. *Inorg. Synth.* **1998**, *32*, 149–153.

Chapter 3

Oxidative Addition as a Metallation Strategy for the Preparation of Aminocarbene Complexes of Palladium and Platinum

Some of the results reported below are the work of Nick A. Piro.

Abstract

The oxidative addition of 2-chloro-3,3-dimethyl-3*H*-indole (**1**) and 2-chloro-1,3,3-trimethylindolium triflate (**2**) to tetrakis-triphenylphosphine palladium(0) and platinum(0) were studied as a route to transition-metal aminocarbene complexes. The reaction of **2** with palladium(0) in CD_2Cl_2 produced the *cis*- oxidative addition product which, upon refluxing for 12 hours, converted to [*trans*-$(PPh_3)_2$(InMe)PdCl]$^+$[OTf]$^-$ (**3**) (InMe = 1,3,3-trimethyl-indole-2-ylidene; $OTf^- = CF_3SO_3^-$) (δ = 240.7 ppm). Reaction of **1** with platinum(0) produced [*trans*-$(PPh_3)_2$(Ind)PtCl] (**4**) (Ind = 3,3-dimethyl-indole-2-yl) that could be converted to the carbene complex [*trans*-$(PPh_3)_2$(InMe)PtCl]$^+$[OTf]$^-$ (**5**) by addition of methyl triflate. A crystal structure of **3** (1.9894(18) Å) shows a typical Pd–C single bond distance between the carbene ligand and the palladium atom. Comparing the C–N distance in **3** (1.288(2) Å) and **4** (1.341(2) Å) shows a lengthening of the typical C–N double bond in **3** to a longer distance that falls short of typical N–C single bonds. Reduction of **2** with Reicke magnesium produces the carbene dimer (**6**) as well as carbene rearrangement products - 1,2,3-trimethylindole (**7**) and 2,3,3-trimethyl-2*H*-indole (**8**). Reaction of stannous chloride with **2** in the presence of added chloride generates an unassigned indole containing species with a ^{13}C NMR resonance at δ = 220 ppm. Attempted crystallization of this species gave dark green blocks of the carbene dimer radical cation as its pentachlorostannate salt. A discussion of the bonding in these carbene complexes is presented.

Introduction:

Continued interest in the development of N-heterocyclic carbene ligands stems from their utility in catalysis as well as an interest in their electronic structure.[1] The electron-rich nature of these neutral carbon donors is frequently argued as their important electronic characteristic with the vast majority of reports claiming that π-effects make a negligible contribution to their bonding with transition metals.[2]

Arguments that imidazole derived carbenes are at best weak π-acceptors often cite the adjacent nitrogen lone pair π-donation as stabilizing the carbene empty orbital.[1] With this in mind, carbenes with only one adjacent donating group might be expected to display increased π-acidity and hence different reactivity and structure when bound to transition metals. It is expected that an increased number of inductively electron withdrawing and π-donating substituents raise the singlet-triplet gap.[1] According to this model aminocarbenes should have a more electron-rich σ-orbital as well as a more acidic π-orbital as compared to their imidazol-2-ylidene cousins.

Figure 1

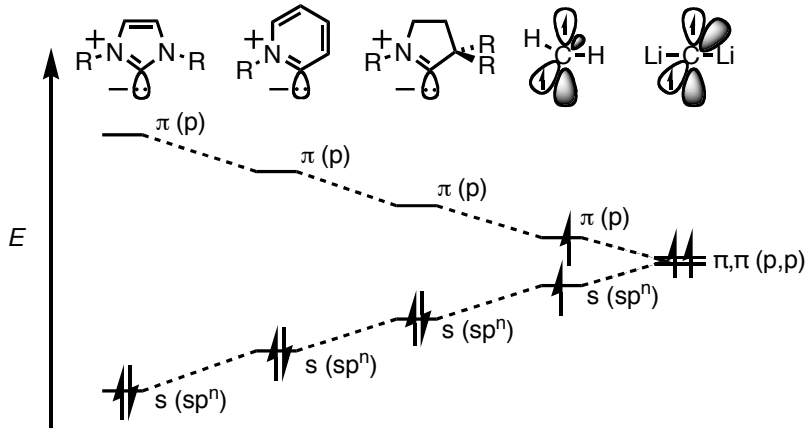

The vast number of studies on the diamino imidazole-derived N-heterocyclic carbenes is well documented in several recent reviews.[1] Numerous examples of these carbenes have been prepared *in situ* or isolated and stored. On the other hand, aminocarbenes have only recently appeared in the literature with the only example of a "free" aminocarbene coming from the Bertrand group.[3] The difficulty of their preparation and isolation inhibits the study of these carbenes and limits our knowledge of their bonding characteristics.

To avoid the need to prepare and isolate a free aminocarbene, we synthesized chloro-imminium salts that upon oxidative addition of the C–Cl bond would produce more stable transition-metal-bound aminocarbene complexes. At least one example of this metalation strategy was reported to make an analogous palladium complex of 1,3-dimethylimidazole-2-ylidene (IMe).[4] The synthesis of aminocarbene complexes using this method as well as their crystal structures and NMR parameters are reported. The reduction of C–Cl precursor with magnesium and tin reagents is also presented.

Results and Discussion

Preparation of 2-chloro-1,3,3-trimethylindolium triflate (**2**) is readily accomplished by methylation of 2-chloro-3,3-dimethyl-3*H*-indole (**1**) with methyltriflate in anhydrous methylene chloride (Scheme 1). Addition of diethylether provides 2-chloro-1,3,3-trimethylindolium triflate as an extremely hygroscopic white powder that is stable at room temperature when stored under inert atmosphere. The imidoyl carbon in **2** has a downfield ^{13}C NMR resonance at 184.7 ppm, an additional 7 ppm downfield of the same carbon in **1**.

Scheme 1

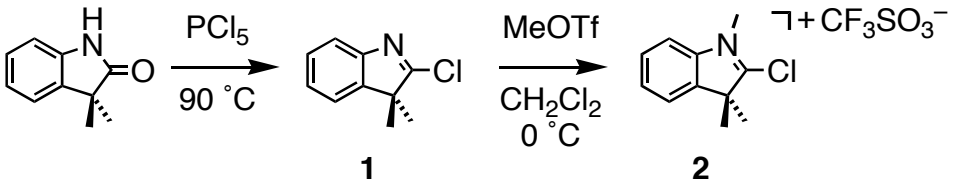

Mixing a CD_2Cl_2 solution of **2** with *tetrakis*-(triphenylphosphine) palladium causes a color change from yellow to orange which, upon continued refluxing (12 hours), changes to a pale yellow color. Following the reaction by ^{31}P NMR spectroscopy indicates that a new palladium complex with two inequivalent phosphorus nuclei (δ = 19.8, 30.0 ppm (J_{P-P} = 25.7 Hz)) is formed upon mixing the starting materials. Upon continued refluxing, this species decays with the appearance of a single ^{31}P resonance (δ = 24.0 ppm). ^{1}H NMR spectra of these samples at early reaction reveal a new indole containing species with three inequivalent methyl groups for the indole fragment. Along with the above mentioned changes in the ^{31}P NMR spectrum the asymmetric indole fragment converts to a new species with equivalent methyl groups for the quaternary center. These observations are consistent with the rapid formation of a palladium carbene complex containing *cis*-triphenylphosphine groups that converts to the *trans*-complex upon heating.[5] ^{13}C NMR spectra of the final product contain a resonance at δ = 240.7ppm (J_{P-C} = 6.0 Hz) confirming the presence of a carbene complex of palladium (**3**) (Scheme 2).

Scheme 2

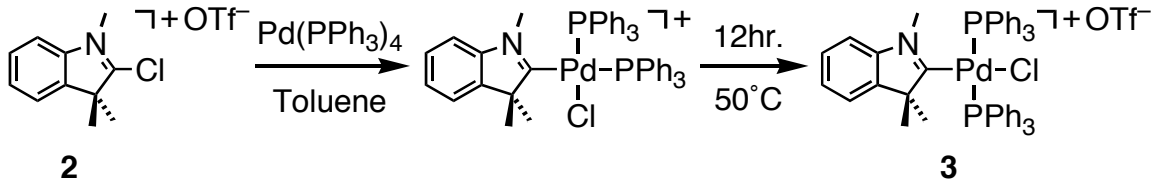

Attempts to prepare the platinum analogue of **3** by the method outlined in Scheme 2 were not successful. Instead of the desired carbene complex, reaction of **2** with *tetrakis*-triphenylphosphine platinum in methylene chloride, THF or diethylether showed the eventual formation of *bis*-triphenylphosphine platinum(II)dichloride by ^{31}P NMR spectroscopy.[6] Instead, the platinum analougue of **3** was prepared via oxidative addition of **1** to *tetrakis*-triphenylphosphine platinum and subsequent methylation of the indole nitrogen (Scheme 3). Consistent with the successful metylation of **4**, the ^{13}C NMR spectra of the carbon bound to platinum shifts from δ = 197.3 ppm to δ = 223.9 ppm and the platinum carbon coupling constant increases by >10% ($J_{Pt\text{-}C}$ = 1096 Hz (**4**), $J_{Pt\text{-}C}$ = 1216 Hz (**5**)).

Scheme 3

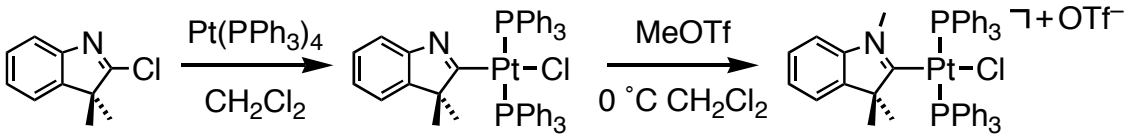

1 **4** **5**

X-Ray quality crystals of **3** and **4** were grown from methylene chloride solutions by slow diffusion of diethyl ether and pentane (Figure 2). Both complexes exhibit distorted square planar structures with both triphenylphosphine ligands bending away from the quaternary carbon of the carbene ligand (P(1) - M - P(2) = 164.758(14)° (**4**) and 167.692(16)° (**3**)). The platinum carbon distance in **4** (2.0006(17) Å) is typical for a single bond to an sp^2-carbon,[7] and the C–N distance (1.288(2) Å) consistent with typical nitrogen–carbon double bonds. This same bond in the carbene complex ((**3**) 1.314(2) Å), though slightly longer, is still significantly shorter than the C–N distance in

formamide (1.38 Å).[8]

A palladium complex of 1,3-dimethylimidazole-2-ylidene ([*cis*-$(PPh_3)_2$(IMe)PdCl]$^+$), provides a useful comparison for understanding the bonding and NMR parameters of **3**, **4**, and **5**.[4] For instance, the carbene carbon of the imidazole-derived ligand resonates at 194.9 ppm with a similar P–C coupling constant (6.9 Hz) indicating a smaller paramagnetic contribution to its chemical shift compared with **3** and **5**. The crystal structure of **3** shows that the Pd–C distance in **3** (1.989(2) Å) is similar to its imidazole-2-ylidene cousin (1.975(3) Å), and the Pd–Cl distance (2.3511(5) Å) a bit shorter than in the diamino complex (2.3359(7) Å). A more distinct difference between the two molecules is visible in the P(1) - Pd - P(2) angle (167.69(2)° (**3**), 176.01(3)° ([(InMe)Pd$(PPh_3)_2$Cl]$^+$)) and Pd - P distances (2.3680(5) Å (**3**), 2.3432(8) ([(InMe)Pd$(PPh_3)_2$Cl]$^+$)) in these two complexes with compound **3** showing a larger distortion from a square planar structure. These observations indicate a larger steric influence of the InMe ligand that is likely due to the bulk of the "neoheptylidene-like" framework. Though the crystal structure **3** does not reveal any shortening of the metal–carbon bond, this does not rule out an increased π-acidity of the aminocarbene carbon compared with its imidazole-2-ylidine cousin. These effects are likely masked by the steric differences that might prohibit shortening of this distance and the weak π-basicity of palladium(II).

Mixing active magnesium•2KBr, described by Rieke *et. al.*[9], with solutions of **2** in THF at -78 ˚C gives an immediate darkening of the orange suspension. Analysis of the filtrate by GC-MS shows a mixture of three predominant products (>90%) with the major product (>70%) being a broad peak for the carbene dimer (**9**). The other two products, 2,3,3-trimethyl-2*H*-indole (**7**) and

Figure 2

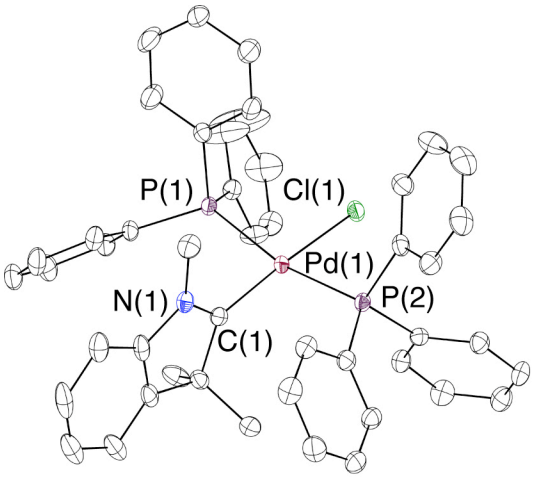

3

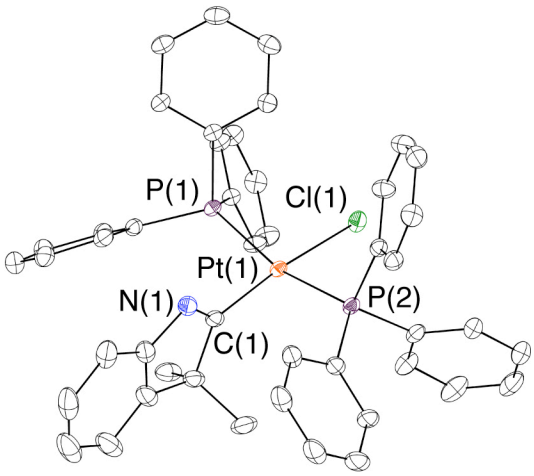

4

Pd(1)-C(1)	1.9894(18)
Pd(1)-Cl(1)	2.3511(5)
Pd(1)-P(2)	2.3639(5)
Pd(1)-P(1)	2.3722(5)
N(1)-C(1)	1.314(2)
C(1)-Pd(1)-P(1)	92.88(5)
C(1)-Pd(1)-P(2)	95.37(5)
P(1)-Pd(1)-P(2)	167.692(16)
P(2)-Pd(1)-Cl(1)	85.661(16)
P(1)-Pd(1)-Cl(1)	87.189(16)
C(1)-Pd(1)-Cl(1)	173.46(5)

Pt(1)-C(1)	2.0006(17)
Pt(1)-P(1)	2.3155(4)
Pt(1)-P(2)	2.3251(4)
Pt(1)-Cl(1)	2.4028(4)
N(1)-C(1)	1.288(2)
C(1)-Pt(1)-P(1)	93.23(4)
C(1)-Pt(1)-P(2)	94.44(4)
P(1)-Pt(1)-P(2)	164.758(14)
P(1)-Pt(1)-Cl(1)	86.648(14)
P(2)-Pt(1)-Cl(1)	87.691(14)
C(1)-Pt(1)-Cl(1)	171.47(5)

Ellipsoids are shown at 50% probability with relevant distances [Å] and torsional angles shown [°].

1,2,3-trimethylindole (**8**), are presumably the result of methyl group migration to a transient carbene (**6**) (Scheme 6). Conducting the same reduction at room temperature shows similar products with a much larger percentage of the products arising from unimolecular decomposition (**7,8**).

Scheme 4

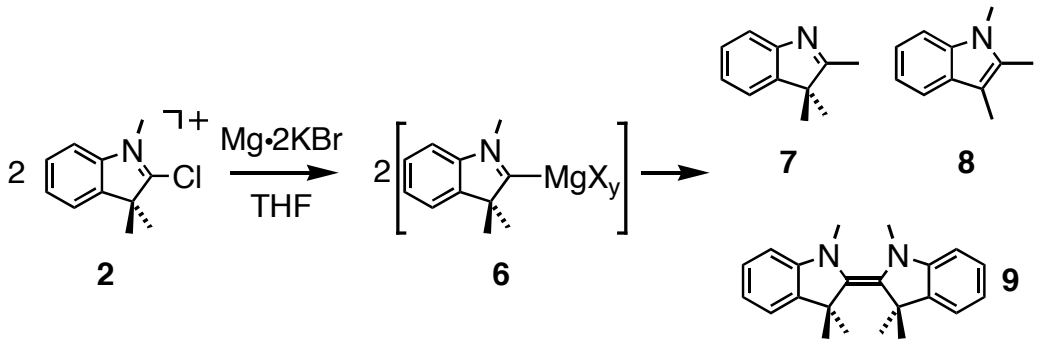

Upon mixing a THF solution of **2** with anhydrous tin(II) chloride and *n*-butylammonum chloride the colorless solution darkens to a deep purple color. Analysis of these solutions by ^{13}C NMR spectroscopy shows one predominant set of resonances (~85%) for the indole fragment product and a single resonance appearing at 220ppm that is tentatively assigned to a tetrachlorotin bound carbene (**10**) (Scheme 5). Attempts to crystallize this species gave dark green blocks that were characterized with X-ray crystallography as a radical cation of the carbene dimer (**11**) with a THF bound pentachlorostannate anion in the lattice (Figure 3). This radical cation presumably arises by dimerization of **10** and subsequent oxidation by tin(IV)chloride.

Scheme 5

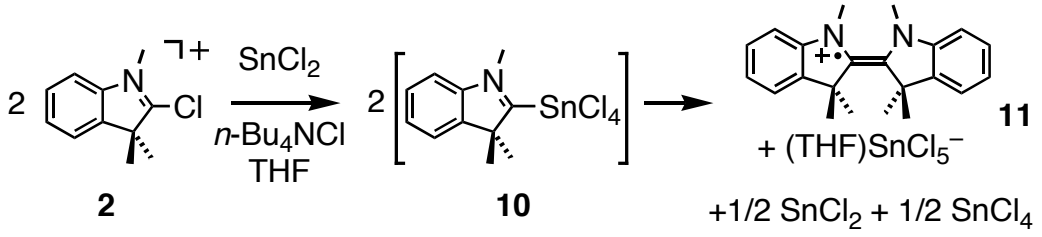

ESR analysis of the crystals at room temperature shows an eleven-line pattern for an organic radical (g = 2.004). In order to provide support for the assignment of this radical cation a semi-empirical PM3 calculation of the dimer was performed that gave good structural agreement with its X-ray crystal

structure (Figure 3). A picture of the SOMO indicates that the upaired electron is delocalized symmetrically over both sides of the molecule with orbital contributions from both nitrogens and four carbons that have bound hydrogens. Using this as a model, the ESR spectrum could be simulated with the unpaired electron coupling to four hydrogens and two nitrogens providing excellent agreement with the observed spectrum (Figure 4).[10]

Figure 3

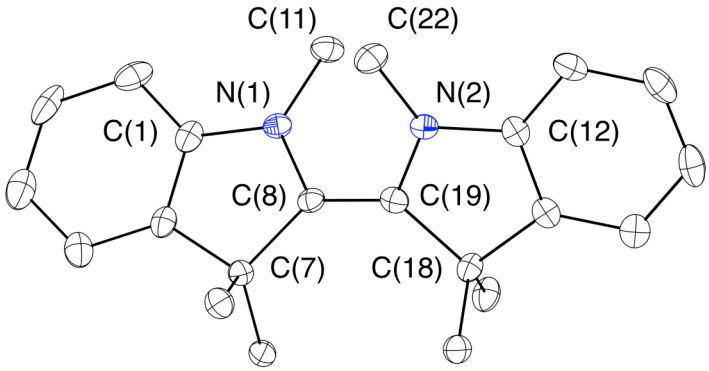

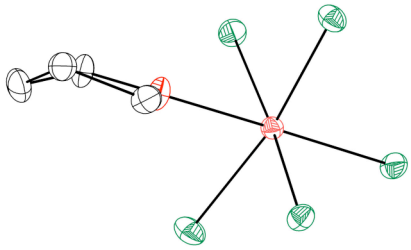

C(8)-C(19)	1.414(2)
N(1)-C(8)	1.359(2)
N(1)-C(1)	1.405(2)
N(1)-C(11)	1.467(2)
N(2)-C(19)	1.361(2)
N(2)-C(12)	1.407(2)
N(2)-C(22)	1.471(2)

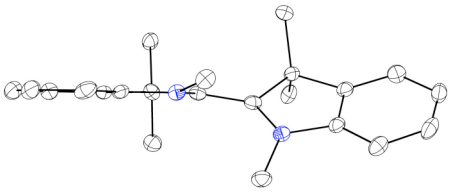

N(1)-C(8)-C(19)-N(2)	31.1
C(7)-C(8)-C(19)-C(18)	53.6

Ellipsoids are shown at 50% probability with relevant distances [Å] and torsional angles shown [°]. An additional representation of the radical cation without its anion is shown below on the right to illustrate the deviation from planarity.

Figure 4

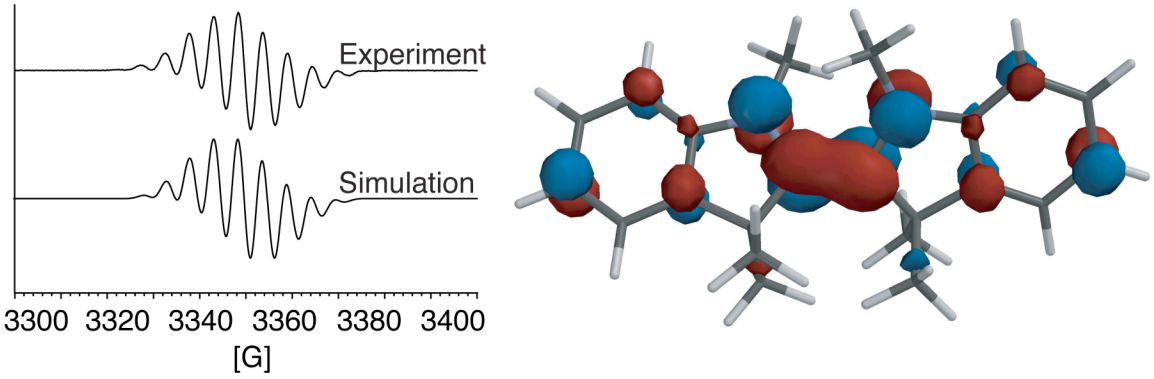

Conclusions

In conclusion, transition-metal aminocarbene complexes were prepared by oxidative addition either of a chloroindolium (**2**) precursor or by methylation of an indol-2-yl platinum complex (**4**). Crystallographic analysis of **3** reveals no shortening of bond between the palladium center and the carbene ligand compared with a typical Pt–C(sp^2) distance. A steric interaction between the quaternary center of the indole and the adjacent triphenylphosphine ligands distorts the square planar structure by repelling the adjacent triphenylphosphine ligands. Reduction of **2** with magnesium gave 1,2 and 3,2 methyl-migration products as well as the carbene dimer consistent with the formation of a reactive carbene intermediate. Reductive insertion of stannous chloride into the C–Cl bond of **2** is tentatively proposed to give a tetrachlorotin-bound carbene complex that undergoes subsequent one-electron oxidation to a stable radical cation. The radical cation was characterized by X-ray crystallography, ESR spectroscopy, and semi-empirical PM3 modeling showing a delocalized electron despite the large distortion of the heterocycle from a planar structure.

Experimental

Table 1. Crystal[a] and refinement data for complexes **3,4,** and **11**.

	3	**4**	**11**
Empirical formula	$[C_{47}H_{43}ClNP_2Pd]^+$ $[CF_3O_3S]^-$	$C_{46}H_{40}NP_2ClPt$ $\frac{1}{2}C_5H_{12}$ $\frac{1}{2}C_5H_{12}$	$[C_{22}H_{26}N_2]^+$ $[SnCl_5(C_4H_8O)]^-$
a, Å	11.6901(4)	8.8273(3)	11.1772(3)
b, Å	11.7520(4)	13.4824(5)	15.1585(5)
c, Å	19.7241(7)	18.7845(7)	16.9830(5)
α, deg	81.1380(10)	73.6130(10)	90
b, deg	81.1550(10)	88.1440(10)	90
γ, deg	88.8250(10)	72.1040(10)	90
Volume, Å^3	2645.54(16)	2037.40(13)	2877.42(15)
Z	2	2	4
Crystal system	Triclinic	Triclinic	Orthorhombic
Space group	P-1	P-1	$P2_12_12_1$
d_{calc}, g/cm^3	1.224	1.525	1.585
θ range, deg	1.60 to 28.30	1.66 to 50.07	1.80 to 36.02
μ, mm^{-1}	0.547	3.623	1.375
Abs. Correction	None	Face indexed and SADABS	None
GOF	1.639	1.479	1.360
R_1,[b] wR_2[c] [I>2σ(I)]	0.0745, 0.0823	0.0517, 0.0759	0.0359, 0.0510

[a] 100(2) K. [b] $R_1 = \sum||F_o| - |F_c||/\sum|F_o|$. [c] $wR_2 = [\sum[w(F_o^2-F_c^2)^2]/\sum[w(F_o^2)^2]]^{1/2}$.

Computational Details. The lowest energy doublet groundstate structure of **11** was calculated using semi-empirical PM3 calculations on the Spartan '02 software package for the Macintosh operating system. This wave function was used to calculate the SOMO shown in Figure 4.

General Synthetic Methods. All air and/or moisture sensitive compounds were manipulated using standard Schlenk techniques or in a glove box under a nitrogen atmosphere, as described previously.[11] Methyltriflate was purchased from Aldrich, distilled from P_2O_5, and stored under argon. *Tetrakis-*

triphenylphosphine palladium, *tetrakis*-triphenylphosphine platinum, stannous chloride and phosphorus pentachloride were purchased from Strem and stored in the freezer under argon. 3,3-dimethyl-2-chloro-3*H*-indole[12] was prepared from 3,3-dimethyl-2-oxindole[13] as described previously. CD_2Cl_2 was purchased from Cambridge Isotope Laboratories, distilled from CaH_2, and stored under argon. Other solvents were dried by passing them over a column of activated alumina. NMR spectra were recorded on a Varian ^{UNITY}INOVA 500 (499.853 MHz for ^{1}H) or a Varian Mercury 300 (299.868 MHz for ^{1}H) spectrometer.

1,3,3-Trimethyl-2-chloroindolium triflate. (**2**) Freshly distilled 3,3-dimethyl-2-chloroindole (~6 g, 33 mmol) was dissolved in anhydrous methylene chloride (40 mL) under argon and cooled to 0 ˚C in an ice bath. Methyltriflate (7.6 mL, 67 mmol) was added dropwise *via* syringe over a few minutes. The solution was allowed to warm to room temperature and stirring continued for 2 hours. After this time the solution was concentrated and diethylether added until the product precipitated. The white powder was isolated by cannula filtration and purified by washing with diethyl ether. Drying under vacuum over night gave an exteremely hygroscopic free flowing white powder. ^{1}H NMR (300 MHz, $CDCl_3$): δ = 1.59 (s, 6H, $C(CH_3)_2$), 4.10 (s, 3H NCH_3), 7.55 (br s, 3H), 7.65 (br s, 1H); $^{13}C\{^1H]$ NMR (125 MHz, CD_2Cl_2): δ = 23.5, 37.0, 56.6, 116.1, 123.8, 130.2, 131.4, 140.9, 141.5, 185.0.

[*trans*-$(PPh_3)_2$(InMe)PdCl]$^+$ [OTf]$^-$. (**3**) *Tetrakis*-triphenylphosphine palladium (1.419 g, 1.228 mmol) was dissolved in anhydrous methylene chloride

(50 mL) to which was added a solution of **2** (0.4221 g, 1.228 mmol) in 20 mL methylene chloride. An additional 10 mL was used to rinse the remaining residue into the reaction vessel. The Teflon stopper was tightly closed and the orange solution was heated overnight at 50 ˚C. In the morning the yellow solution was concentrated and diethyl ether added to precipitate the product. Isolation of this colorless solid by filtration and washing with diethyl ether gave a crude product that was recrystalized by slow diffusion of diethyl ether into methylene chloride solution at -40 ˚C. Large clear blocks of the product were isolated by filtration and dried under vacuum (1.01g, 84%). ^{1}H NMR (500 MHz, $CDCl_3$): δ = 1.03 (s, 6H, $C(CH_3)_2$), 3.73 (s, 3H, NCH_3), 7.2 – 7.8 (m, 34H); $^{13}C\{^{1}H\}$ NMR (125 MHz, $CDCl_3$): δ = 26.9, 42.0 ($J_{C–P}$ = 65.1 Hz), 113.8, 121.8, 127.5, 128.9, 129.3, 132.1, 134.6, 144.2, 145.3, 240.7 ($J_{C–P}$ = XXX Hz); $^{31}P\{^{1}H\}$ NMR (202 MHz, $CDCl_3$): δ = 24.0.

***trans*-$(PPh_3)_2$(Ind)PtCl.** (**4**) *Tetrakis*-triphenylphosphine platinum (0.50 g, 0.40 mmol) was dissolved in anhydrous toluene (6 mL) to which was added a solution of **1** (0.072 g, 0.40 mmol) in 6 mL toluene. The yellow solution was heated for 20 hours at 100 ˚C over which time the color lightened. The solution was pumped to dryness and the powder dissolved in a minimal amount of methylene chloride. Diethyl ether was added to precipitate the product as a microcrystalline solid. The solid was isolated by filtration and washed with diethyl ether. After drying under vacuum, 0.24g of product was recovered. (84% yield). ^{1}H NMR (500 MHz, CD_2Cl_2): δ = 0.50 (s, 6H, $C(CH_3)_2$), 3.73 (s, 3H, NCH_3), 7.2 – 7.8 (m, 34H); $^{13}C\{^{1}H\}$ NMR (125 MHz, CD_2Cl_2): δ = 25.5, 62.2, 117.5, 120.1,

122.2, 126.5, 128.4 (m), 131.0, 135.8 (m), 148.2, 158.069, 197.3 (J_{C-P} = 8.3 Hz, J_{C-Pt} = 1096 Hz,); $^{31}P\{^{1}H\}$ NMR (202 MHz, $CDCl_3$): δ = XXX.

[*trans*-$(PPh_3)_2$(InMe)PtCl]$^+$ [OTf]$^-$. (**5**) Methylation of **4** (0.150g, 0.176 mmol) with methyltriflate (28 μL, 0.252 mmol) was conducted in a similar fashion as described in the synthesis of **3**. (0.160 g, 90% yield). ^{1}H NMR (500 MHz, CD_2Cl_2): δ = 0.96 (s, 6H), 3.52 (s, 3H), 7.0-7.8 (m, 34H); $^{13}C\{^{1}H\}$ NMR (125 MHz, CD_2Cl_2): δ = 27.5, 41.5, 63.1, 113.2, 122.6, 127.9, 128.9, 128.9 (br, C_{ipso}-P), 129.5 (m), 132.5, 135.1 (br), 144.5, 144.9, 223.9 (J_{C-Pt} = 1216 Hz,); $^{31}P\{^{1}H\}$ NMR (121.4 MHz, $CDCl_3$): δ = 20.7 (J_{C-P} = 2615 Hz).

(InMe)$SnCl_4$. (10) **2** (0.0553 g, 0.2403 mmol) was dissolved in THF-d_8 (1.0 mL) and mixed with a suspension of tin dichloride (0.0456 g, 0.2403 mmol) and *tetra*-butylammonium chloride in THF-d_8 (1.0 mL). A dark purple color quickly developed upon addition. After approximately one hour the sample was analyzed by ^{13}C NMR spectroscopy showing predominantly one set of resonances (~80%) for the aromatic portion of the molecule (δ = 110 - 150 ppm) and a single high field resonance proposed to be the carbene carbon of **10** (δ = 220 ppm). An irregular baseline was observed which is likely due to the presence of **11**.

References

1) a) Herrmann, W. A. *Angew. Chem., Int. Ed. Engl.* **2002**, *41*, 1290-1309. b) Bourissou, D.; Guerret, O.; Gabbai, F. P.; Bertrand, G. *Chem. Rev.* **2000**, *100*(1), 39.

2) a) Kocher, C.; Herrmann, W. A. *J. Organomet. Chem.* **1997**, *532* 261. b) Green, J. C.; Scurr, R.G.; Arnold, P. L.; Cloke, F. G. N. *J. Chem. Soc, Chem. Comm.* **1997**, 1963. c) Boehme, C.; Frenking, G. *Organometallics* **1998**, *17*, 5801-5809.

3) Lavallo, V.; Mafhouz, J.; Canac, Y.; Donnadieu, B.; Schoeller, W. W.; Bertrand, G. *J. Am. Chem. Soc.* **2004**, *126*, 8670. b) Cattoën, X.; Gornitzka, H.; Bourissou, D.; Bertrand, G. *J. Am. Chem. Soc.* **2004**, *126*, 1343.

4) Fürstner, A.; Seidel, G.; Kremzow, D.; Lehmann, C. W. *Organometallics*, **2003**, *22*, 907.

5) The same *cis-trans* isomerization was proposed on the basis of similar spectroscopic changes by Fürstner et al.. See reference 4.

6) Farkas, E.; Kollar, L.; Moret, M.; Sironi, A. *Organometallics* **1996**; *15*(5); 1345.

7) A search of Cambridge Crystal Strucuture Database for platinum-phenyl complexes revealed 1662 structures with an average and a mean Pt-C distance of 2.033 Å. Only 10% of the reported structures showed distances less than 1.98 Å.

8) March, J. *Advanced Organic Chemsitry*, 4th Edition, Wiley-Interscience, John Wiley and Sons, New York, p. 21.

9) Sell, M. S.; Hanson, M. V.; Rieke, R. D. *Synth. Commun.* **1994**, *24*, 2379.

10) The assignement of this radical cation was corroborated by one electron oxidation of (**9**) with silver triflate. The same dark purple color developed immediately upon mixing these reagents. A similar darkerning of the pale-orange oil developed, though more slowly, if **9** was left exposed to air.

11) Burger, B. J.; Bercaw, J. E. *New Developments in the Synthesis, Manipulation, and Characterization of Organometallic Compounds*; Wayda, A.; Darensbourg, M. Y., Eds.; American Chemical Society: Washington, DC, **1987**; Vol. 357.

12) Ugi, I.; Beck, F.; Fetzer, U. *Chem. Ber.* **1962**, *95*, 126.

13) Robertson, D. W.; Krushinski, J. H.; Kau, D. *J. Labelled Compounds and Radiopharmaceuticals* **1986**, *23*(4), 343-54.

Appendix A

Equipment For High Pressure NMR Spectroscopy

Some of the design and construction of the equipment shown below are the work of Dan Nieman, Mike Roy and Steve Olson.

Introduction

Below is a series of diagrams showing the design of the high-pressure NMR equipment used in my PhD research. Diagrams of the high pressure manifold including the gas regulators, vents and NMR tube filling tree is shown in Figures A1-A4. Figure A5 is a hand drawing of the columns used for purification of gases at high pressure. Figures A6 and A7 show the blast container used to shield the user from the tube while it is being filled on the manifold and as the tube is being inserted into the NMR probe. Dimensions of the blast container as well as a description of its use are provided so that this design can be copied or modified by others.

Figure A1. High-Pressure NMR Manifold – Gas Regulators.

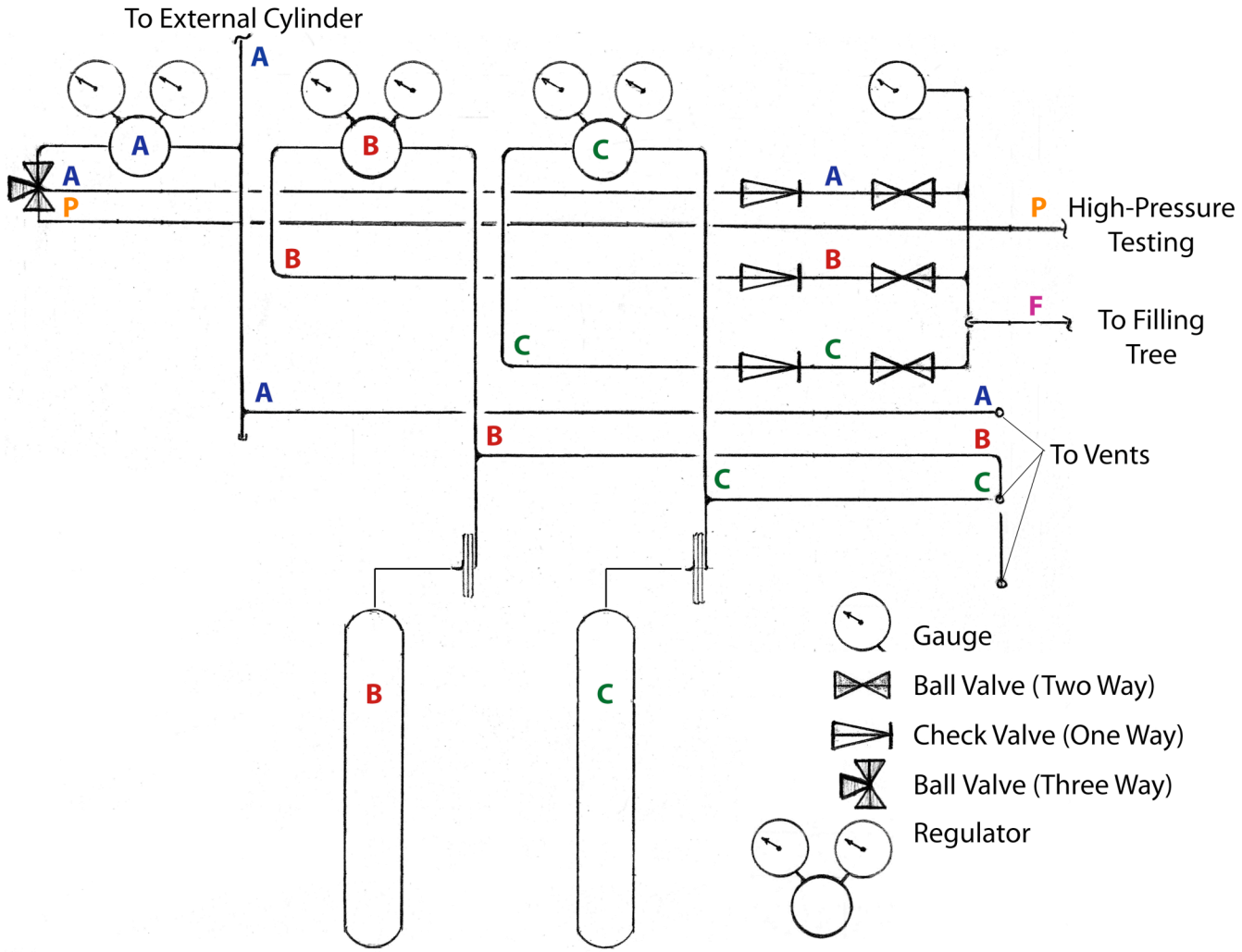

Figure A2. High-Pressure NMR Manifold – Regulator Venting System.

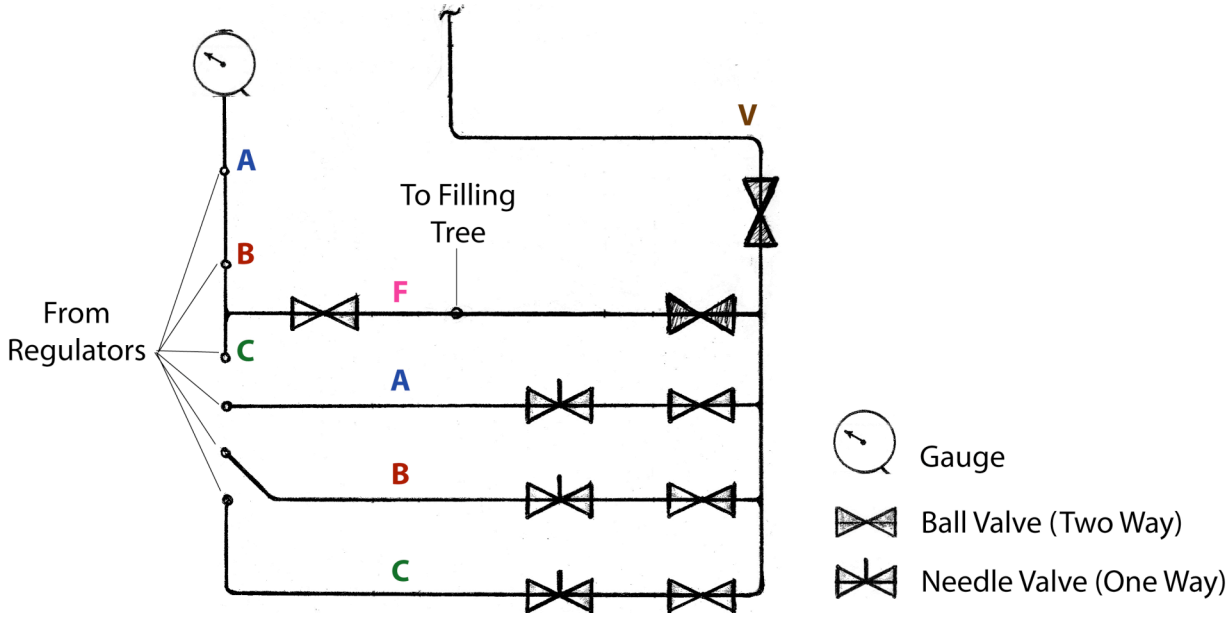

The above diagrams (Figures A1 and A2) depict equipment for regulating the pressure of gases from attached lecture bottles (shown) (Figure A1), or external cylinders. Three separate pathways with regulators and venting system are outlined and labeled A,B, and C. These three paths meet to form the main feed line, labeled F, on their way to the Filling Tree (See Below). The vent for the gas regulators is labeled V.

Figure A3. High-Pressure NMR Manifold – Filling Tree.

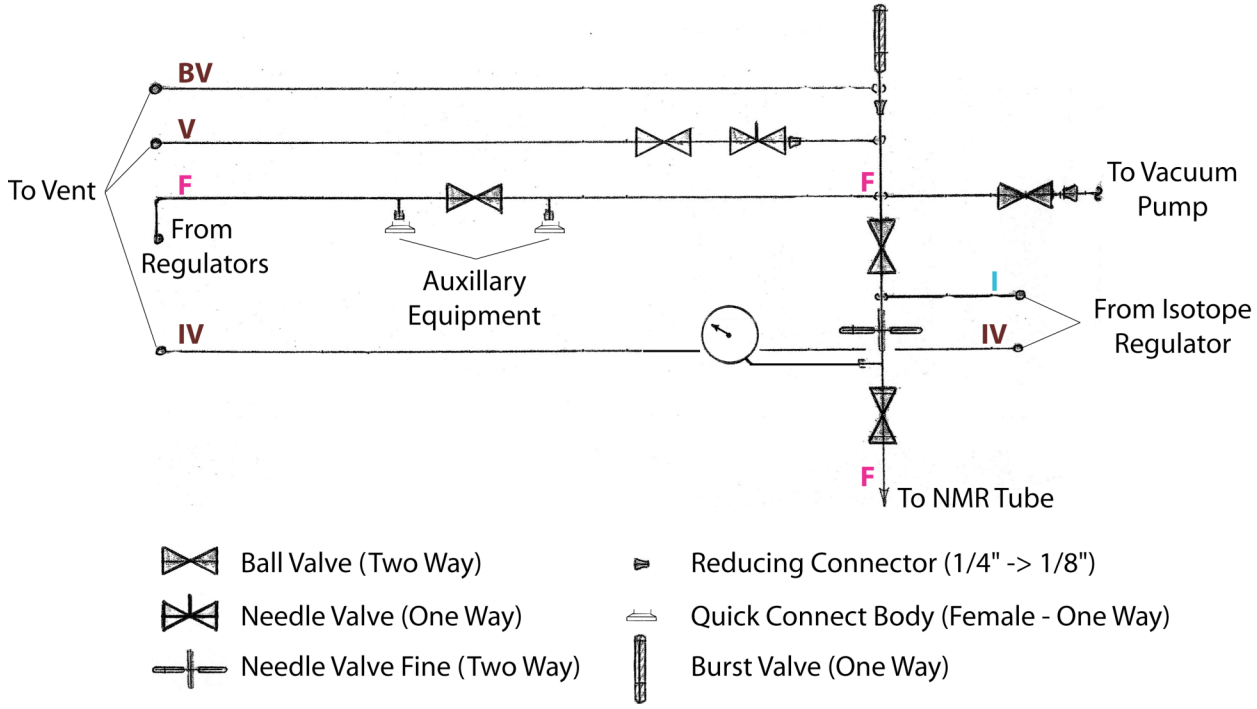

A diagram for the Filling Tree (Figure A3) depicts equipment for delivering gasses from the main feed line - labeled F - or expensive and/or isotopically labeled gasses - labeled I - to auxiliary equipment or high-pressure NMR tubes. In addition, venting systems, including a burst valve and its vent - labeled BV - and a vent for an adjacent regulator for expensive and/or isotopically labeled gases - labeled IV - (Figure A4) are shown.

Figure A4. High-Pressure NMR Manifold – Isotope Regulator and Venting System for Filling Tree.

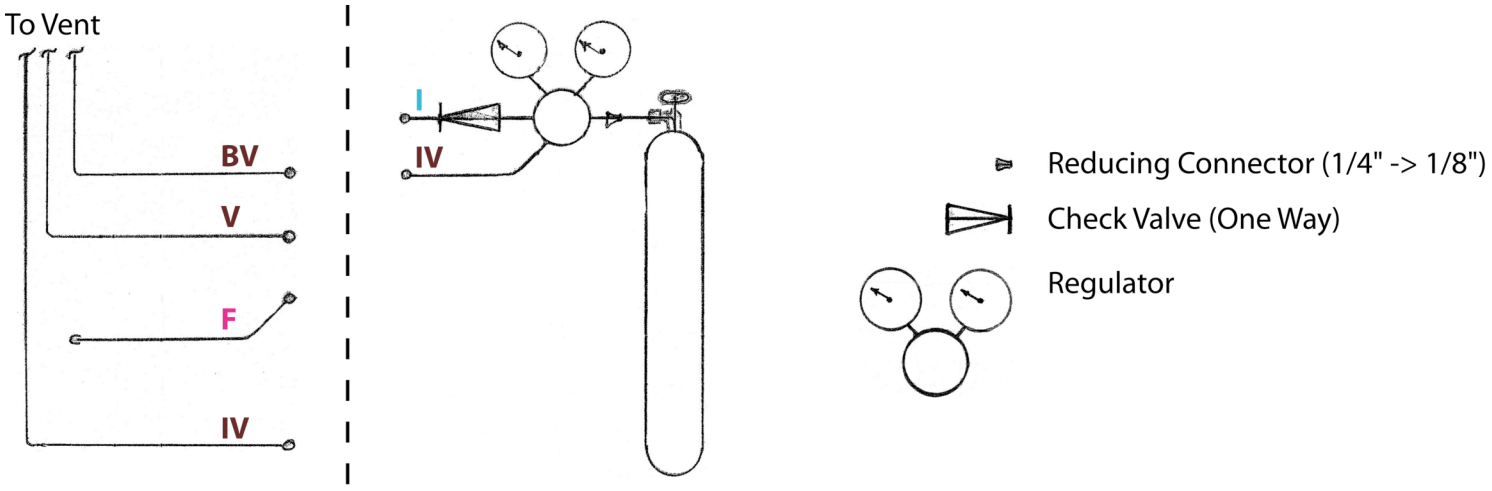

Figure A5. High-Pressure NMR Manifold – Gas Scrubbing Column.

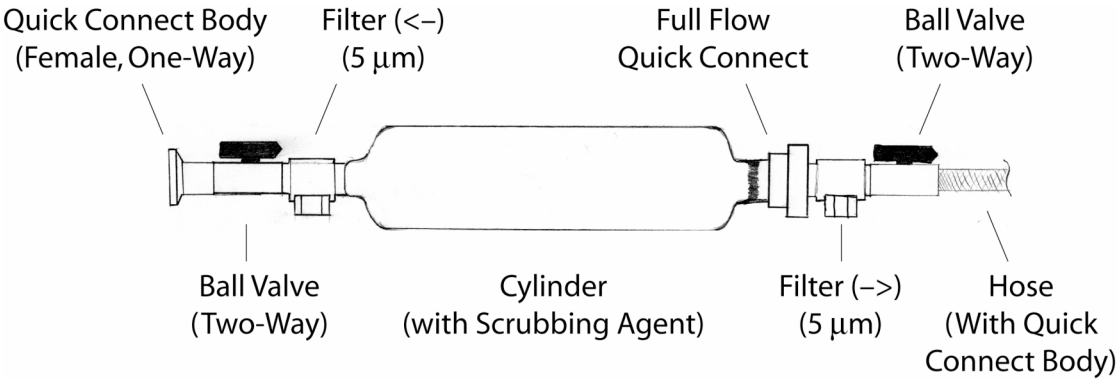

Figure A6. High-Pressure NMR Tubes – Blast Container (60% Scale).

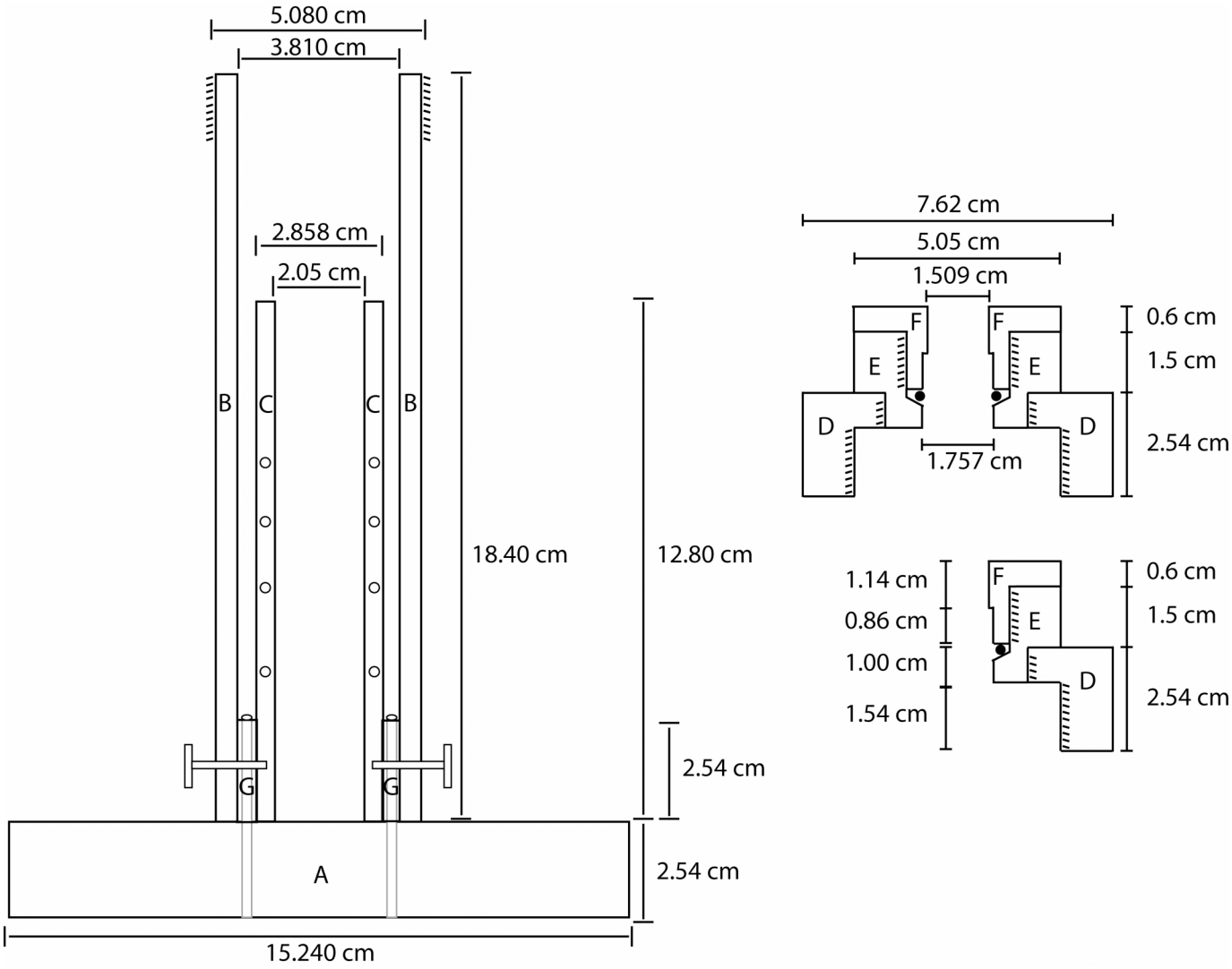

Figure A7. High-Pressure NMR Tubes – Blast Container with NMR Tube (50% Scale).

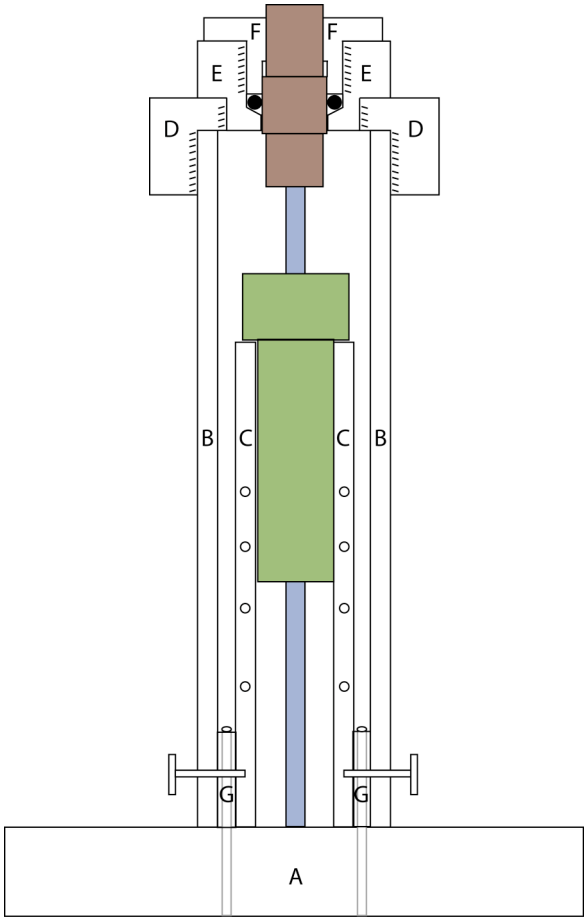

A cross section of a blast container for shielding the NMR spectroscopist from the danger of explosion is shown above in Figures A6 and A7 with the tube included. The individual pieces were cut from polycarbonate rods by Steve Olson in the machine shop. The container is divided into several parts that function 1) as a depth gauge and stand (Parts A,C, and G), 2) As a clasp (Parts E and F), and 3) as a shield and mount for the clasp (Parts D and B). While the depth gauge and stand are fastened to one another more permanently with screws, all other parts can be unscrewed from one another. Thumbscrews are used for convenient removal of the top portion, so that the shield and clasp can be lifted from the base. The clasp functions to hold the tube with an O-ring that

is squeezed around the NMR tube top by screwing F down onto the o-ring and against the beveled edge. This squeezing action holds the tube while the spectroscopist lifts the shield off of the base and transfers it to the top of the NMR spectrometer. This method of handling the tube minimizes ones contact with the tube while under pressure. If the tube were to break while pressurized within the container, vents have been drilled through the walls of C, and vertically thorugh G and A to relieve the gases though the bottom of the apparatus. Protection against the cap or tube rocketing up and through the clasp is provided by a constriction in F. Finally, the clasp was designed with the need to vent these tubes upon completion of the experiment. By separating parts E and D the ends of the cap are exposed and can be used to release the pressure. This limits the exposure to the tube and minimizes the handling of the tube while partially removing it from the container. Because this procedure can be performed behind the safety of an additional blast shield, the consequences of an explosion are minimized during this step. No tests of the effectiveness of this container have been performed, limiting the confidence of those with a more fragile constitution, though under the typical working pressures, the total amount of gas is less than the volume of the blast container when expanded to one atmosphere.